Université Lille 1
École Doctorale de Sciences de la Matière, du Rayonnement et de l'Environnement

Spécialité

Molécules et Matière Condensée

Thèse de Doctorat

En Cotutelle avec le Harbin Institute of Technology (Chine)

Par

Yi WANG

ayant pour titre

Synthesis and Catalytic Performance of Hierarchical Zeolites Supported Nickel-Tungsten Hydrodesulfurization Catalysts

Soutenance publique prévue le 23 Nov 2015 devant la commission d'examen composée de :

Rapporteurs : Yannick Pouilloux, Professeur, Université de Poitiers.
Changmin Hou, Professeur, Jilin University.

Examinateurs : Carole Lamonier, Professeur, Université de Lille-Sciences et Technologies
Christine Lancelot, Maitre de Conférences, Université de Lille-Sciences et Technologies
Yang Gang, Professeur, Harbin Institute of Technology
Min Yang, Professeur, Harbin Institute of Technology
Alain RIVES, Maitre de Conférences habilité à diriger les Recherches, Université de Lille-Sciences et Technologies
Yinyong Sun, Professeur, Harbin Institute of Technology

Remerciement

First of all, I would like to thank my tutor, M. Alain Rives. Thanks for the opportunity he gave me. His careful guidance leads me standing here. Thank you for your patience and support on me. Secondly, Thanks to M. Yinyong Sun, my co-supervisor, sharing me a lot of experience and knowledge in this domain.

Thanks to my co-director Christine Lancelot and Ms. Carole Lamonier. They helped me a lot in operation and paper writing. I love the environment working with you.

Thank to Mr. Olivier Gardoll, Mr. Pascal Blanchard, Martine Frere-Trenteseaux, Mr. Jean-Charles Morin, Mr. Bertrand Revel, Mr. Laurent Delevoye and Mr. Frederic Richard. They helped me a lot in the characterizations.

Moreover, thanks for the help of Alexia Cordova, Andre Mino, Kunyue Leng, Bingteng Wang and other partners.

Acknowledgement for the financial supporting of the Program Caiyuanpei (project N°30323NF) between China (CSC) and France (Campus-France).

Contents

Abstract

More and more strict regulations were drawn up in many countries to limit the concentration of sulfur below 10 or 15 ppm in transportation fuel oil. However, it is difficult to reach such standard because of the presence of refractory sulfur-containing molecules like 4,6-dimethyl-dibenzothiophene (4,6-DMDBT) due to the steric hindrance from alkyl groups. To overcome this problem, more efficient solids than the conventional CoMo supported on alumina catalysts have to be developed. In this work hierarchical Beta and Mordenite zeolite supported nickel-tungsten catalysts were prepared and their catalytic performance in HDS reactions were evaluated.

Firstly, hierarchical Beta zeolite was prepared by post-treatment and characterized by X-ray diffraction (XRD), N_2-sorption, scanning and transmission electron microscopy (SEM/TEM) and NMR techniques. It was found that more than half of acid sites in Beta was lost after base-treatment due to the transformation of tetrahedral coordinated aluminum. Subsequent acid treatment could increase the concentration of tetrahedral coordinated aluminum and allowed to recover the acidity of Beta zeolite. Moreover, the formation of mesopores greatly increased the number of accessible acid sites. As a result, hierarchical zeolite Beta prepared by base-acid treatment exhibited excellent catalytic activity in acid-catalytic reactions, especially towards large molecules.

NiW catalysts supported on Al_2O_3, commercial Beta and Mordenite zeolites (HB and HM), and hierarchical Beta and Mordenite prepared by post treatment (HB-M and HM-M) were characterized by XRD, N_2 sorption, Infrared spectroscopy (IR), TEM and X-ray photoelectron spectroscopy (XPS). Their catalytic performance were evaluated in the hydrodesulfurization (HDS) of dibenzothiophene (DBT) and 4,6-dimethyldibenzothiophene (4,6-DMDBT). In the HDS of DBT, NiW/Al_2O_3 exhibited better catalytic activity than zeolite supported catalysts. On the contrary, zeolite supported catalysts exhibited higher catalytic performance in the HDS of 4,6-DMDBT, which could be attributed to the strong acidity of the zeolitic support that supplied an additional isomerization reaction route. The use of hierarchical zeolite Beta and Mordenite could further improve the isomerization ability of catalyst. As a result, the HDS activity of 4,6-DMDBT over NiW/HM-M and NiW/HB-M was more than twice as that of NiW/Al_2O_3 in the HDS of 4,6-DMDBT.

The deactivation of hierarchical Beta zeolite supported catalysts was studied in the HDS of thiophene. The results indicated that NiW/HB as well as NiW/HB-M

endured serious and rapid deactivation during the first 3h of reaction. The introduction of additional mesopores/macropores in support could not prevent the deactivation tendency. Interestingly, mixing NiW/HB or NiW/HB-M with NiW/Al_2O_3 and the utilization of Na^+-exchanged Beta as support improved remarkably the anti-deactivation ability of the catalysts. As a result, the catalysts NiW/NaB-M (NiW catalyst supported on Na^+-exchanged hierarchical Beta) and NiW/20HB-M (20% NiW/HB-M mixed with 80% NiW/Al_2O_3) gave superior catalytic activity than NiW/HB-M and NiW/Al_2O_3. Moreover, these two methods may be utilized to enhance the anti-deactivation ability of NiW catalysts supported on different types of zeolites in the HDS of thiophene.

Keywords: NiW supported catalyst, Hierarchical zeolite, Hydrodesulfurization, 4,6-DMDBT, Deactivation.

Résumé

Des règles environnementales de plus en plus strictes imposent une concentration en soufre dans les carburants en-dessous de 10 à 15 ppm. Cependant, il est difficile d'atteindre cette norme en raison de la présence de molécules réfractaires comme le 4,6-diméthyl-dibenzothiophène (4,6-DMDBT), difficilement désulfurables en raison de l'encombrement stérique des groupes alkyles adjacents à l'atome de soufre. Pour résoudre ce problème, des catalyseurs plus efficaces que les catalyseurs conventionnels à base de cobalt et molybdène supportés sur alumine doivent être développés. Dans ce travail, des catalyseurs nickel-tungsten supportés sur zéolites Beta et Mordenite hiérarchisées ont été préparés et leurs performances en hydrodésulfuration (HDS) ont été évaluées.

Tout d'abord, des zéolites Beta hiérarchisées ont été obtenues par post-traitement et caractérisées par diffraction des rayons X (DRX), adsorption-désorption d'azote, microscopie électronique à balayage et à transmission (SEM, TEM) et résonnance magnétique nucléaire (RMN). Plus de la moitié des sites acides de la zéolite Beta sont perdus après le traitement basique, en raison de la diminution du nombre d'atomes d'aluminium en coordination tétraédrique. Après le traitement acide, la concentration en aluminium tétraédrique est récupérée, et le nombre de sites acides est augmenté. En outre, la hiérarchisation de la zéolite Beta permet d'augmenter considérablement le nombre de sites acides accessibles. En conséquence, la zéolite Beta hiérarchisée préparée par post-traitement base-acide présente une excellente activité dans les réactions en catalyse acide, en particulier pour la conversion de grosses molécules.

Des catalyseurs NiW supportés sur Al_2O_3 (NiW/Al_2O_3), zéolite Beta commerciale et hierarchisée (NiW/HB et NiW/HB-M), zéolite Mordenite commerciale et hierarchisée (NiW/HM et NiW/HM-M) ont été préparés et caractérisés par XRD, adsorption-désorption d'azote, spectroscopie infrarouge (IR), microscopie électronique à transmission et spectroscopie de photoélectrons induits par rayons X (XPS). Leurs performances catalytiques ont été évaluées en HDS du dibenzothiophène (DBT) et du 4,6-diméthyldibenzothiophène (4,6-DMDBT). Le catalyseur à base d'alumine NiW/ Al_2O_3 présente la meilleure activité catalytique en HDS du DBT. Par contre, les catalyseurs supportés sur zéolite présentent une performance catalytique plus élevée en HDS du 4,6-DMDBT, la forte acidité du support zéolite permettant une voie de réaction supplémentaire par isomérisation. L'utilisation de zéolite hiérarchisée améliore encore la capacité d'isomérisation du catalyseur. En conséquence, l'activité en HDS du 4,6-DMDBT sur NiW/HM-M et NiW/HB-M est plus du double de celle du catalyseur à base d'alumine NiW/Al_2O_3.

La désactivation de catalyseurs supportés sur zéolite Beta a été étudiée dans la réaction d'HDS du thiophène. Les résultats indiquent que les catalyseurs NiW/HB et

NiW/HB-M subissent une importante et rapide désactivation pendant les 3 premières heures de réaction. L'introduction de mésopores/macropores supplémentaires ne permet pas de limiter la désactivation. Par contre, le mélange des solides NiW/HB ou NiW/HB-M avec un catalyseur à base d'alumine NiW/Al_2O_3 et l'utilisation de zéolite Beta après échange avec des ions Na^+ comme support (NiW/NaB-M) améliorent remarquablement la capacité anti-désactivation des catalyseurs. En conséquence, les catalyseurs NiW/NaB-M et NiW/20HB-M (20% NiW/HB-M mélangé avec 80% NiW/Al_2O_3) conduisent à une activité catalytique supérieure à celle de NiW/HB-M et NiW/Al_2O_3. Par ailleurs, ces deux méthodes peuvent être étendues à des catalyseurs supportés sur d'autres types de zéolites.

Mot clés: Catalyseurs NiW, Zéolite hiérarchisée, Hydrodésulfuration, 4,6-DMDBT, Déactivation.

Chapter 1. Introduction

1.1 Purpose and significance of petroleum desulfurization

Petroleum industry, as one of pillar industries, plays an important role in economy. At present, most of transportation tools are driven by petroleum refining products. Thus, the quality and price of the transportation oil is closely related to our daily life. Usually, petroleum refinery includes two departments, distillation and oil refining (as shown in Figure 1-1) [1]. Distillation department could separate desalted and dewatered crude oil into various fractions such as naphtha, gas oil (GO), vacuum gas oil (VGO), etc., by atmospheric distillation and vacuum distillation. Oil refining was then carried out to improve the quality of fractions, such as availability, stability (anti-explosion) and combustion value. Finally, different transportation fuels such as gasoline, diesel, jet, kerosene and other fuels could be obtained by mixing various treated fractions.

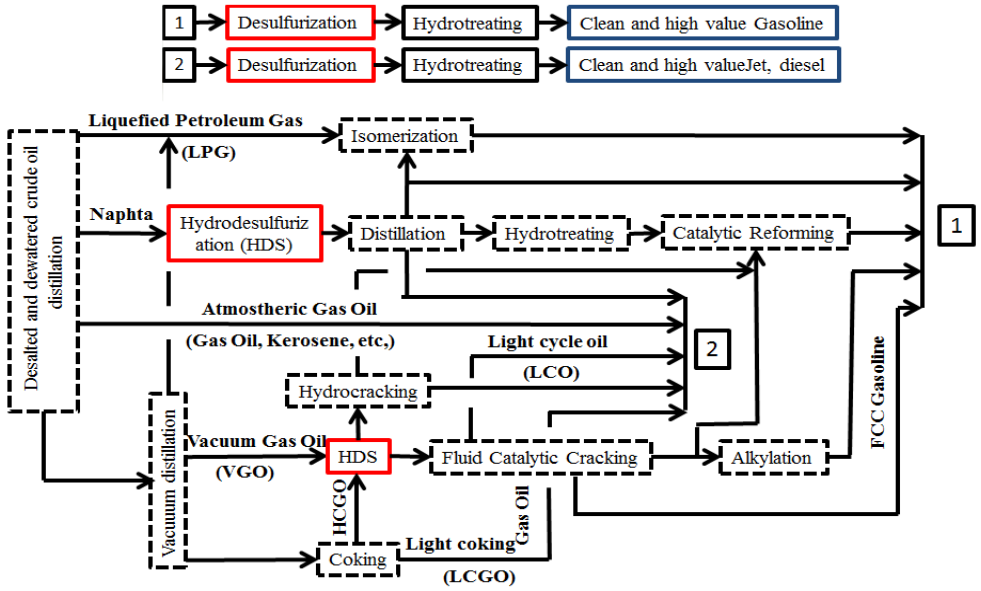

Fig.1-1 Scheme of petroleum industry

Desulfurization is a necessary process in refinery, because sulfur compounds in fuels is known as one of catalytic poison, which could negatively influence the performance of refining catalysts such as catalytic reforming catalyst and catalytic cracking catalyst. Moreover, sulfur in crude oil could cause corrosion problems in pipelines, pumps and reactors. Therefore, desulfurization process is generally carried out at the beginning of petroleum refining (as indicated in red squares in Fig. 1-1) to protect refining catalysts. However, due to the danger of naturally occurring sulfur compounds left in fuels for environment, a new important meaning has been given to

hydrodesulfurization of transportation fuel, to protect the environment [2].

Sulfur in the fuel will produce sulfur oxide gases. These gases react with water in the atmosphere to form sulfates and acid rain which damages buildings, destroys automotive paint finishes, acidifies soil, and ultimately leads to loss of forests and various other ecosystems [2]. Moreover, the sulfur compounds could react with metal salts during combustion. Part of formed sulfite, sulfate, hydrogen sulfate salts and other substances would be finally converted into particulate matter (PM), causing respiratory system disease and heart disease. According to the determination of PM2.5 in Beijing [3], sulfate and sulfite salt has become the most important artificial pollution sources, the influence of which was much higher than that of nitrate and ammonium salt. However, the PM emissions caused by car could be reduced by more than 30% when using ultra-low sulfur fuel [2]. In addition, sulfur in gasoline and diesel would greatly affect the performance of engine and the exhaust gas treatment device, leading the increase of automobile exhaust gas. It is reported [2] that the automobile exhaust gas (hydrocarbon, carbon monoxide and nitrogen oxide pollutants) can be reduced by 13%, 16% and 9%, respectively, when the sulfur content in gasoline decreasing from 450 ppm to 50 ppm. Therefore, reducing the sulfur content in the fuel has been recognized as the primary goal to produce clean energy.

Based on this, more and more strict regulations were drawn up in many countries to limit the concentration of sulfur below 10 ppm or 15 ppm in transportation fuel oil, such as standard mandated by Environmental Protection Agency (EPA) and European Parliament (Table 1-1) [4]. It could be observed in Table 1-1 that the limitation of sulfur content in transportation fuels was significantly changed from 1996 to 2008. Despite other limitations for cetane number and aromatic hydrocarbon value were also listed in these standards, their changes were much smaller than that of sulfur content, which illustrated the importance to limit the sulfur content in transportation fuels from another point of view.

Table 1-1 Roadmap of emission standards worldwild[4]

	Sulfur content (ppm)	Year	Adopted region
Euro II	500	1996	Indonesia
Euro III	150	2001	India, Malaysia
Euro IV	50	2005	Thailand, Singapore
Euro V	10	2008	Europe
EPA Tier	500	1996	-
EPA Tier	300	2004	-
EPA Tier	80	2006	-
EPA Tier	15	2008	USA

In addition, there are some other standards, such as the California CARB standards and China GB IV/V [5], which can be roughly equal to the corresponding EPA Tier or EU standards. Now, how to meet the more and more strict regulations became one big challenge for petroleum industry.

1.2 Desulfurization methods

1.2.1 Type and distribution of sulfur containing compounds in fuels

Sulfur containing products are one of the most important impurities in crude oil. Table 1-2 showed the sulfur content in crude oil from different region (US EPA) [4]. It could be observed in Table 1-2 that most of crude oil contain 1-2% sulfur element (10000-20000 ppm S). Moreover, it should be noticed that the sulfur content in crude oil in 2010 was higher than that of 1990, indicating that the quality of crude oil is declining and the sulfur content is gradually increasing with the large scale application.

Table 1-2 Sulfur levels in the global supplies of crude oil[4]

Region	Sulfur weight (%，1990)	Sulfur weight (%，2010)
Alaska	1.11	0.99
Canada	1.52	1.62
California	1.59	2.60
USA (Others)	0.86	0.88
Africa	0.17	0.18
Europe	1.09	1.10
Latin America	1.62	1.82
Middle East	1.69	1.71
Far East	1.09	1.10
World Average	1.13	1.27

Sulfur containing products in crude oil could be classified into inorganic and organic sulfur-components. Most of them are in organic form, and a small amount of inorganic sulfur components such as sulfur, hydrogen sulfide, sulfur oxides, sulfides are dissolved or suspended in crude oil.

Generally speaking, inorganic sulfur compounds are easy to remove by dewatered and distillation, because the inorganic sulfur components are soluble in water and their boiling points are relative low. Therefore, the removal of organic sulfur compounds is the main objective of petroleum desulfurization. The chemical analysis of crude oil from different regions indicated that four types of organic sulfur

compounds could be found in crude oil, including thiols, thioethers, disulfides and thiophenes, as shown in Fig. 1-2.

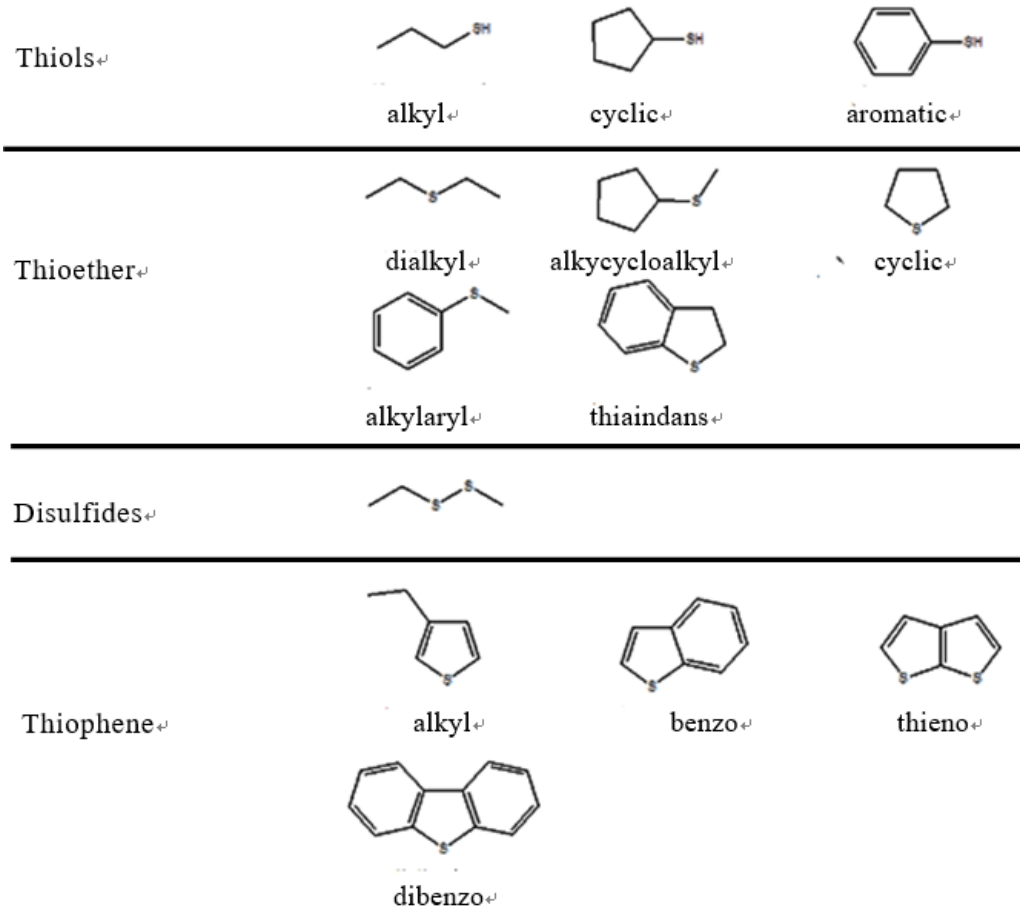

Fig. 1-2 Classification of organic sulfur-containing components in crude oil[1]

About 80%-90% sulfur containing products in crude oil are located in heavy fraction such as atmospheric gas oil (GO, all kinds of fractions can be found in Fig. 1-1) and vacuum gas oil (VGO). Table 1-3 [2] indicates the proportion of thiophene and non-thiophenes in sulfur containing products in some of heavy fractions such as GO and VGO from different regions. It could be observed that the content of thiophenes occupies more than 60% of entire sulfur resource in these heavy fractions. Moreover, the content of thiophenes would be higher in heavier fractions such as cocking gas oil (CGO). Therefore, thiophenes were the main sulfur containing products left in transportation fuels. For gasoline, thiophenes occupy more than 60% of the total sulfur number, thioethers occupy about 25%, and disulfides and thiols occupy less than 15% [6]. Importantly, it should be noticed that thiophenes in crude oil are usually in the form of thiophene derivatives such as benzothiophene (BT), dibenzothiophene (DBT) and dimethyl dibenzothiophene (DMDBT).

Table 1-3 Proportion of thiophene in sulfur containing products in some of fractions[2]

Fraction	Region	Non Thiophene (%)	Thiophenes (%)
VGO	Northern China	33.7	66.3
VGO	Estern China	30.6 (12.0[a])	69.4 (88.0[a])
VGO	Iran	30.8	69.2
GO	Middle China	26.9	73.1
GO	Western China	28.9	71.1
GO	Russia	30.3	69.7
GO	Oman	26.0	74.0
GO	Iran	29.8 (14.6[a])	70.2 (85.4[a])
GO	Saudi Arabia	27.1 (13.8[a])	72.9 (86.2[a])
VGO/GO	Iran	34.4	65.6
VGO/GO	Estern China	38.3	61.7
CGO	Middle China	19.5	80.5
CGO	Northern China	19.2	80.8

[a] after pre-treatment

1.2.2 Industrial desulfurization technologies

(1) Alkali washing and solution extraction

Alkali washing was a traditional process in petroleum refining, which is still used in many factories [7]. The principle of this method is that alkali solution can extract part of sulfur because some of sulfur containing products prefers to dissolve in solution. However, this process would produce a lot of waste water, and alkali washing cannot well treat organic sulfur compounds. Therefore, extraction process is used instead of washing process. Sulfur could be separated from extraction liquid by distillation, and extraction liquid could be recycled. Moreover, polar organic solvents such as tetraethylene glycol, furfuryl alcohol, acetone and other oxygen containing compounds were usually added into extraction solution to improve the distribution coefficient of organic sulfur in extraction liquid. High concentration thiols can be obtained by solution extraction. However, this method is not efficient for thioether and thiophenes. So, alkali washing or solution extration is usually used as the pretreatment process, which is normally labelled as sweetening process.

(2) Hydrodesulfurization

Hydrodesulfurization (HDS) is a major choice of industrial desulfurization process [2,4]. Typically, the HDS process involves catalytic treatment with hydrogen to convert the various sulfur compounds to H_2S and sulfur-free organic compounds at

high temperature and partial pressure of hydrogen. Through a gas-liquid separation, H_2S can be removed and the obtained sulfur-free hydrocarbons could be maintained in fuels. In comparison, HDS process has a lot of advantages, such as high capacity, low hydrocarbon loss and the simply separation of H_2S, which are suitable for industrial application. Thus, hydrodesulfurization technology is widely applied in oil refining industry.

(3) Other desulfurization methods

Non hydrogen based desulfurization technology were studied in recent years, such as oxidative desulfurization technology (ODS) which converts sulfur compounds into sulfones products and then removes sulfones by extraction [8], bio desulfurization (BDS) which cut C-S bonds through microorganism [9] and adsorptive desulfurization technology (ADS) which selectively adsorbs sulfur compounds by using adsorbent [10]. These methods can be operated at relatively mild condition, and are more efficient to convert refractory molecules with steric hindrance such as 4,6-dimethyl dibenzothiophene (4,6-DMDBT). However, these non-hydrogen desulfurization technologies are still in a laboratory scale due to several problems such as separation and capacity. Till now, only the adsorption desulfurization technology is used in few plants, as an additional process of HDS to remove refractory molecules left in fuels.

1.3 Hydrodesulfurization catalysts

From the viewpoints of business and technology, hydrodesulfurization technology has been proven to be a good petroleum desulfurization technology, which possessed many advantages such as the high capacity (continuous reaction and high tolerance to sulfur), high hydrocarbon yield (preservation of sulfur-free hydrocarbon in fuels), easy separation (gas-liquid separation) and long life time. Moreover, as one hydrotreating process, HDS can greatly reduce other impurities in the fuel, such as aromatic and olefins, to improve the quality of diesel fuel.

1.3.1 Conventional HDS catalyst

Catalyst displays a vital role determining the performance of HDS technology. Hydrodesulfurization catalyst is usually supported on carrier like alumina, using noble metals or transition metal sulfide (TMS) as active phases. According to the high price of noble metals, alumina supported TMS catalysts was major choice for industrial HDS process.

Figure 1-3 shows the structure of conventional $CoMo/Al_2O_3$ catalyst. This catalyst was generally prepared by depositing Co and Mo precursors (usually nickel nitrate and ammonium heptamolybdate) on alumina support by wet-impregnation.

After calcination, Co and Mo could be translated into oxidic state and be located on alumina support. After pre-sulfidation, molybdenum oxide could be transformed into hexagonal layered MoS_2 structures. The plane part of MoS_2 is inactive, and the edge of the top layer possessed hydrotreating properties, according to the Daage model. Moreover, the Co atom could act as a promoter of MoS_2 and form a more active phases CoMoS. This model is accepted for other TMS catalysts such as NiW catalyst.

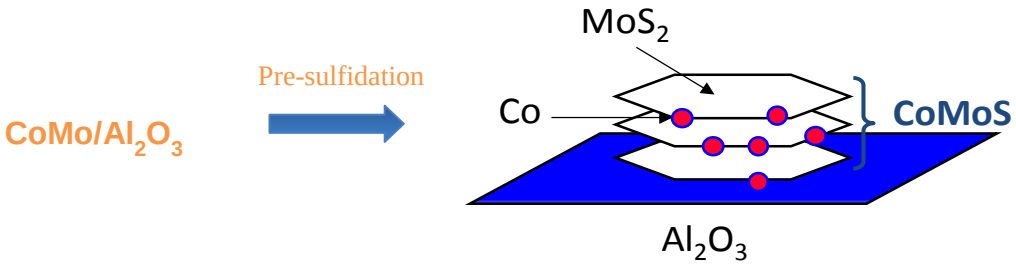

Fig. 1-3 Structure of conventional HDS catalyst

Moreover, triangular MoS_2 structure with lower activity might be formed [11] in some cases (the absence of promotor, low pre-sulfidation condition or the use of non-appropriate support). However, the shape of active phases could be only observed over gold or carbon support.

This catalyst is highly efficient for HDS reactions. The sulfur content of SRGO (Straight Run Gas Oil, containing about 12000 ppm sulfur) could be decreased to below 300 ppm through one single catalytic unit. However, the sulfur content of transportation fuels is hardly to be continuously reduced to below 10-15 ppm over conventional catalysts.

1.3.2 Main problem of conventional HDS catalyst

Although the conventional HDS catalyst has been proven to be efficient for most of sulfur containing products, the activity of this catalyst for refractory molecules such as 4,6-dimethyl dibenzothiophene (4,6-DMDBT) is relative low [12-21]. This made the sulfur content in desulfurized transportation fuels higher than that of adopted standard (below 10 or 15 ppm).

Nag et al. [14] tested the performance of $CoO\text{-}MoO_3/Al_2O_3$ in the HDS of various organic sulfur compounds. They found that the activity of catalyst was in the following order: TH (thiophene) > BT (benzothiophene) > DBT (dibenzothiophene). Moreover, the substitution of these compounds by ring alkylation further affected the activity of catalyst. Kilanowski et al. [15] used $CoMo/A1_2O_3$ catalyst in the HDS of methyl-substituted DBTs at atmospheric pressure. They found that the reactivity of DBTs with methyl substitution at different positions was in the following order: 2,8-dimethylDBT (2,8-DMDBT) > DBT (DBT) > 4-methyldibenthothiophene

(4-MDBT) > 4,6-dimethylDBT (4,6-DMDBT), as indicated in Figure 1-4 [16].

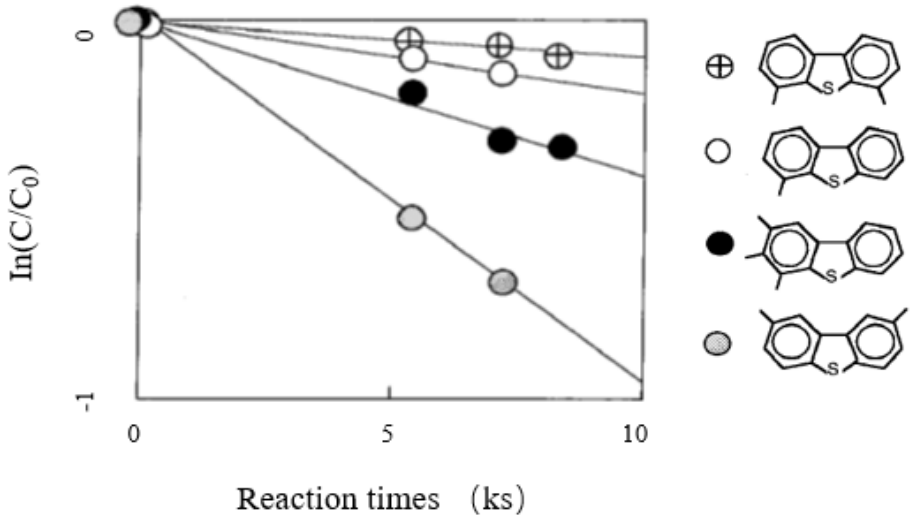

Fig. 1-4 First order plots of alkyl-DBTs over the $CoMo/Al_2O_3$ catalyst[15]

This was generally recognized as the influence of steric hindrance of molecules. For thiophene derivatives with polyaromatics rings, sulfur site is hard to associate with catalyst. Ring alkylation could further increase this steric hindrance, as indicated in Figure 1-5 [16]. It has been reported that the reactivity of 4,6-DMDBT over $CoMo/Al_2O_3$ and $NiMo/Al_2O_3$ was only 1/6 to 1/8 as that of DBT [17-21]. Therefore, the presence of 4,6-DMDBT in fuels became the biggest challenge for the more and more strict regulations.

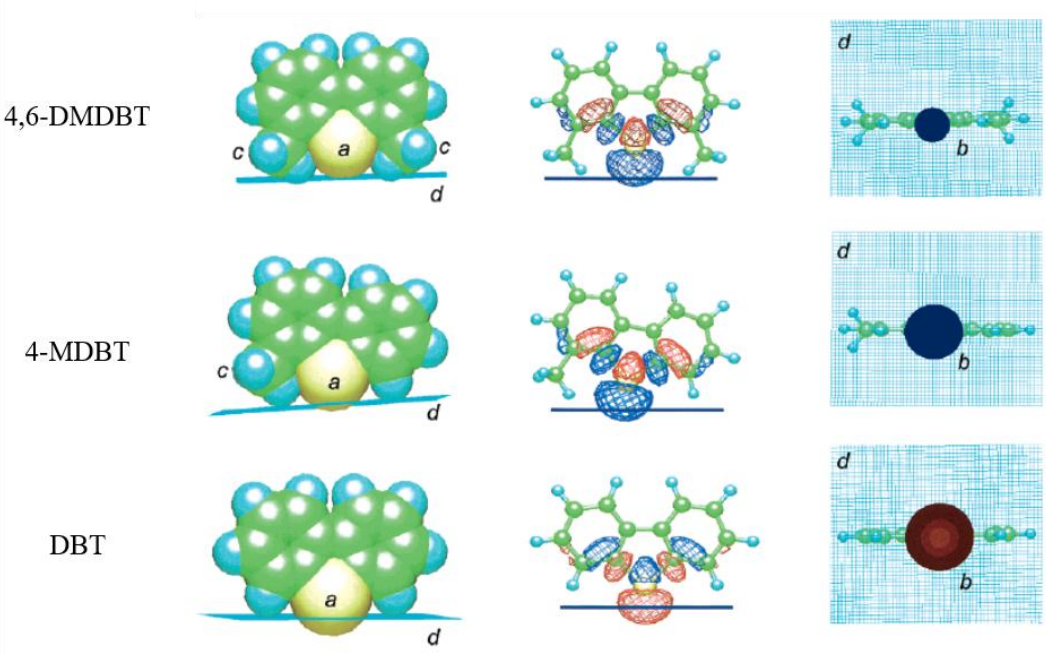

Fig. 1-5 Steric hindrance in DBT, 4-MDBT and 4,6-DMDBT[16]
a) S site, b) S site, c) metyl group, d) catalyst plane

1.3.3 Deep HDS catalyst

An additional hydrodesulfurization process for refractory molecules such as 4,6-DMDBT could effectively decrease the sulfur content in transportation fuels. This additional hydrodesulfurization process for 4,6-DMDBT is generally called deep hydrodesulfurization or second layer hydrodesulfurization [22].

Nowadays, second layer hydrodesulfurization has been widely adopted by refinery industry (See Fig. 1-1) because it could be easily realized. However, industrial deep hydrodesulfurization is usually carried out by increasing the H_2 pressure or reaction temperature, which is much expensive. Thus, novel HDS catalysts able to convert refractory molecules such as 4,6-DMDBT have attracted much attention. It was found that a higher hydrogenation ability or a higher acidity was beneficial to improve the performance of catalyst in the HDS of 4,6-DMDBT, because 4,6-DMDBT could be converted and the steric hindrance effect of methyls at 4 and 6 position could be removed.

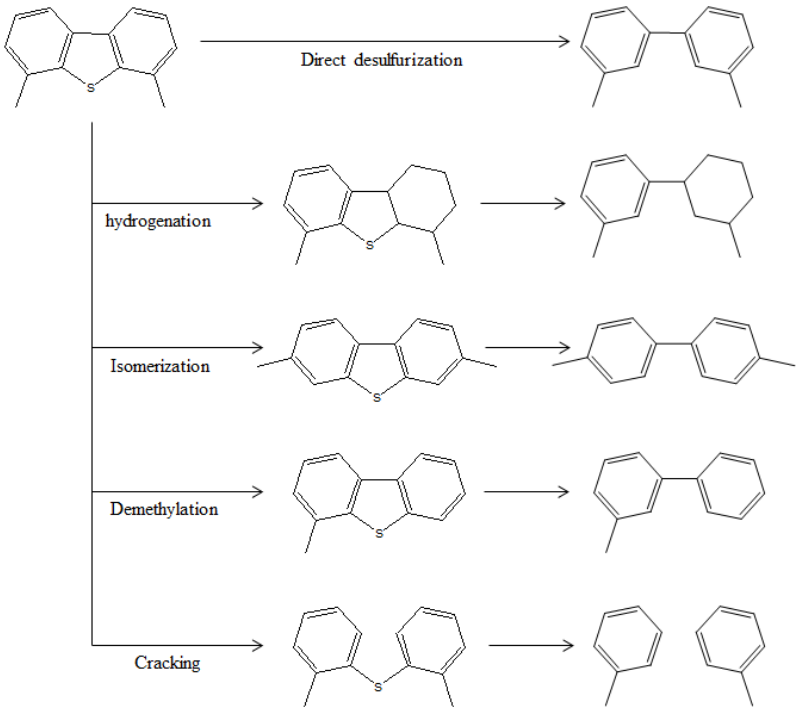

Fig. 1-6 Possible reaction pathways for enhancing the reactivity of 4,6-DMDBT[23]

Lecrenay et al. [23] found that the commercial $NiMo/Al_2O_3$ exhibited three times higher activity than that of the commercial $CoMo/Al_2O_3$ on the HDS reaction pathways of 4,6-DMDBT. This was ascribed to the higher hydrogenation activity of $NiMo/A1_2O_3$ catalyst as compared to $CoMo/A1_2O_3$. Hydrogenation of the aromatic ring leads to easing of steric hindrance, as indicated in Figure 1-6. Thus, catalysts with higher hydrogenation capability show higher catalytic activity towards the HDS

of 4,6-DMDBT. Isoda et al [24] also found that the performance of catalyst in the HDS of 4,6-DMDBT depended on its hydrogenation property. Such an enhancement could be also observed when increasing acidity of catalyst [25]. Moreover, to increase the acidity of HDS catalyst could improve the electron property of active phase, to enhance the adsorption property to sulfur-containing molecules [26] and decrease the deactivation of catalyst [27].

The change of catalyst support was thought to be one efficient method, because the content of support in catalyst is relative high, which made the improvement more significant. Moreover, the support plays an important role, determining its catalytic performance. Firstly, the support provides high surface area to maximize active phase dispersion. Secondly, the support could influence the performance of active phase by the synergetic effect. In the past few decades, there has been intense activity to evaluate the impact of supports such as metal oxides, amorphous-silica-alumina (ASA), active carbon, mesoporous aluminosilicate and zeolite-based materials. Among of them, zeolites with high acidity, high thermo/chemical stability and large surface area have attracted much attention.

1.4 Zeolite supported HDS catalysts

1.4.1 Zeolites

Zeolite is a crystalline aluminosilicate, consisting of a crystalline network of SiO_4 and AlO_4 tetrahedra, connected through oxygen bridges [28]. So far, about 200 different zeolite structures were classified. Zeolites have high specific surface area of regular array microporous structure. Thus, zeolites are also labelled as “molecular sieve” and widely used in adsorption and separation. However, catalysis is the most important application of zeolites. It occupies more than 40% of the entire solid catalysts in the current chemical industry [29,30]. The catalytic ability of zeolites is due to its special structure. In zeolites, trivalent Al atoms are tetrahedrally coordinated by oxygen in the crystalline silicate framework. This causes a charge mismatch between Al and the oxide framework, which is compensated by extra-framework Na^+ ions. These Na^+ ions can be exchanged by other cations like H^+. H^+-ion exchanged form zeolite can exhibit Lewis acidity and also Brönsted acidity, which is comparable to sulfuric acid [31].

1.4.2 Performance of various active phases over zeolite supports

Recent researches reported that noble metals and TMS active phases could exhibit good activity over zeolite supports. Navarro et al. [32] evaluated the catalytic performance of different noble and semi-noble metals supported on HUSY. The

results suggested that the order of catalytic activity is: Ir > Pt > Pd > Ru≈Ni.

The comparison between zeolite supported NiMo and CoMo catalysts seemed to depend on the reaction temperature (Table 1-4). Azizi et al. [33] found that alumina-coating zeolite supported CoMo catalyst was more active at high temperature (360 °C) but less active at 340 °C than supported NiMo catalyst in the HDS of LCO. Another group also observed that Beta supported CoMo catalyst gave higher activity than supported NiMo catalyst at a reaction temperature of 400 °C in the HDS of thiophene [34].

The comparison between active phase W and Mo is difficult because the optimal content of two metals in support could be different. For instance, the optimal loading content is 6% wt for Mo and 17% wt for W over pure Beta zeolite, respectively [34,35]. Although Mo catalyst may show higher activity than W catalyst at low loading content, Beta supported 17% wt W catalyst could give much higher activity than that supported 6% wt Mo catalyst under the same reaction condition in the HDS of thiophene.

The comparison of active phase NiMo and NiW took place over the desulfurization of vacuum gasoil (2890 ppmw) with the loading content of 4% wt NiO and 15% wt MoO_3/WO_3 (10% Mo and 11.9% W, respectively) [36]. The results suggested that NiW supported on alumina-ASA-USY/Beta generally had relatively high catalytic activity in the range of reaction temperature from 380 to 410 °C. Moreover, NiW catalyst was very sensitive to the particle size of zeolite support, whereas NiMo catalyst was not. Thus, the performance of NiW catalyst could be improved by optimizing zeolite support [37].

Table 1-4 Activity comparison of different catalysts with same active support and different active phase

Support	Temperature（°C）	Active phase	Ref
HUSY	320	Ir>Pt>Pd>Ru>>Ni	[32]
Al_2O_3 coated Z	340	NiMo>NiW	[33]
Al_2O_3 coated Z	360	CoMo>NiMo	[33]
Beta	400	CoMo>NiMo	[35]
Beta	400	W>Mo	[35,38]
Al_2O_3-nano Beta	375	NiW≈NiMo	[37]
Al_2O_3-ASA-Beta	375	NiW>NiMo	[37]
ASA-Beta	380	NiW>NiMo	[36]
ASA-USY	410	NiW>NiMo	[36]

Z: Zeolites

1.4.3 Performance of various zeolites

Tatsumi et al. [39] compared the catalytic performance of different zeolite supported catalysts. The $[Mo_3S_4(H_2O)_9]^{4+}$ species was located on various supports (NaY, HUSY, NaHBeta, KL and NaMOR) by ion-exchanged method. The loading of Mo on HUSY, NaHBeta, KL and NaMOR was between 2.0 and 2.5% wt. They found that KL and NaMOR exhibited relatively high activity for HDS of benzothiophene, while HUSY displayed similar activity to NaHBeta (Table 1-5).

Table 1-5 Activity comparison of catalysts with same active phase and different support

Catalyst	Temperature (°C)	Zeolite type	Ref
Mo/Z	300	KL>NaMOR>NaY>HUSY≈NaHBeta	[39]
NiMo/Z	<390	Y>Beta	[41]
NiMo/Z	390-430	Beta>Y	[41]
NiMo/Z	>430	Beta≈Y	[41]
Mo/Z	400	USY>NaY>HBeta	[45]
NiMo/Z	400	USY>NaY>HBeta	[45]
CoMo/Z	400	USY>NaY>HBeta	[45]
NiW/Al_2O_3-Z	375	Beta>Y	[40]
NiMo/Al_2O_3-Z	350	Beta≈Y	[42]
NiMo/Al_2O_3-ASA-Z	380-410	Beta>Y	[36]
NiW/Al_2O_3-ASA-Z	380-410	Beta>Y	[36]

Z: Zeolites

Most of studies have been focused on zeolite Beta and Y mainly because of their larger pore size. Compared with zeolite Y supported catalyst, Beta supported catalyst exhibited higher hydroisomerization activity, lower hydrogen-transfer capacity, and lower catalyst deactivation by self-poisoning [36,40]. However, it was observed that the catalytic activity greatly depended on the reaction temperature. Camblor et al. [41] showed that zeolite Y supported catalyst possessed higher activity than Beta supported catalyst below 390 °C in the HDS reaction of vacuum gasoil. Above a reaction temperature of 430 °C, the catalytic activity of both catalysts is almost the same. The comparisons between different supports are summarized in Table 1-6. It could be observed that Beta zeolite is suitable for HDS catalyst.

Moreover, the performance of zeolite support was influenced by reactants, crystal size and Si/Al ratio. It has been proposed that the HDS conversion of transportation fuel depends on the Si/Al ratio of zeolite and high Si/Al is favorable [42], which could be partly attributed to many mesopores created by dealumination. Ismgilov et al. [43] prepared ZSM-5-containing monolith support. They found that the HDS activity has a

good relationship with Si/Al molar ratio (from 45 to 17) of ZSM-5 (Table 1-6). Lara et al. [44] evaluated the catalytic performance of CoMoP supported commercial USY (with different Si/Al molar ratio) catalyst. It was found that the catalyst with higher Si/Al molar ratio had higher HDS activity. Similar phenomenon was also observed by Marin [45].

Table 1-6 Effect of Si/Al molar ratio on the performance of catalyst

Catalyst	Performance of different Si/Al	Ref
CoMoP/USY	160>60>24	[42]
CoMoP/Al_2O_3-USY	160>120≈60≈80[a]	[45]
CoMoP/Al_2O_3-USY	160>60>120≈80[b]	[45]
CoMoP/Al_2O_3-USY	160>60>120≈80[c]	[45]
Pt/ZSM-5	17>45>30	[43]
NiW/USY	11.6>10	[44]

[a] measured at 370°C [b] measured at 360°C [c] measured at 350°C。

The effect of Si/Al molar ratio was observed by several authors. Kadono et al. [46] showed that smaller sulfide particles can be formed when the Si/Al molar ratio is higher. They deposited Mo metal on NaY, USY (Si/Al molar ratio of 2.4∼3.5) and USY (630) by vapor exposition. They found that Mo atoms were transformed into dimer clusters of molybdenum sulfide at lower Si/Al molar ratio (<3.5) and the distance of Mo-Mo was varied with the Si/Al molar ratio (0.31 nm for Si/Al = 2 and 0.28 nm for 2 < Si/Al < 4). Moreover, the coordination number of Mo-Mo shell also had a correlation with the Si/Al molar ratio. High Si/Al molar ratio in zeolite is also beneficial to the formation of the metal-Si intermetallic phase [47], which can improve HDS activity due to the introduction of electron-deficient metal. For example, catalysts containing zeolite with high Si/Al molar ratio gave high HDS activity and good sulfur tolerance for the zeolite supported NiMo(W) catalyst.

1.4.4 Main problem of zeolite supported catalyst

Despite much of the outstanding features of the microporous structure, the sole presence of micropores often imposes significant limitations. Reactants and products with sizes beyond the micropore dimensions cannot diffuse into and out of zeolite crystals. Even in the case of smaller molecules, the catalytic performance can be seriously limited by the diffusion of reactants or products. Bulk zeolite crystals are often several thousand times larger than the pore diameter. In such a diffusion-controlled regime, less than 10% of zeolite active sites at the edge of the bulky crystal might actually participate in the catalytic reaction simply due to the limited mass transport to and from the active sites. In addition, slow diffusion can

cause polymerization of by-products or reaction intermediates covering catalytic active sites within the microporous channels. This can cause serious loss of catalytic activity, that is, catalytic deactivation [30]. When using zeolite as the support of HDS catalyst, the dispersion of active phases would be also negatively influenced. The size of 4,6-DMDBT is generally more than 3 nm, which is much larger than the size of micropores. Thus, active phases and acid sites located in micropores are inaccessible for 4,6-DMDBT [48].

1.5 Hierarchical zeolite supported HDS catalysts

1.5.1 Hierarchical zeolites

Four strategies were proposed in recent years in order to overcome these adverse effects, as indicated in Figure 1-7 [49].

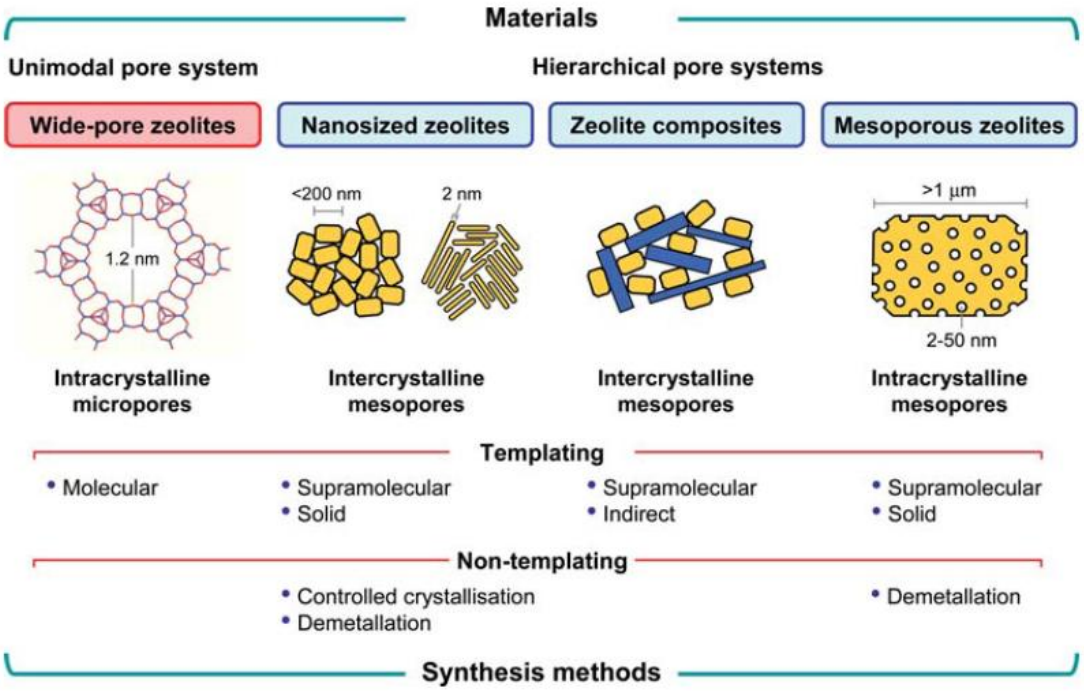

Fig. 1-7 Categorization of zeolite materials with enhanced transport characteristics [49]

Synthesis of zeolites with extra-large pores is one of these approaches. Another approach is to synthesize zeolites in the form of small nanoparticles possessing inter crystalline mesopores. A third class of approach is to obtain zeolite samples with intracrystalline mesopores (defined as pores with diameters ranging from 2 to 50 nm). Moreover, mix zeolite with mesoporous/macroporous materials can also introduce some mesopores in final product. Recently, several zeolites with large pore sizes such as VPI-5 have been found [50]. However, the pore size of these zeolites is still in the range of micropores, and the acidity and stability of these zeolites are much lower

than that of the conventional zeolite materials. As a result, these zeolites usually exhibit unexpected catalytic performance. Moreover, mixing method would decrease the acidity of final catalyst and nano sized zeolites prepared by varying the synthesis conditions, such as temperature, to stop crystallization before growth to bulk crystals, would negatively influence the crystallinity and stability of zeolite. Therefore, hierarchical zeolite was thought as the main solution to overcome the develop the performance of zeolite [28-30].

Two methods have been proposed to prepare hierarchical zeolites: templating method and post-treatment method. The direct generation of intracrystalline mesopores can be achieved by the addition of a hard template of a mesopore diameter, such as carbon nanoparticles and nanotubes, or soft-templates such as surfactant micelles and silylated polymers. After calcination, template could be removed and ordered hierarchical zeolite could be obtained [28-30,51,52]. Moreover, mesopores could be also introduced by desilication or dealumination, which was usually labelled as post-treatment. In comparison, this method is suitable for a large-scale production due to its relative low cost. Thus, post-treatment was widely studied in recent few decades [28-30].

Nowadays, dealuminated zeolite such as ultra-stable Y (USY) has been used in industry. However, hierarchical zeolite prepared by dealumination would reduce the content of aluminum, and subsequently decrease the acidity of zeolite. To overcome this limitation, desilication has become one of the most versatile procedures to generate mesoporosity in zeolites. Firstly, desilication have few influence on the aluminum. Secondly, more mesopores could be introduced in zeolite by desilication due to the much higher content of silicium than aluminum in zeolite. A series of studies on desilicated hierarchical zeolite has been drawn in the laboratory, pilot and industrial unit [53-68]. Desilication now is considered to be a most promising way for large-scale production [28-30].

The alkaline desilication treatment was firstly reported by Ogura et al. [53] and the mechanism of mesopore formation upon desilication was studied [54]. The performance of desilicated hierarchical zeolite could be greatly influenced by the alkali concentration, treatment time, temperature and the property of zeolite itself such as zeolite type and Si/Al ratio. From the viewpoint of catalytic performance, Perez-Ramirez et al. have deeply studied the desilicated hierarchical zeolites, and proposed relative optimal post-treatment conditions: 30 min 0.2M NaOH at 60-70°C, Si/Al≈25-50 [49]. These preparation conditions could be used with Mordenite zeolite, Y zeolite and ZSM-5 zeolite. Moreover, it was indicated that other additional operations such as the adding of pore directing agents (PDAs) and partial desilication might further improve the performance of desilicated hierarchical zeolite.

1.5.2 Performance and problem of hierarchical zeolites supported catalysts

Prins et al. [69] firstly investigated the catalytic performance of noble metal supported on hierarchical ZSM-5 in the HDS of DMDBT. The results indicated that sulfur removal by these catalysts was much more efficient than those on microporous zeolites and Al_2O_3. The sulfur removal by Pd/MNZ-5 was 29 times higher than for Pd/NZ-5 and 4 times higher than for Pd/Al_2O_3. Further, Tang et al. [70] studied the catalytic performance of Pd supported on mesoporous Beta and mesoporous Y. The results displayed that Pd supported on mesoporous Y exhibited much higher HDS activity than that on microporous Y, mesoporous beta and ZSM-5. Recently, Tojholt et al. [71] reported the catalytic performance of hierarchical ZSM-5 supported CoMo catalyst in the HDS reaction. They used a new approach to prepare tight bi-functional HDS catalyst for controlling the location of active phase. The desilicated zeolite would present more Si-OH at the position of the created mesopores, which can give different surface properties. So the location of CoMo phase could be optimized by using (3-amoinopropyl) trimethoxysilane (APTMS) as a linker molecule. By this approach, a highly efficient HDS catalyst $CoMo_6$-ZSM-5 (anchored) was obtained. These results indicated that hierarchical zeolites supported catalysts could exhibit good activity in the HDS reactions.

However, these researches were mainly based on hierarchical zeolite prepared by templating method, which was expensive and not suitable for industrial applications. In comparison, hierarchical zeolite prepared by post-treatment was suitable for large-scale application. However, this method was still studied in laboratories, and not favorable for many zeolite frameworks, such as zeolite Beta. Moreover, the studies about mechanism of post-treatment and its influence on the local structure of zeolite was still rare, which was not beneficial for the further development of post-treatment method.

Additionally，the performance of HDS catalysts could be influenced by the presence of nitrogen containing products. This product could adsorb on the active sites of the catalyst, inhibiting the adsorption of sulfur compounds over active sites of catalyst and greatly decreasing the desulfurization activity of catalysts [4]. Similarly, olefin, aromatics and polar components such as oxygen containing molecules can also hinder the efficiency of HDS catalyst. To overcome this limitation, the hydrogenation ability of catalyst need to be enhanced, because these products could be converted by hydrogenation, and then quickly desorbed. NiW active phases possessed the highest hydrogenation property than other TMS active phases. However, the research of hierarchical zeolite supported NiW HDS catalysts was not reported.

Moreover, HDS catalysts regularly undergo some degree of deactivation in

commercial operation, depending on the feed source [4]. The heavier the feedstock, the faster the catalyst deactivates. The deactivation of Mo/Al_2O_3 and $NiMo/Al_2O_3$ catalysts has been widely reported [26], which was generally caused by coke deposition. This deactivated catalyst could be regenerated by calcination. However, this is not beneficial for industrial application. The deactivation of zeolite supported catalysts should be heavier due to the higher acidity of zeolite. However, the deactivation of hierarchical zeolite supported catalysts was not discussed in literatures.

1.6 Main research contents of this subject

The hydrodesulfurization of petroleum is an important process in petroleum refining, which could effectively decrease the pollution of transportation oil. In order to overcome the limitations of conventional HDS catalysts, we prepared NiW catalysts based on hierarchical zeolite Beta and Mordenite supports. NiW active phase with high hydrotreating ability could decrease the interference of nitrogen containing molecules, and zeolite support with high acidity could help the conversion of refractory molecules such as 4,6-DMDBT.

In the present work, the preparation of hierarchical zeolite by post-treatment was investigated. The hierarchical zeolites and their corresponding NiW catalysts were deeply characterized. The performance of hierarchical zeolite supported catalysts were evaluated in HDS of simulated SRGO (straight run gas oil) containing 500 ppm DBT or 4,6-DMDBT. Moreover, the anti-deactivation of hierarchical zeolite supported catalysts was studied in thiophene HDS reaction.

Chapter 2. Experimental section

2.1 Reagents and equipment

2.1.1 Reagents and materials

The used reagents and materials are listed in Table 2-1.

Table 2-1 List of reagents

Reagents	Place and purity	Formula
zeolites	Catalyst plant of Nankai Uni.	-
nickel nitrate	Sigma-Aldrich, AR	$Ni(NO_3)_2\ 6H_2O$
ammonium metatungstate	Sigma-Aldrich, AR	$(NH_4)_6H_2W_{12}O_{40}$
nitric acid	Sinopharm Chemical, AR	HNO_3
sodium hydroxide	Sinopharm Chemical, AR	NaOH
ammonium nitrate	Sinopharm Chemical, AR	NH_4NO_3
benzene	Sinopharm Chemical, AR	C_6H_6
mesitylene	Sinopharm Chemical, AR	C_9H_{12}
benzyl alcohol	Sinopharm Chemical, AR	C_7H_8O
pyridine	Sigma-Aldrich, AR	C_5H_5N
pivalonitrile	Sigma-Aldrich, AR	C_5H_9N
n-heptane	Carlo-Erba, AR	C_7H_{16}
n-decane	Sigma-Aldrich, AR	$C_{10}H_{22}$
dimethyl disulfide (DMDS)	Fluka, AR	$C_2H_6S_2$
hydrogen sulfide	PRAXAIR	H_2S
dibenzo thiophene（DBT）	Eburon, AR	$C_{12}H_8S$
4,6-dimethyl dibenzo thiophene（4,6-DMDBT）	Eburon, AR	$C_{14}H_{12}S$
thiophene	Sigma-Aldrich, AR	C_4H_4S
deionic water	HIT/UCCS	H_2O
hydrogen	PRAXAIR, 99.9999%	H_2
azote	PRAXAIR, 99.9999%	N_2

2.1.2 Experimental facilities

The used equipment is listed in Table 2-2.

Table 2-2 List of experimental facilities

Products	Type	Mark
Filter Paper	Quantitative filter	Wohua Filter
circulating water vacuum pump	SHZ-III	Zhixin equip.
drying oven	DZF-6020	Qixin equip
muffle furnace	L3-L40	Nabertherm
tubular furnace	-	Eurotherm
heating magnetic stirrer	ETS-D5	IKA
analytical balance	JJ124BC	G&G
X-ray diffraction	D-5000	Siemens
specific surface and pore size analyzer	TriStar II 3020	Micromeritics
inductively coupled plasma optical emission spectrometer	PE5300	Agilent
scanning electron microscope	S-4700	Hitachi
transmission electron microscope	Tecnai	FEI
magic angle solid-nuclear magnetic resonance	Avance II 400	Bruker
multi quantum MAS NMR	Avance III 800	Bruker
vacuum infrared device	460	Nicolet Protege
ammonia temperature programmed desorption	AutoChem II 2920	Micromeritics
X-ray photoelectron spectroscopy	Axis Ultra DLD	Kratos
gas chromatography mass spectrometry	7890A-5975C	Agilent
gas chromatography	6890	Agilent
generic desulfurization equipment	-	-
gas chromatography	430	Varian

2.2 Preparation method

2.2.1 Hierarchical zeolite Beta

(1) Hierarchical zeolite Beta

Typically, the commercial Beta zeolite calcined at 823 K for 5 h was labeled as

HB. The sample HB was treated with a solution of 0.2 M NaOH with a liquid-to-solid ratio of 30 ml·g^{-1} at 338 K for 0.5 h. Then, the product was filtered, washed with deionized water, dried, ion-exchanged into NH_4-form, and calcined at 823 K for 5 h. The resultant sample was named as HB-B. It was then treated with a solution of 0.1 M HNO_3 at 338 K for 6 h with a liquid-to-solid ratio of 30 ml·g^{-1}. The product was ion-exchanged as described above, followed by calcination at 823 K for 3 h to obtain the sample labeled as HB-M, as illustrated in Fig 2-1.

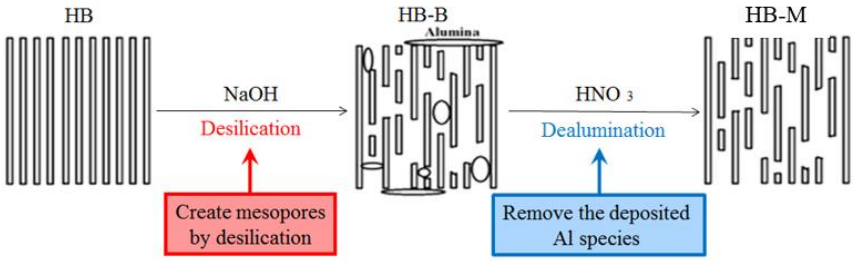

Fig. 2-1 Hierarchical zeolite Beta prepared by base-acid treatment

(2) Na^+-exchanged hierarchical Beta

HB or HB-M was treated with 1 M $NaNO_3$ with a liquid-to-solid ratio of 100 ml·g^{-1} at room temperature for 2 h. This ion-exchanged process was repeated twice. Then, the product was dried overnight, calcined at 823 K for 5 h and labelled as NaB or NaB-M.

2.2.2 Hierarchical zeolite Mordenite

As another important industrial zeolite [72], Mordenite zeolite with relative low cost was also hierarchized by the same base-acid post-treatment in our parallel research [73].

The commercial Mordenite (Si/Al=15) was ion-exchanged with a solution of 1 M NH_4NO_3 at 353 K for 1 h, under stirring with a speed of 1000 rpm, followed by calcination at 823 K for 3 h. The obtained sample was labeled HM.

It should be noticed the optimal Si/Al of Mordenite zeolite for desilication is about 30. Thus, an additional acid treatment was supplied to change the Si/Al of HM before desilication. The HM sample was refluxed with a solution of 2 M HNO_3 at 373 K for 2 h with a liquid-to-solid ratio of 20 ml·g^{-1}, under stirring with a speed of 1000 rpm. Then, the solid sample was filtered, washed with deionized water, dried at 393 K for 12 h, and ion-exchanged thrice with a solution of 1 M NH_4NO_3 at 353 K for 1 h, followed by calcination at 823 K for 3 h. The final product was labeled HM-A.

The HM-A sample was treated with a solution of 0.2 M NaOH with a liquid-to-solid ratio of 20 ml·g^{-1} at 343 K for 0.5 h under stirring with a speed of 1000 rpm. The product was filtered, washed with deionized water, dried, ion-exchanged,

and then calcined at 823 K for 3 h. The obtained sample was called HM-AB.

The HM-AB sample was treated with a solution of 0.2 M HNO_3 at 323 K for 1.5 h with a liquid-to-solid ratio of 20 ml·g^{-1}, under stirring with a speed of 1000 rpm. The product was ion-exchanged as described above, followed by calcination at 823 K for 3 h to obtain the sample labeled HM-M, as illustrated in Fig. 2-2.

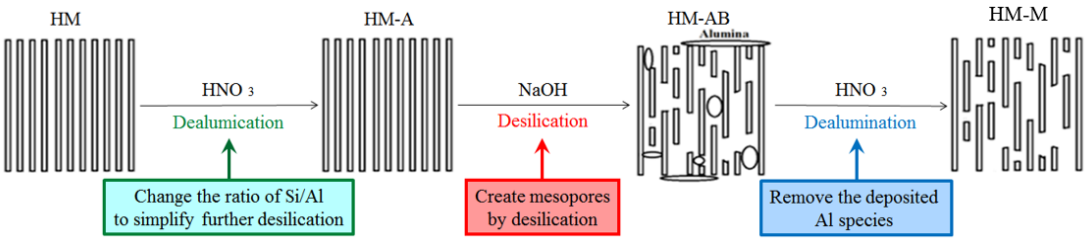

Fig. 2-2 Hierarchical zeolite Mordenite prepared by base-acid treatment

Moreover, the Na^+-exchanged Mordenite could be obtained by ion-exchange with $NaNO_3$, as indicated before, which were labelled as NaM and NaM-M, respectively.

2.2.3 Zeolite supported NiW catalysts

(1) Commercial and hierarchical zeolite supported catalysts

The NiW supported catalysts were prepared by co-impregnation using the incipient wetness technique. Typically, the impregnation solution was obtained by dissolution of nickel nitrate hexahydrate and ammonium metatungstate $[(NH_4)_6H_2W_{12}O_{40}]$ in water with a Ni/W molar ratio of 0.36, which has been described as an appropriate molar ratio [74,75]. The calculated content of WO_3 was set at 15 % in the calcined catalyst. The pore volume of various supports obtained by water adsorption was listed in Table 2-3.

Table 2-3 Pore volume obtained by water adsorption of various supports

Samples	Pore volume (ml·g^{-1})
Al_2O_3	0.60
HM	1.03
HM-M	0.64
HB	1.00
HB-M	1.84

After impregnation and maturation, the solids were dried at 373 K overnight and calcined at 773 K for 4 h in air, using a temperature rate of about 2 K·min^{-1}. The commercial and hierarchical Mordenite supported NiW catalysts were labelled as NiW/HM and NiW/HM-M, respectively. The commercial and hierarchical Beta supported NiW catalysts were labelled as NiW/HB and NiW/HB-M, respectively. For comparison, commercial alumina (BET surface area: 220 m^2 g^{-1}, pore volume

obtained by water adsorption: 0.6 $cm^3 \cdot g^{-1}$) supported NiW catalyst was prepared by the same method and named as NiW/Al_2O_3.

(2) Mixed catalysts

The mixed catalysts were prepared by mechanically mixing zeolite supported catalyst (NiW/HB, NiW/HM, NiW/HB-M or NiW/HM-M) with NiW/Al_2O_3. In our research, these catalysts were labelled in the form as "NiW/xHB", where x was the content of zeolite supported catalyst in mixed catalyst (x = 20, 50 or 80).

(3) Na^+-exchanged catalysts

NaB, NaB-M, NaM and NaM-M supported NiW catalysts were prepared by the incipient wetness method, as mentioned above. The obtained catalysts were labelled as NiW/NaB, NiW/NaB-M, NiW/NaM and NiW/NaM-M, respectively.

2.3 Characterization technologies

2.3.1 X-ray diffraction

X-ray diffraction (XRD) was used to understand the structural modification of the zeolite supports after acid/base treatments. Moreover, the change of structural stability could be evaluated by calculating the crystallinity from XRD patterns. X-ray powder diffraction (XRD) patterns were recorded using a Siemens D-5000 diffractometer equipped with the Cu Kα radiation (wavelength of λ = 1.5418 Å) and using the two cycle diffractometer equipped by six detectors having Si(111) analyzer crystals and Na-I scintillation counters. The determination of the relative crystallinity value was based on the intensity of the characteristic peaks (22.1° for Mordenite and 6-9° for Beta). The parent zeolite was assigned a crystallinity of 100%.

2.3.2 N_2-sorption isotherm

N_2-sorption isotherms were used to measure the textural parameters of the prepared solids: surface areas, pore volume and pore size distributions, where t-plot method was used to evaluate the microporesity and BJH method was used to evaluat the mesoporosity. It was obtained at 77 K on a Micromeritics TriStar II 3020 Gas Sorption and Porosimetry system. Prior to the experiments, the samples were outgassed at 423 K under vacuum for 3 hours.

2.3.3 Scanning electron microscope

Scanning electron microscope (SEM) images were used to observed the morphology of treated zeolite, which was recorded on Hitachi S-4700 Scanning Electron Microscope system operated with an acceleration voltage of 10 kV.

2.3.4 Nuclear magnetic resonance

^{29}Si NMR experiments were performed at room temperature on a 400MHz Bruker Advance Avance II 400 spectrometer at a spinning rate of 12 kHz using a 4 mm probe and the ^{29}Si MAS NMR chemical shift was referenced to at 0 ppm relatively to tetramethylsilane (TMS). The ^{27}Al MAS NMR spectrawere recorded on a 800 MHz Bruker Avance III 800 spectrometer by using single pulse length of $\pi/6$ and a relaxation delay of 1s. The ^{27}Al chemical shift was referenced to $[Al(H_2O)_6]^{3+}$ (Chemical shift=0 ppm). The ^{27}Al MQMAS spectra were collected using the Z-filter sequence[39], which consists of two hard pulses of 6 and 1.4 μs at an RF field of 90 kHz, for triple-quantum excitation and reconversion, respectively, followed by a central transition selective pulse of 7 μs at an RF field of 12 kHz [76]. The decomposition of NMR spectra was realized by using Topspin and DMfit.

2.3.5 Ammonia temperature programmed desorption

Temperature-programmed desorption of NH_3 (NH_3-TPD) was carried out on a Micromeritics AutoChem II 2920 system equipped with a thermal conductivity detector. The samples were first outgassed under 823 K for 1 h before the measurement. After cooling to 373 K, the samples were saturated in an NH_3 stream (5% in Ar) for 1 h and consequently treated in Ar (30 ml·min^{-1}) for 2 h for removing physisorbed NH_3. Finally, the TPD profile was determined by increasing temperature from 373 K to 873 K with a heating rate of 5 K·min^{-1} while recording NH_3 desorption with a thermal conductivity detector.

2.3.6 Infrared studies of pyridine and pivalonitrile adsorption

The IR studies of pyridine and pivalonitrile adsorption were carried out to measure the number of acid sites and accessible acid sites, respectively, recorded with a Nicolet Protege System 460 equipped with a DTGS detector. All samples were ground in an agate mortar and were pressed into the form of self-supporting wafers (5 mg·cm^{-2}), then heated at 723 K under high vacuum (10-6 mbar) for 2 h and cooled down before probe molecule adsorption. All recorded spectra were recalculated to a normalized wafer of 10 mg. The concentration of Brönsted and Lewis acid sites was determined by quantitative IR studies of probe molecule adsorption experiments. In order to quantify Lewis and Brönsted acid sites, FTIR spectrum of the activated surface was subtracted from the pivalonitrile and pyridine adsorbed one. For experiments based on pyridine adsorption, the following bands and absorption coefficients were used: Pyridinium (PyH^+) band at 1545 cm^{-1}, εB = 1.23 cm·μmol^{-1} and pyridine (PyL) 1454 cm^{-1}, εL = 1.73 cm·μmol^{-1} [77]. The concentration of

accessible Brönsted and Lewis acid sites was determined by quantitative IR studies of pivalonitrile adsorption experiments using the following bands and absorption coefficients were used: pivalonitrile (PiH^+) band at 2274 cm^{-1}, $\varepsilon B = 0.11$ $f \cdot cm \cdot \mu mol^{-1}$ and pivalonitrile (PiL) 2302 cm^{-1}, $\varepsilon L = 0.15$ $f \cdot cm \cdot \mu mol^{-1}$, where f was a constant depending on the IR system [78]. For bands with several contributions spectra were decomposed using Omnic software 8.3.

2.3.7 Inductively coupled plasma optical emission spectrometer

Inductively Coupled Plasma-Optical Emission Spectroscopy (ICP-OES) results were determined after acidic digestion of zeolites based catalysts in a mixture of fluorhydric acid (3mL) and nitric acid (5 mL) under closed vessels microwave (600 watts) for a duration of 40 minutes. Acidic mineralizations were then analyzed using ICP-OES for nickel, aluminum and tungsten. Silicon was analyzed by Flame Atomic Absorption Spectroscopy (FAAS) in order to avoid spectral interference that could exist in ICP-OES.

2.3.8 Transmission electron microscope

Transmission electron microscopy (TEM) analysis was performed on a TECNAI microscope operating at 200 kV with a LaB_6 crystal. Freshly sulfided samples were ground under an inert atmosphere and dispersed in ethanol. The suspension was collected on carbon films supported on copper grids. Statistical analysis was performed on 600 WS_2 slabs to obtain a reliable determination of the distribution of size and stacking number of the slabs for each sample.

2.3.9 X-ray photoelectron spectroscopy

X-ray photoelectron spectroscopy (XPS) were performed on an Axis ultra DLD (Kratos analytical) using a monochromatic Al Kα X-ray source (hν = 1486.6 eV). The emission voltage and the current of this source were set to 15 kV and 10 mA, respectively. The pressure in the analyzing chamber was maintained at 10^{-9} Pa or lower during analysis, and the size of the analyzed area was 300 × 700 μm^2. After their sulfidation under H_2/H_2S (90/10) for 2 h at 673 K, samples were transferred into the spectrometer chamber using a gloves box in order to avoid any reoxydation. Surveys (0~1300 eV) were recorded at pass energies of 160 eV with a step of 1 eV and high-resolution (W4f, Ni2p, S2p and C1s zone) spectra were recorded at pass energies of 40 eV with a step of 0.1 eV. Data treatment and peak-fitting procedures were performed using Casa XPS software. Obtained spectra were calibrated in respect of C1s (C-C bond) at 285 eV. The peaks were decomposed using Gaussian-Lorentzian peak shapes by CasaXPS.

2.4 Catalytic evaluations

2.4.1 Friedel-Crafts alkylation

The support would determine the activity of HDS catalysts by influencing the acidity and mass transfer ability of catalyst. However, the mass transfer ability was hard to be characterized. To simplify this research, acid-catalyzed reactions were used to evaluate the global performance of hierarchical zeolite supports. Considering the importance of Brönsted acid sites for the conversion of 4,6-DMDBT, Friedel-Crafts alkylation was used as a probe in our research.

(1) Benzylation of benzene with benzyl alcohol

The liquid phase benzylation of benzene with benzyl alcohol (BA) (Fig. 2-3) was carried out in a three-necked round-bottom flask equipped with a reflux condenser and heated in a temperature-controlled oil bath under atmospheric pressure. The reaction temperature for the benzylation of benzene was at 353 K. 160 mmol of benzene was added to 100 mg catalyst. The reaction mixture was maintained for 30 min at the required reaction temperature and then 2 mmol of benzyl alcohol was added. This moment was regarded as the initial reaction time. Liquid samples were withdrawn at regular intervals and analyzed by gas chromatography on an Agilent 6890 GC with an FID detector using a 50 m packed HP5 column. The products were also identified by GC-MS (HP-5975C) analysis. Since benzene was in excess, conversion was calculated based on the benzylating reagent, i.e. BA. The selectivity to the product diphenylmethane (DPM) was expressed as the amount of particular product divided by the amount of total products and multiplied by 100.

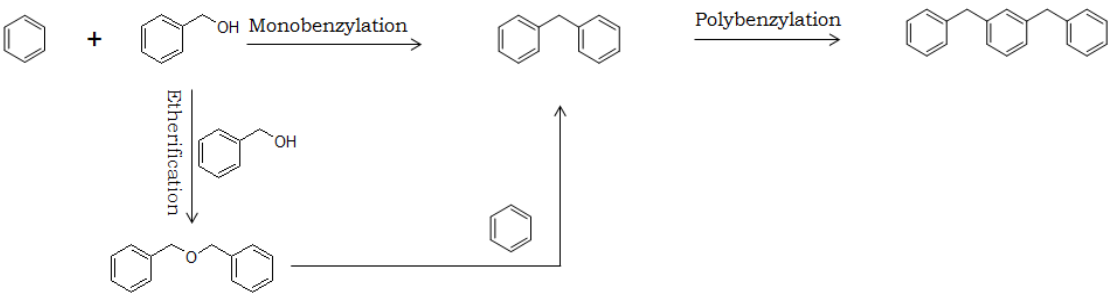

Fig. 2-3 Benzylation reaction pathway of benzene with benzyl alcohol

The size of benzene was smaller than the micropore size in zeolite Beta and Mordenite. Therefore, this reaction could be used to evaluate the performance of zeolites in the acid-catalyzed reactions with small molecules. Moreover, the liquid phase benzylation of aromatic compounds by benzyl chloride or benzyl alcohol is of significance for the production of diphenylmethane and substituted diphenyl methanes which are key industrial compounds used as pharmaceutical intermediates and fine chemicals [79-81].

(2) Benzylation of mesitylene with benzyl alcohol

The benzylation of mesitylene with benzyl alcohol was carried out in the similar condition as that in the benzylation of benzene, in a three-necked round-bottom flask equipped with a reflux condenser and heated in a temperature-controlled oil bath under atmospheric pressure. The reaction temperature for the benzylation of mesitylene was at 373 K. 160 mmol of mesitylene was added to 100 mg catalyst. The reaction mixture was maintained for 30 min at the required reaction temperature and then 2 mmol of benzyl alcohol was added.

The products in this reaction are 2-benzyl-1,3,5-trimethylbenzene (BTB), polybenzylation products and dibenzyl ether (DBE), as indicated in Fig. 2-4. However, the size of mesitylene and its products were larger than the micropore size in zeolite Beta and Mordenite. Therefore, the reaction could be only occurred on the external surface of zeolite Beta and Mordenite. This reaction could be used to evaluate the performance of zeolite in the acid-catalyzed reactions involving large molecules.

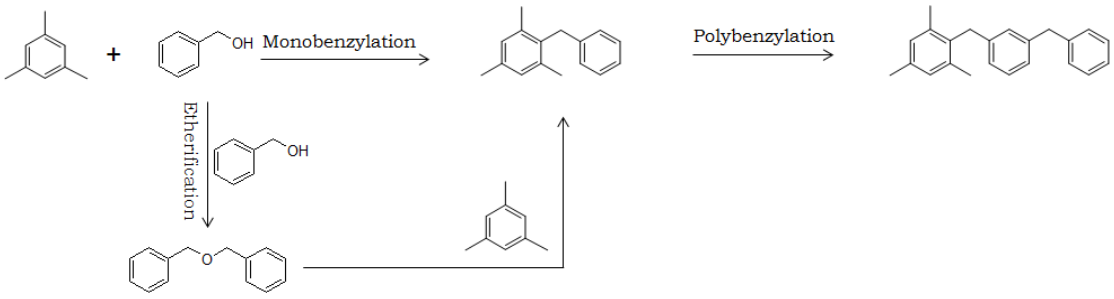

Fig. 2-4 Benzylation reaction pathway of mesitylene with benzyl alcohol

2.4.2 HDS of thiophene

The HDS of thiophene was used to evaluate the deactivation of catalysts. Due to the relative small size of thiophene, the influence of accessibility of reactants to the active phase could be reduced as much as possible. The HDS of thiophene was shown in Fig. 2-5. Generally, thiophene could be converted into tetrahydrothiophene and 1,3-butadiene by direct desulfurization (DDS) and hydrogenation (HYD) reaction routes. Then, 1,3-butadiene could be converted in butene and butane by hydrogenation.

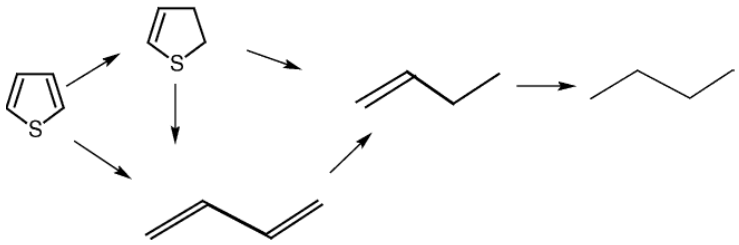

Fig. 2-5 Reaction pathways of conventional catalysts in the HDS of thiophene[15]

This reaction was performed in a fixed-bed tubular reactor. The reactor was

loaded with 0.2 g of catalyst. Then the catalysts were pre-sulfided at atmospheric pressure at 673 K for 3 h (6 $K \cdot min^{-1}$) using a mixture of 10 vol% H_2S in H_2 at a total flow rate of 100 $ml \cdot min^{-1}$. The reactions were then carried out at 623 K with 20 $ml \cdot min^{-1}$ H_2 and 1.4 $ml \cdot min^{-1}$ thiophene. The reaction samples were withdrawn at regular intervals and analyzed by gas chromatography on an Agilent 6890 GC with an FID detector.

2.4.3 HDS of DBT

In our research, the HDS of DBT was carried out to evaluate the performance of catalysts in the first layer HDS and to deeply study the different behavior of catalysts in the first and second layer HDS. It is generally accepted that DBT convert by two routes: the direct desulfurization pathway (DDS) yielding biphenyls (BPh) and the hydrogenation pathway (HYD) yielding tetrahydrodibenzothiophene (THDBT), Then THDBT could be converted into cyclohexylbenzenes (CyBz), as indicated in Fig. 2-6.

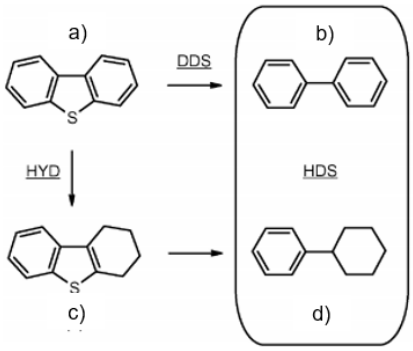

Fig. 2-6 Reaction pathways of conventional catalysts in the HDS of DBT[21]
a) DBT, b) BPh, c) THDBT, d) CyBz

The HDS of DBT were performed in a high-pressure fixed-bed microreactor (length: 40 cm, inner diameter: 1.25 cm) at 613 K under 4 MPa of total pressure. Before catalytic test, the solids were sulfided by a mixture containing DMDS (5.8 wt%) diluted in n-heptane introduced at 8 $ml \cdot h^{-1}$ as volume flow in presence of hydrogen (volume flow equal to 4.7 $NL \cdot h^{-1}$). This sulfiding solution was injected at 423 K. After 1h, the temperature was increased to 623 K by 5 $K \cdot min^{-1}$ and was maintained for 14 h to ensure a good sulfidation of the catalyst. Then, the temperature was decreased to reaction temperature (613 K).

The composition of the model feedstock was designed to simulate a straight run gas oil (SRGO) containing 10000 ppm of sulfur, as indicated in table 2-4. DBT (500 ppm S) was dissolved in n-heptane to which DMDS (1.4 wt%) was added to generate H_2S. Decane was used as a reference for quantitative analysis using a GC apparatus. The liquid effluents were collected at regular intervals after stabilization of the catalyst (observed after 1 hour on stream irrespective of the type of solid used) and

analyzed by gas chromatography (Varian 430) equipped with a FID detector and a DB1 capillary column (length: 30 m; inside diameter: 0.25 mm; film thickness: 0.25 μm). In order to obtain similar conversion (close to 50%), experiments were carried out at different LHSV values depending on the reactivity of the sulfur reactant and on the activity of the sulfide catalyst.

Table 2-4 Composition of feed in HDS

DBT (ppm)	n-C7 (wt%)	n-C10 (wt%)	DMDS (ppm)
500	97.8	0.5	9500

Assuming a first order reaction, the total activity of sulfided catalyst was determined according the following equation:

$$A = - F_S/W_{cat}. \ln (1 - X_S)$$

where A is the total activity (expressed in mol h^{-1} g^{-1}), F_S the molar flow of DBT, W_{cat} the weight of the sulfided catalyst and X_S the conversion of the DBT.

2.4.2 HDS of 4,6-DMDBT

The HDS of 4,6-DMDBT was used to evaluate the performance of catalysts in the second layer HDS. Generally, it is accepted that 4,6-DMDBT could be converted by HYD and DDS reaction routes yielding 4,6-tetrahydrodimethyldibenzothiophene (4,6-THDMDBT) and 3,3-dimethyl biphenyl (3,3-DMBPh), respectively. Then, 4,6-THDMDBT could be further desulfurized into 3,3-methylcyclohexyl toluene (MCHT), as indicated in Fig. 2-7.

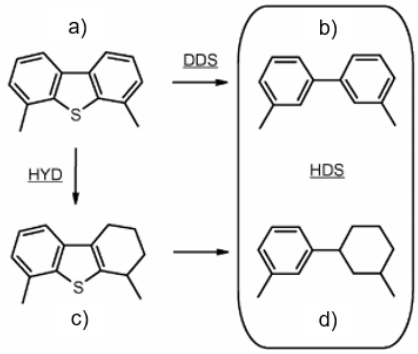

Fig. 2-7 Reaction pathways of conventional catalysts in the HDS of 4,6-DMDBT[21]
a) 4,6-DMDBT, b) 3,3-DMBPh, c) THDMDBT, d) MCHT

In order to compare with their results in the first layer HDS, the operation condition in this reaction was same as that in the HDS of DBT, only the feed was changed, as indicated in Table 2-5.

Table 2-5 Composition of feed in deep HDS

4,6-DMDBT (ppm)	n-C7 (wt%)	n-C10 (wt%)	DMDS (ppm)
500	97.8	0.5	9500

Chapter 3. Preparation and characterization of hierarchical zeolite support

3.1 Introduction

Although desilication post-treatment has been proven to be an efficient method to introduce mesopores into zeolite framework, this approach appeared less favorable for Beta zeolite, because the stability of Beta zeolite is relative low. In this case, uncontrolled dissolution would be amplified in beta zeolites synthesized in basic medium, and the severely damaged of zeolite Beta structure during desilication would occur [60,68,82-84]. However, Tian et al. currently reported that the Si/Al molar ratio in parent Beta had a big influence on the properties of hierarchical Beta prepared by desilication. The Beta zeolite with a low Si/Al molar ratio less than 30 could well preserve its microporosity and acidic properties after desilication [84,85].

On the other hand, it was suggested that desilication could result in part of Al species deposited on the external surface of zeolite framework and thus disadvantage the improvement of catalytic reactivity [72]. Acid wash after desilication may remove the deposited Al species to improve the catalytic performance. Some experimental results seemed to support this viewpoint. For example, zeolites ZSM-5, Mordenite, and Y acid washed after desilication exhibited better catalytic activities than the only desilicated ones [55,57,73]. However, the effect of such treatment on desilicated Beta has not been presented yet. Additionally, literature about the local structural change in Beta zeolite before and after post treatment is scarce.

In the present work, we firstly prepared hierarchical Beta by desilication based on a commercial Beta with a low Si/Al molar ratio of 12.5. Then, acid treatment was employed to study its effect on the structure and properties of the obtained hierarchical Beta. The catalytic performance of the catalysts was first evaluated in the benzylation of benzene with benzyl alcohol, then in the benzylation of mesitylene (tri methyl benzene) with relatively large molecular size. The change of local structure and acidity in Beta zeolite before and after post-treatment was deeply studied. The relationship between the structural properties of catalysts and catalytic performance was discussed.

3.2 Preparation and Characterization of hierarchical Beta

3.2.1 Preparation of Hierarchical zeolite Beta

Hierarchical zeolite Beta was prepared by post-treatment method, according to

Chapter 2.2.1.

3.2.2 Characterization of hierarchical zeolites Beta

The powder XRD patterns of HB, HB-B, HB-M are shown in Fig. 3-1. All the samples exhibited well-resolved diffraction peaks, which are characteristic of the Beta framework structure. This result indicated that the structure of zeolite Beta can be well preserved after base and acid treatment. However, the crystallinity of the sample decreased to 60%, perhaps due to the formation of debris. After acid treatment, the crystallinity was recovered to 73%.

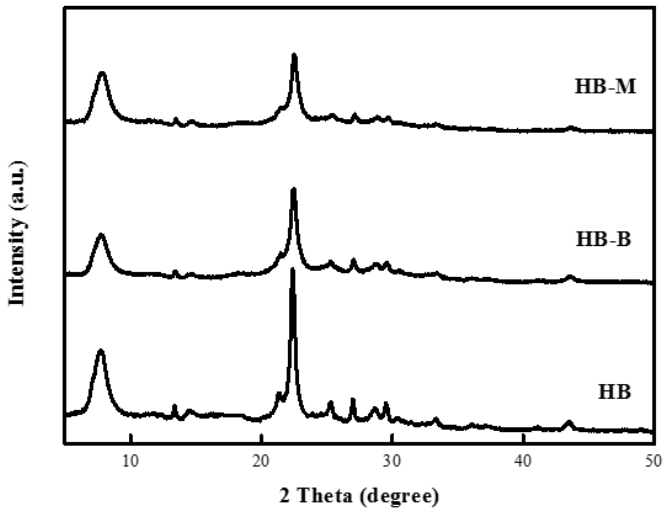

Fig. 3-1 XRD patterns of HB, HB-B and HB-M

Fig. 3-2a exhibits N_2 sorption isotherms of HB, HB-B and HB-M. It can be seen that all the samples gave a type I isotherm at low relative pressure and a type IV/II isotherm with a hysteresis loop at high relative pressure, indicating the existence of hierarchical pores. The detailed sorption data are shown in Table 3-1. Obviously, BET surface area, external surface area, mesopore volume of zeolite Beta increased after base treatment from 550 $m^2 \cdot g^{-1}$, 134 $m^2 \cdot g^{-1}$, 0.34 $cm^3 \cdot g^{-1}$ to 676 $m^2 \cdot g^{-1}$, 329 $m^2 \cdot g^{-1}$, 0.70 $cm^3 \cdot g^{-1}$, respectively. The external surface area and mesopore volume of HB-B is twice more than that of HB. These results indicated that the base treatment had a great influence on the pore structure of Beta zeolite. The mesoporosity in Beta zeolite can be greatly improved by desilication. Further, subsequent acid treatment slightly increases those values to 717 $m^2 \cdot g^{-1}$, 348 $m^2 \cdot g^{-1}$, 0.74 $cm^3 \cdot g^{-1}$ for HB-M. This means that acid treatment had a minor effect on the pore structure. Fig. 3-2b showed the curves of pore distribution obtained by BJH method for various samples. All the samples exhibited the existence of mesopores (average pore size around 4 nm) and macropores (average pore size around 75 nm). Differently, HB-B and HB-M had richer mesopores and macropores than HB. However, the pore distribution curve of HB-B is very similar to that of HB-M. Additionally, it can be noted that micropore

volume could be mostly maintained after base and acid treatment, suggesting the persistence of Beta micropore structure.

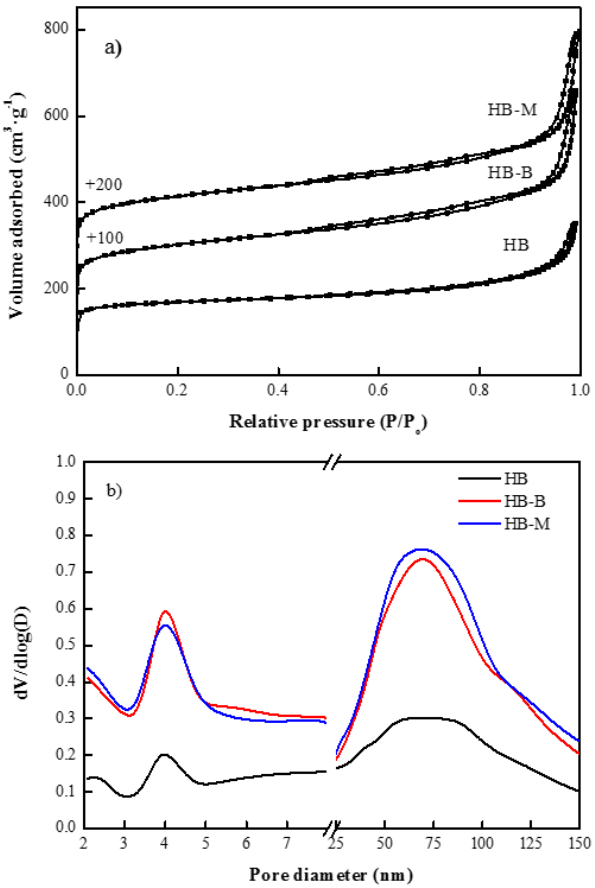

Fig. 3-2 N_2 sorption data of HB, HB-B and HB-M
a) Isotherms curves, b) pore distribution

Table 3-1 Textural properties and chemical composition of various Beta samples

Sample	S_{BET} ($m^2 \cdot g^{-1}$)	S_{ext} ($m^2 \cdot g^{-1}$)[a]	S_{micro} ($cm^3 \cdot g^{-1}$)[a]	V_{meso} ($cm^3 \cdot g^{-1}$)[b]	Crystallinity (%)[c]	Si/Al[d]	Si/Al[e]
HB	550	134	0.20	0.34	100	16.5	15.9
HB-B	676	329	0.17	0.70	60	13.4	10.0
HB-M	717	348	0.18	0.74	73	15.3	17.8

[a] t-plot； [b] BJH（adsorption branch）； [c] XRD； [d] ^{29}Si NMR； [e] XPS

The SEM images of HB, HB-B and HB-M were shown in Fig. 3-3. From SEM images, some particle aggregates can be observed. They formed the mesopores in HB. Moreover, the particle size of HB was small, between 100 and 200 nm. Therefore, more mesopores could be obtained in HB, which could explain the relative high mesopore volume and external surface area in HB.

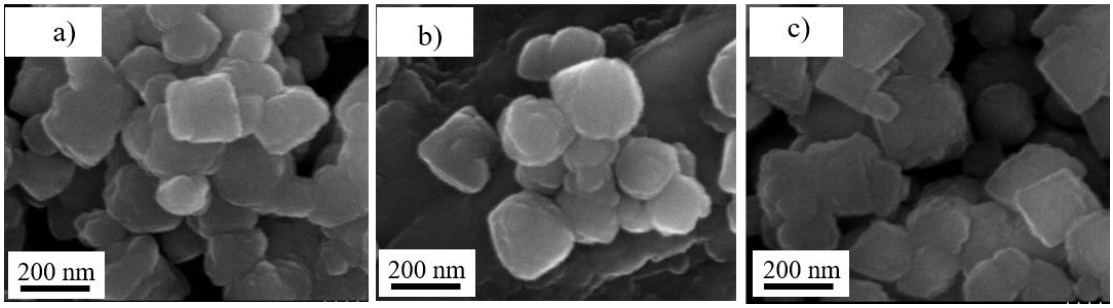

Fig. 3-3 SEM images of various Beta samples
a) HB, b) HB-B, c) HB-M

Further, TEM images revealed the presence of porosity between the particles formed for HB-B and HB-M (see the circled images in Fig. 3-4) compared with HB. Meanwhile, the crystal fringe characteristic of Beta structure in HB-B and HB-M can be clearly seen, suggesting again that micropore structure of zeolite Beta was well kept after post treatment. These results are in accordance with N_2 sorption data concerning the creation of mesopores and macropores and XRD analysis concerning the preservation of the zeolite structure.

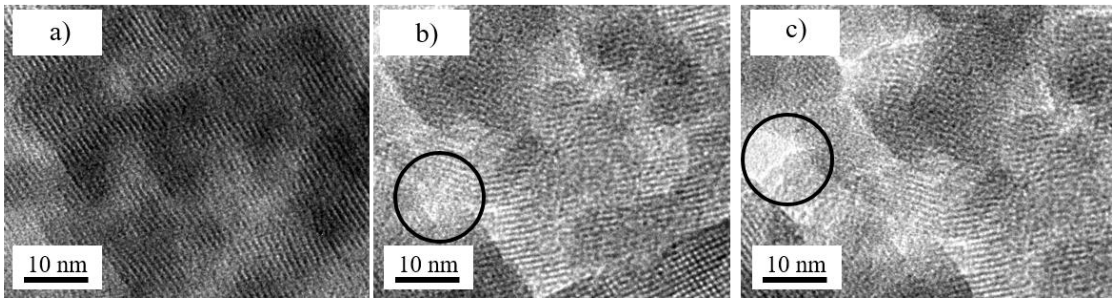

Fig. 3-4 TEM images of various Beta samples
a) HB, b) HB-B, c) HB-M

The IR studies of pyridine adsorption were performed to measure the number of acid sites in HB, HB-B and HB-M. The data are listed in Table 3-2.

Table 3-2 The number of acidic sites and accessible acid sites of various Beta samples

Sample	B_{py} ($\mu mol \cdot g^{-1}$)	L_{py} ($\mu mol \cdot g^{-1}$)	Tot_{py} ($\mu mol \cdot g^{-1}$)	B_{pi} ($f \cdot \mu mol \cdot g^{-1}$)	L_{pi} ($f \cdot \mu mol \cdot g^{-1}$)	Tot_{pi} ($f \cdot \mu mol \cdot g^{-1}$)
HB	269	313	582	2.0	3.4	5.4
HB-B	129	125	254	5.9	10.5	16.4
HB-M	209	236	445	9.5	7.5	17.0

Obviously, the number of total and Brönsted acid sites (582 $\mu mol \cdot g^{-1}$, 269 $\mu mol \cdot g^{-1}$) in HB is twice more than that (254 $\mu mol \cdot g^{-1}$, 129 $\mu mol \cdot g^{-1}$) in HB-B. The number of acid sites was greatly decreased after desilication, which is in agreement with some reported results [60,68,82-84]. Comparatively, the number of total and Brönsted acid sites (445 $\mu mol \cdot g^{-1}$, 209 $\mu mol \cdot g^{-1}$) for HB-M is much larger than that of HB-B (nearly twice). This result indicated that the number of total acid sites can be

greatly recovered by subsequent acid treatment after desilication.

Due to its larger size than that of pyridine, pivalonitrile with steric hindrance has been proven to be a good probe molecule to characterize the number of acid sites in zeolites accessible to larger molecules [78]. The band of 2274 cm^{-1} and 2302 cm^{-1} corresponds to the adsorption of pivalonitrile on Brönsted acid sites and Lewis acid sites, respectively. The data of the corresponding acid sites in HB, HB-B and HB-M are listed in Table 3-2. As shown, HB-B and HB-M had more acid sites accessible to larger pivalonitrile than HB. The number of accessible acid sites in HB-B is three times larger than that in HB. This means that desilication of zeolite Beta can increase the number of accessible acid sites, which should be attributed to the improvement of external surface area due to the introduction of additional mesopores. After acid treatment, the number of total accessible acid sites was slightly increased. Apparently, HB-M had larger number of accessible Brönsted acid sites than HB-B.

3.2.3 Catalytic performance of hierarchical zeolite Beta

(1) Benzylation of benzene with benzyl alcohol

The conversion of BA and yield of DPM with reaction time over various catalysts are shown in Fig. 3-5. Obviously, the conversion of BA was increased with reaction time and reached nearly 100% at a reaction time of 30 min over all the catalysts (Fig. 3-5a). Meantime, the yield of DPM was increased with reaction time until the formed DBE was completely converted (Fig. 3-5b). Considering that the product distribution in the liquid phase reaction system might be not homogeneous during the earlier reaction time (5 min), the catalytic activity of various catalysts at a relatively long reaction time (10 min) was selected for comparison.

Furthermore, the apparent reaction rate constant was calculated. As seen in Table 3-3, HB gave higher catalytic activity than HB-B.

Table 3-3 Catalytic reaction data about various catalysts in the benzylation of benzene

Sample	BA conversion（%）	DPM yield（%）	*ka*（x10^{-3} min^{-1}）
HB	58	49	87
HB-B	37	31	46
HB-M	52	45	73

Reaction time: 10min, Reaction temperature: 353K

After a reaction time of 10 min, the conversion of BA and yield of DPM for HB reached 58% and 49%, respectively. Comparatively, HB-B showed the BA conversion of 37% and DPM yield of 31%. The reaction rate constant of HB is 1.9 times that of HB-B. This means that hierarchical Beta prepared by desilication had poorer catalytic activity than parent one in the benzylation of benzene. It needs be noted that HB-M had better catalytic activity than HB-B. After a reaction time of 10 min, the

conversion of BA and yield of DPM for HB-M reached 52% and 45%, respectively. The reaction rate constant of HB-M is 1.6 times that of HB-B. This result indicates that acid treatment may improve the catalytic performance of desilicated hierarchical Beta in this reaction.

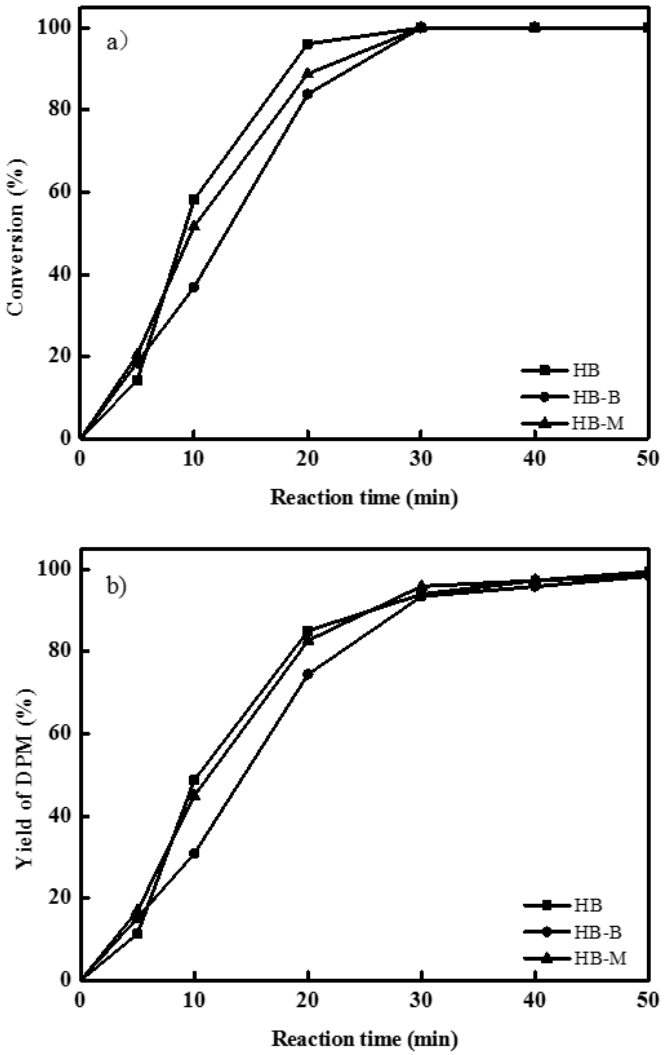

Fig. 3-5 Benzlyation of benzene with benzyl alcohol HB, HB-B and HB-M
a) Conversion of BA, b) yield of DPM

(2) Benzylation of mesitylene with benzyl alcohol

The conversion of benzyl alcohol and yield of BTB with reaction time over various catalysts is shown in Fig. 3-6. As seen, the conversion of BA was rapidly increased with reaction time and reached nearly 100% after a reaction time of 120 min over HB-M and HB-B except for HB (Fig. 3-6a). Meantime, the yield of BTB was increased with reaction time until the formed DBE was completely converted (Fig. 3-6b).

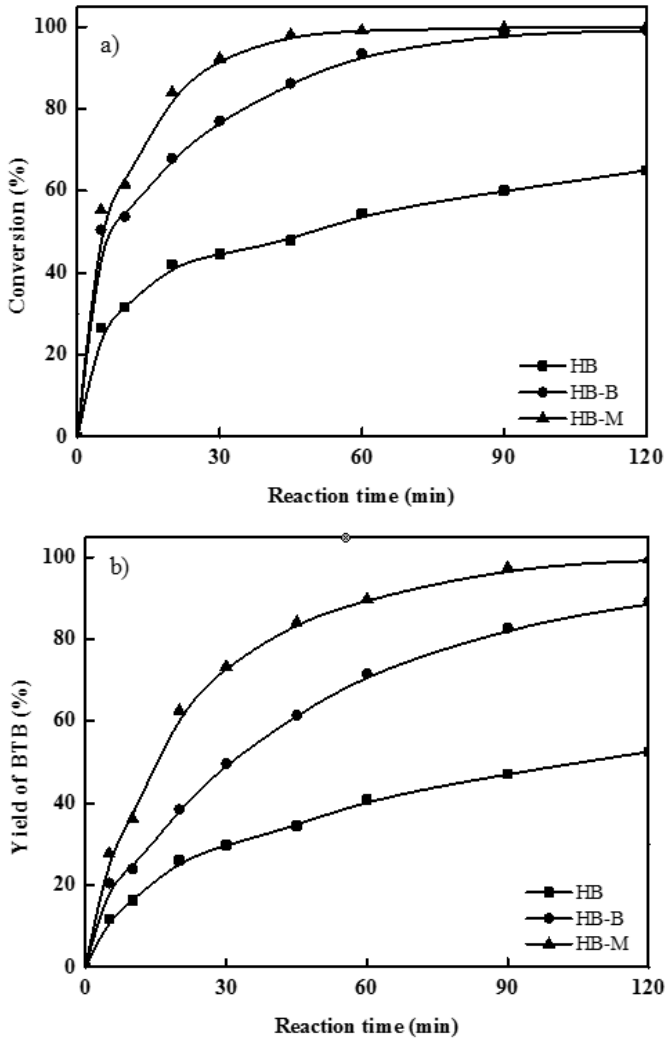

Fig. 3-6 Benzlyation of mesitylene with benzyl alcohol over HB, HB-B and HB-M
a）Conversion of BA, b) yield of BTB

HB showed lower catalytic activity than HB-B. After a reaction time of 30 min, the conversion of BA and yield of BTB for HB reached 45% and 30%, respectively (Table 3-4). In comparison, HB-B gave the BA conversion of 77% and BTB yield of 50%. The reaction rate constant of HB-B is twice as much as that of HB. Further, HB-M exhibited better catalytic activity than HB-B. After a reaction time of 30 min, the conversion of BA and yield of BTB for HB reached 92% and 73%, respectively. The reaction rate constant of HB-M is 1.2 times that of HB-B and 2.5 times that of HB.

Table 3-4 Catalytic reaction data about various catalysts in the benzylation of mesitylene

Sample	BA conversion（%）	BTB yield（%）	*ka*（x10^{-3} min^{-1}）
HB	45	30	38
HB-B	77	50	77
HB-M	92	73	96

Reaction time: 30min, Reaction temperature: 373K

3.2.4 Influence of acidity on the performance of zeolites

In the benzylation of benzene, HB exhibited higher activity than HB-B and HB-M. To clarify the above catalytic results, the factors influencing the catalytic performance in this reaction need to be considered. Because the benzylation of benzene with benzyl alcohol is an acid-catalyzed reaction, the acidity of catalysts should be an important factor. Based on the proposed reaction mechanism [86], it is undoubted that the number of Brönsted acid sites should play a key role in the reaction. In fact, as shown in Table 3-2, HB possessed more Brönsted acid sites characterized by pyridine adsorption than HB-B and HB-M. The number of Brönsted acid sites in HB-B is the lowest. Apparently, the catalytic reactivity of the catalysts had a good relationship with the number of Brönsted acid sites. Additionally, the ability of mass transfer should be also an important factor influencing the catalytic performance. It has been demonstrated that the catalyst with larger external surface area and mesopore volume had better ability of mass transfer [57,72,73]. Obviously, HB-B and HB-M possessed larger external surface area and mesoporous volume than HB but exhibited lower catalytic activity (Table 3-1). The catalytic reactivity seemed to have no good correlation with the ability of mass transfer. Based on these analyses, it can be concluded that the number of Brönsted acid sites played a more vital role than the ability of mass transfer in the reaction. The reason why the desilicated hierarchical Beta exhibited relatively low catalytic activity in the reaction may be mainly attributed to the great loss of acid sites during base treatment. Subsequent acid treatment is helpful for improving the catalytic performance of hierarchical Beta due to the partial recovery of acid sites.

In the benzylation of mesitylene, HB-M exhibited the highest activity. To explain the above catalytic results, the molecular size of reactant and product has to be considered. In the benzylation of benzene, the molecular size of benzene and main product is around 0.5 nm, which is smaller than micropore size of Beta zeolite (0.67 nm). However, in the benzylation of mesitylene, the molecular size of mesitylene and main product is around 0.8 nm [87], which is larger than micropore size of zeolite Beta. This means that the reactant cannot reach acid sites in micropores of zeolite Beta and the reaction has to be carried out on its external surface. Obviously, some acid sites characterized by pyridine (molecular size around 0.5 nm) adsorption cannot effectively be utilized in this reaction. Comparatively, the data of the accessible acid sites characterized by pivalonitrile adsorption should supply some correlated information. As seen in Table 3-2, HB-M and HB-B possessed more Brönsted acid sites accessible to pivalonitrile than HB. The number of accessible Brönsted acid sites in HB-M is the highest and that in HB is lowest. The catalytic reactivity is well correlated with the number of accessible Brönsted acid sites. In earlier reports, it is often displayed that the desilicated zeolites had better catalytic performance than

parent ones in the reactions involving indifferently small or large molecules. However, it is rarely observed that the desilicated zeolite showed poorer catalytic activity with small molecules and better catalytic performance with large molecules than parent one. This means that the desilicated Beta may be used in the benzylation of the reactant with large molecular size although the number of total acid sites characterized by pyridine adsorption was greatly decreased. Further, these results demonstrated again that subsequent acid treatment is helpful for improving the catalytic activity of desilicated Beta in the benzylation reaction.

3.3 Change of local structure during treatments

3.3.1 Change of Si species

To understand the change of local structure in Beta zeolite before and after post treatment, the samples HB, HB-B and HB-M were firstly studied by ^{29}Si MAS NMR and the recorded spectra with their corresponding best fit simulations are displayed in Fig. 3-7.

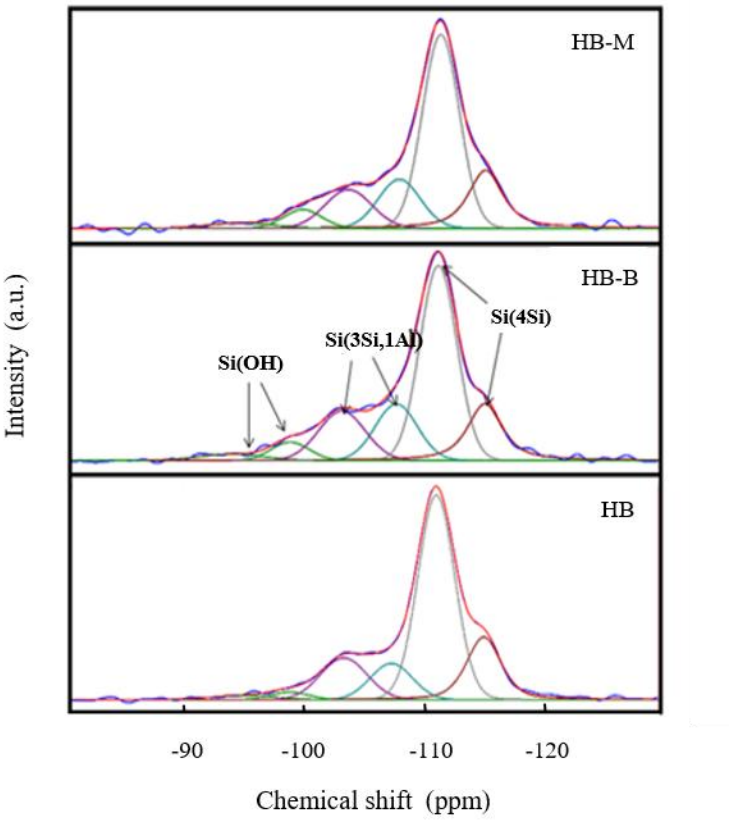

Fig. 3-7 ^{29}Si NMR spectra of HB, HB-B and HB-M
(blue) Experimental,（red）simulated

All the samples showed six resonance peaks centered at -94 to -100 ppm (SiOH), -103 to -108 ppm (Si(3Si,1Al)) [88,89], and -111 to -116 ppm (Si(4Si)) [73,90],

respectively. The data about the proportion of different Si types are listed in Table 3-5. Obviously, the base treatment removed part of Si(4Si) species in the framework because the proportion of Si(4Si) decreased from 71.8% to 63%. The proportion of SiOH was increased from 4% to 7% because the created mesopores extended into the microporous crystalline zeolite framework and would be terminated by silanol groups on the mesopore walls [71]. Further, it could be observed that the proportion of Si(3Si,1Al) was increased from 24.2% to 30% after the desilication. Generally, it was thought that the Si species such as Si(4Si) can be easily leached out during desilication but it is difficult to remove the Si species such as Si(3Si,1Al) because the negatively charged AlO_4^- tetrahedral structure prevented the hydrolysis of the Si-O-Al bond in the presence of OH^- [59]. Therefore, it is reasonable to think that the proportion of Si(3Si,1Al) will increase after the desilication process that removes some Si(4Si) and SiOH species. The Si/Al molar ratio from NMR calculation was decreased from 16.5 to 13.4 after alkaline treatment, indicating that part of silicon species in zeolite Beta has been successfully removed. After acid treatment as shown in Table 3-1, the Si/Al molar ratio was increased from 13.4 to 15.3. These results suggested that a small proportion of Al species should be removed during the acid treatment. In this case, the proportion of Si-OH (7.1%) almost had no change. The proportion of Si(3Si,1Al) and Si(4Si) was changed from 30% to 26.1% and from 63% to 66.8%, respectively. Si/Al molar ratios have also been calculated from XPS analysis. The obtained values are in accordance with those determined by NMR, indicating that the surface species evolve as the bulk species with a decrease of Si surface species after base treatment and a decrease of aluminum surface species after the acid one.

Table 3-5 Relative intensity of different Si types from ^{29}Si MAS NMR

	HB	HB-B	HB-M
SiOH （%）	4.0	7.0	7.1
Si(3Si,1Al)（%）	24.2	30.0	26.1
Si(4Si)（%）	71.8	63.0	66.8

3.3.2 Change of Al species

(1) Type of Al species in zeolite Beta

The ^{27}Al MAS NMR experiments were performed to detect the coordination state of aluminum species in HB, HB-B and HB-M (Fig. 3-8). It can be seen that the recorded spectra exhibited a strong peak centered at around 54 ppm corresponding to tetrahedral coordination aluminum and a small peak centered at around 0 ppm corresponding to octahedral coordination aluminum, indicating that Al coordination in

all the samples mainly consisted of tetrahedral coordination with a small amount of octahedral coordination. Differently, a trace of pentahedral coordination aluminum can be observed in HB-B and HB-M (Fig. 3-8).

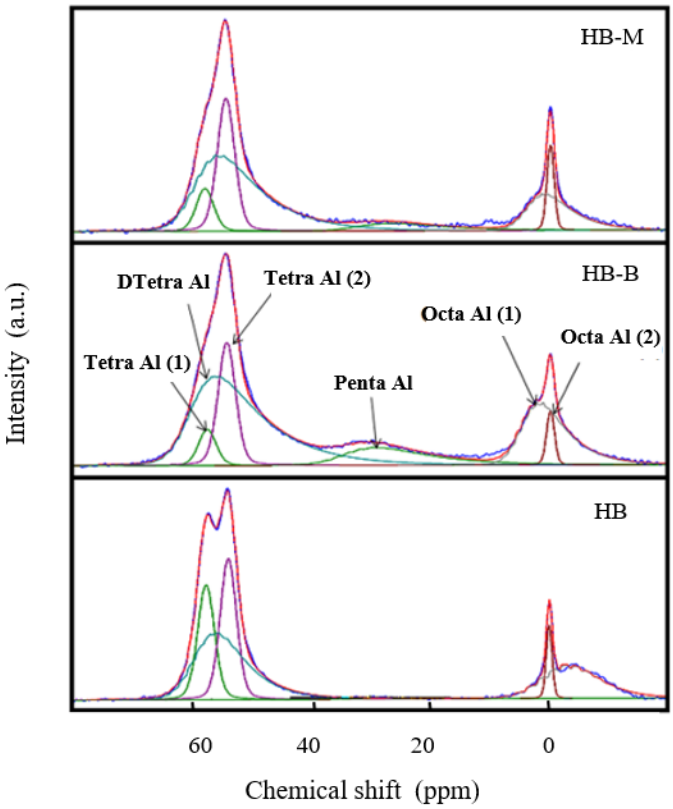

Fig. 3-8 ^{27}Al NMR spectra of HB, HB-B and HB-M
(blue)Experimental，（red）simulated

To deeply uncover the type of aluminum coordination state in the samples, the experiment of two-dimensional ^{27}Al MQ MAS NMR was done. Considering the resonance peaks of ^{27}Al MAS NMR in HB-B and HB-M are similar, here we just showed the results from HB and HB-B for comparison. Moreover, δ_2 projections of the spectra are shown to clearly indicate the position and shape of resonance peaks (Fig. 3-9). As seen, they displayed two resonance peaks with a low quadrupolar effect presented at nearly 58 ppm and 54 ppm and one resonance peak affected by a large quadrupolar interaction at nearly 60 ppm, and two resonance peaks at nearly 0 ppm.

All resonance peaks between 54 ppm and 65 ppm could be regarded as tetrahedral (T) coordination aluminum. The two resonance peaks affected by low quadrupolar interaction were assigned to aluminum atoms occupying different T-sites. It has been proposed that there are nine different T-sites in zeolite Beta based on the difference of the averaged Al-O-Si angles [91-95]. They are T1 at 155.3°, T2 at 155.9°, T3 at 148.0°, T4 at 148.2°, T5 at 151.8°, T6 at 152.1°, T7 at 152.8°, T8 at 151.4° and T9 at 149.7°, respectively [95]. The structure of zeolite Beta and the position of different T-sites was illustrated in earlier literatures [91-95]. According to the

theoretical calculation and experimental results, aluminum atoms on positions T1 and T2 in the framework of Beta would give a resonance peak at nearly 54 ppm (Tetra Al(2)) and aluminum atoms positioned in T3-T9 would show a resonance peak between 56 ppm and 58 ppm (Tetra Al(1)) [96,97]. The resonance peak with large quadrupolar effect visible in the isotropic dimension was from a locally distorted aluminum atom associated with a defective site in the Beta framework (labelled as DTetra Al), which may be regarded as a transition from the crystalline framework lattice state to the amorphous silica-alumina state [98].

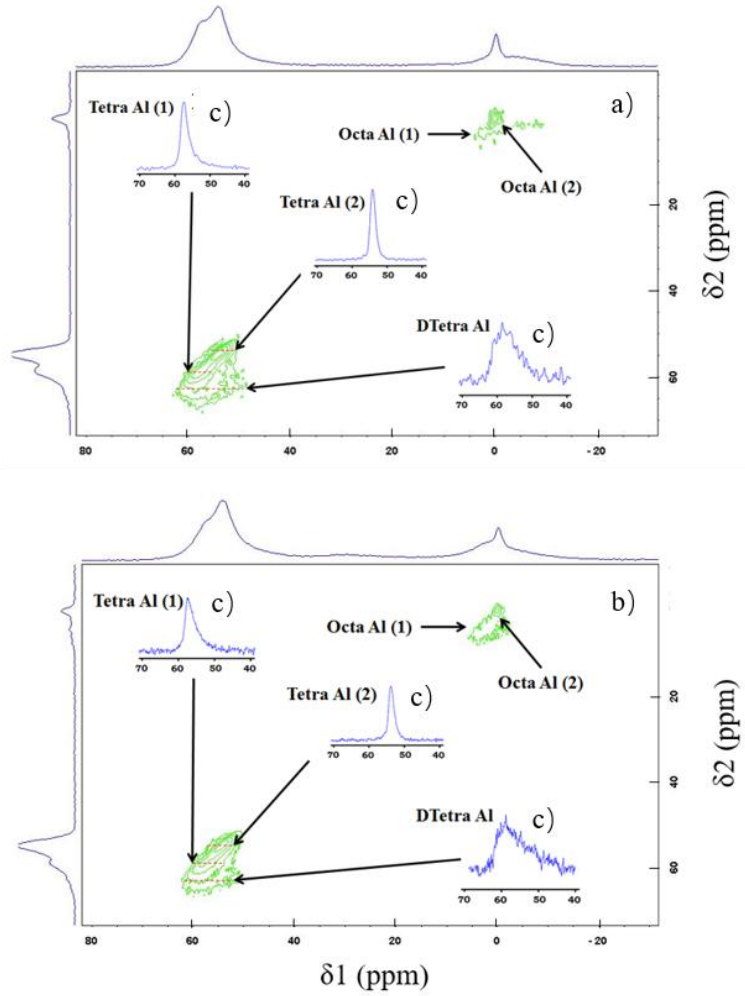

Fig. 3-9 ^{27}Al MQ MAS NMR spectra and their respective projections correspond to the anisotropic δ2 and isotropic δ1 dimensions, respectively
a) HB, b) HB-M, c) projections

In addition, two resonance peaks at nearly 0 ppm were located in the octahedral coordination region. The octahedral coordination aluminum close to 0 ppm (Octa Al(2)) showed a weak quadrupolar interaction and a small distribution in the isotropic chemical shifts. One explanation is that the octahedral coordination aluminum is from the aluminum connected to the framework via one or two oxygen atoms [96,97]. Another is that it is from the aluminum connected via 4 oxygen atoms to the framework and coordinated by one water molecule and one hydronium ion [99]. The

resonance peak with a strong quadrupolar effect centered between 0 ppm and 5 ppm was considered as distorted octahedral coordination aluminum [97].

(2) Content of various Al species

Based on the results from two-dimensional ^{27}Al MAS NMR, the deconvolution of 1D ^{27}Al MAS NMR was done to understand the change of Al sites in zeolite Beta (Fig. 3-8). The used NMR parameter was as in Table 3-6.

Table 3-6 Fit parameters for decomposition of ^{27}Al MAS NMR

	Tetra Al(1)	Tetra Al(2)	DTetra	Penta Al	Octa Al(1)	Octa Al(2)
Shape	Gaus/Lor	Gaus/Lor	CZSimple	CZSimple	CZSimple	Gaus/Lor
Pos.	~58.8	~55.1	~60.4	~34.9	~4.38	~0
CQ	~3.15	~3.21	~10	~5.1	~5.1	~1.47

The detailed data of various coordinative was collected in Table 3-7. As seen, the simulated resonance peaks were identical in shape and position shown in δ_2 projections. HB contained five types of Al sites: DTetra Al, Tetra Al(1), Tetra Al(2), Octa Al(1) and Octa Al(2). Their proportion was 35.7% for DTetra Al, 18.7% for Tetra Al(1), 23.2% for Tetra Al(2), 18% for Octa Al(1) and 4.4% for Octa Al(2), respectively. No pentahedral coordination aluminum (Pent Al) was observed.

Table 3-7 Relative intensity of aluminum species in ^{27}Al MAS NMR

	HB		HB-B		HB-M	
	ppm	%	ppm	%	ppm	%
DTetra Al	59.49	35.7	60.48	47.2	59.59	42.4
Tetra Al(1)	57.71	18.7	57.33	2.8	57.72	6.5
Tetra Al(2)	53.97	23.2	54.05	14.1	54.20	23.8
Pent Al	-	-	34.53	12.6	32.02	5.7
Octa Al (1)	0.10	18.0	1.57	19.6	3.66	16.0
Octa Al (2)	0.04	4.4	-0.31	3.7	-0.26	5.5

After desilication, a small amount of Pent Al in HB-B was formed with a proportion of 12.6%. Meanwhile, the proportion of DTetra Al was increased from 35.7% to 47.2% and the proportion of Tetra Al(1) and Tetra Al(2) was decreased from 18.7% to 2.8% and from 23.2% to 14.1%, respectively. The total proportion of Octa Al was kept around 23%. This result indicates that the Si species connected with Al by oxygen have to be removed. Otherwise, the proportion of different Al sites should be kept constant. Considering that the proportion of Octa Al did not change significantly, Pent Al and DTetra Al with the increased proportion should mainly result from the transformation of partial Tetra Al(1) and Tetra Al(2). Additionally, it can be noted that the decreased proportion of Tetra Al(2) is less than that of Tetra Al(1)

(Table 3-7), suggesting that the Si species of Si-O-Al in Tetra Al(2) should be more difficult to remove than those in Tetra Al(1).

3.3.3 Influence of local structure on the acidity of zeolite Beta

It is well known that the acidity of zeolites mainly depended on the tetrahedral coordination aluminum sites. The proportion of Al sites from Tetra Al in zeolites is higher, the number of Brönsted acid sites could be larger. Thus, the decreased acidity in HB-B should mainly be attributed to the greatly decreased proportion of Tetra Al from 42% to 17% after base treatment. By calculation, the concentration of Tetra Al was decreased from 403 $\mu mol \cdot g^{-1}$ to 198 $\mu mol \cdot g^{-1}$.

After acid treatment, the proportion of Pent Al and DTetra Al was decreased from 12.6% to 5.7% and from 47.2% to 42.4%, respectively. The proportion of Octa Al was changed from 23.23% to 21.53%. Notably, the proportion of Tetra Al was increased from 17% to 30.4%. By calculation, the concentration of Tetra Al was increased from 198 $\mu mol \cdot g^{-1}$ to 313 $\mu mol \cdot g^{-1}$. This suggested that HB-M could possess more Brönsted acid sites than HB-B. These results may well explain the reason why the Brönsted acid sites can be greatly recovered after acid treatment.

Considering that the amount of aluminum species in Beta zeolite is low, it is difficult to assume that the concentration of Tetra Al was greatly enhanced just by the removal of partial Al species on the surface of catalyst. Possibly, such change occurred in the presence of dissolution of the partial Pent Al or/and DTetra Al and realumination under mild acid condition because the aluminum species in acid solution may be easily reinserted into the framework of zeolite Beta [100,101]. Certainly, it is also possible that the number of acid sites was decreased because partial pores might be blocked after base treatment. After subsequent acid treatment, the pores might have been cleared, leading to high accessibility to acid sites in and superior catalytic performance of HB-M.

3.4 Extended study on hierarchical Mordenite

As another important industrial zeolite [72], Mordenite zeolite with relative low cost was also hierarchized by the same base-acid post-treatment in our parallel research [73].

3.4.1 Preparation of hierarchical zeolite Mordenite

Hierarchical zeolite Mordenite was prepared by post-treatment. The detailed process was described in Chapter 2.2.2.

3.4.2 Characterization of hierarchical zeolite Mordenite

Similar characterizations than that of hierarchical zeolite Beta have been performed in hierarchical zeolite Mordenite. Fig. 3-10 showed the XRD pattern of various zeolite Mordenite. The crystallinity (99%, Table 3-8) of HM-A showed a slight decrease from that of HM, meaning that dealumination had a minor influence on the crystallinity of Mordenite. After base treatment, the crystallinity decreased to 82%. Obviously, the effect of desilication on the crystallinity was relatively large. Further, the acid-washing step resulted in a minor decrease in the crystallinity (75%). These results indicated that the post-treatments could lead to crystallinity loss but the long-range crystal ordering in these samples may be kept.

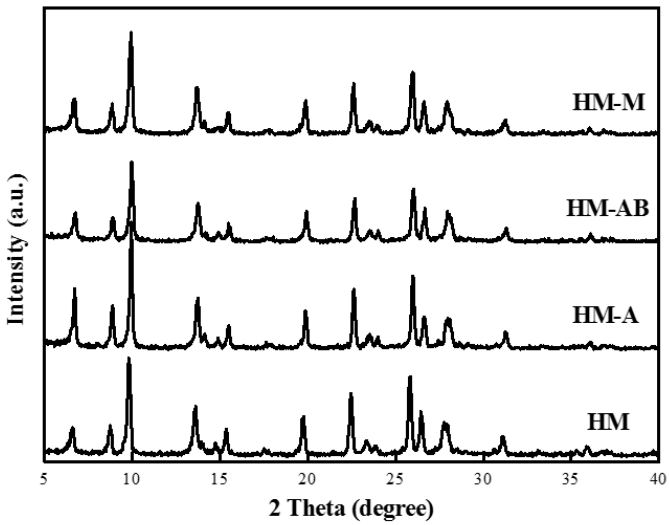

Fig. 3-10 XRD pattern of HM, HM-A, HM-AB and HM-M

The N_2-sorption isotherms of all the samples are shown in Fig. 3-11. The mesopore volume for HM is 0.07 $cm^3 \cdot g^{-1}$, which is lower than that for the treated samples (Table 3-8). The acid-leaching step can improve mesopore volume to some extent, but the enhancement is not significant. Obviously, the Mordenite with base treatment had a relatively high mesopore volume. The mesopore volume for HM-AB and HM-M is 0.17 and 0.21 $cm^3 \cdot g^{-1}$, respectively, which is twice and three times that of the parent Mordenite. Additionally, all the treated Mordenite had a higher BET special surface area and external surface area than the parent Mordenite, which should be attributed mainly to the enhancement of porosity by the additional mesopores. HM-M had the highest external surface area (112 $m^2 \cdot g^{-1}$) among the four samples. The value is more than three times that of HM (45 $m^2 \cdot g^{-1}$) and more than twice that of HM-A (64 $m^2 \cdot g^{-1}$) and HM-AB (83 $m^2 \cdot g^{-1}$). These results indicated that the acid-washing step after base treatment can significantly increase the external surface area.

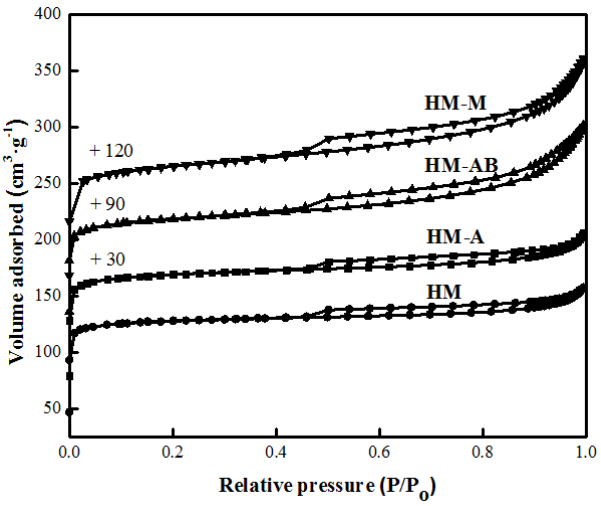

Fig. 3-11 N_2-sorption isotherm of HM, HM-A, HM-AB and HM-M

Table 3-8 Textural properties and chemical composition of various Mordenite zeolites

Sample	S_{BET} ($m^2 \cdot g^{-1}$)	S_{Ext} ($m^2 \cdot g^{-1}$)	V_{micro} ($cm^3 \cdot g^{-1}$)	V_{meso} ($cm^3 \cdot g^{-1}$)	Crystallinity (%)	Si/Al
HM	411	45	0.18	0.07	100	15
HM-A	448	64	0.19	0.08	99	30
HM-AB	448	83	0.16	0.17	82	20
HM-M	471	112	0.18	0.21	75	31

From the SEM images of various samples (Fig. 3-12), it can be observed that there are intercrystalline mesopores and no intracrystalline mesopores in HM. The particle aggregates can explain the reason of mesopores formation in HM.

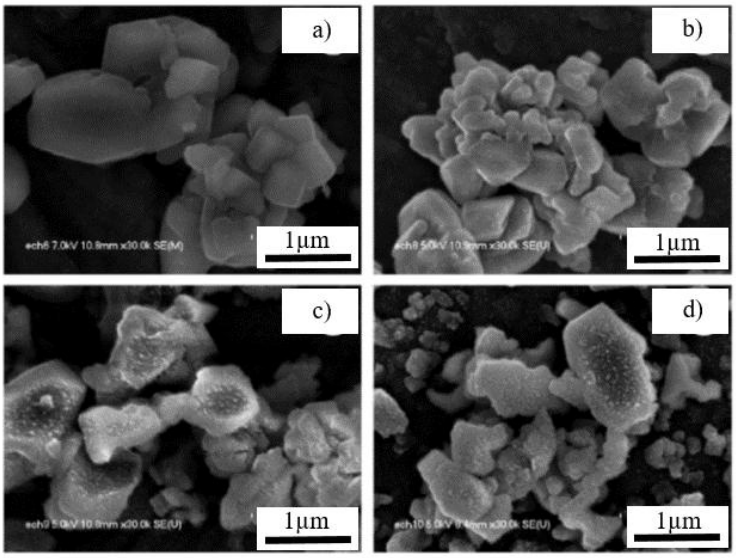

Fig. 3-12 SEM images of various Mordenite zeolites
a) HM, b) HM-A, c) HM-AB, d) HM-M

In contrast, the treated samples (HM-AB and HM-M) displayed the existence of

intracrystalline mesopores (white spots). These results were in accordance with the data from N_2 sorption and TEM results (Fig. 3-13).

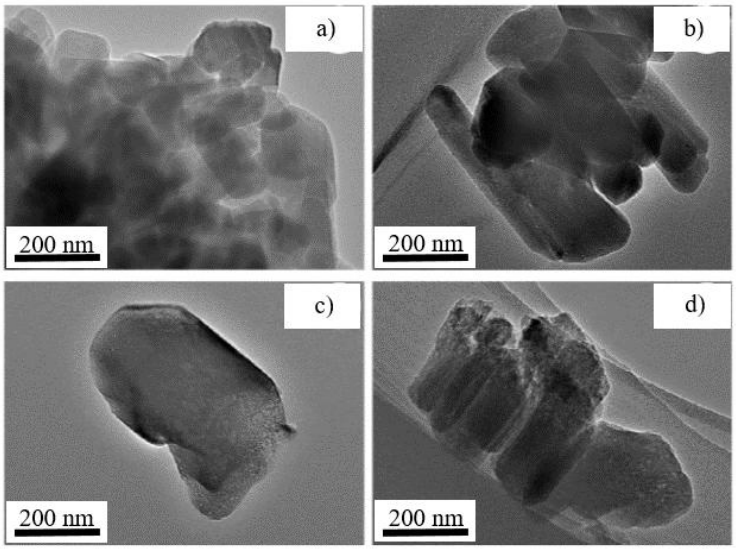

Fig. 3-13 TEM images of various Mordenite zeolites
a) HM, b) HM-A, c) HM-AB, d) HM-M

Fig. 3-14 showed the ^{27}Al spectra of various samples to detect the coordination state of aluminum species in the samples.

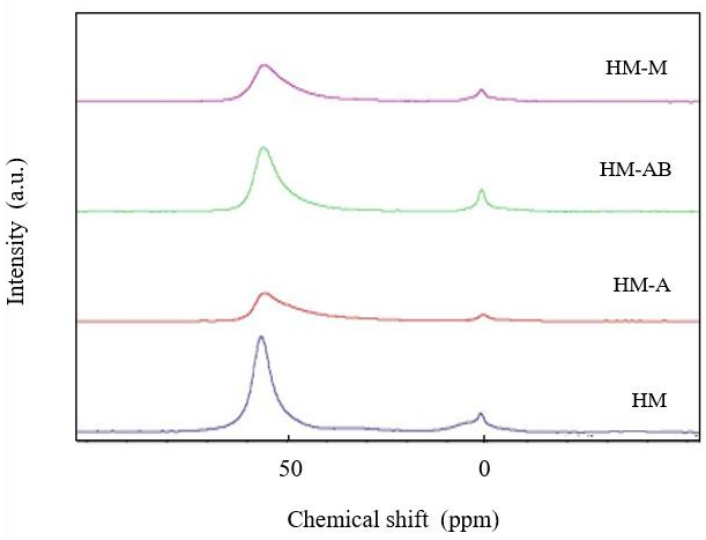

Fig. 3-14 ^{27}Al Spectra of HM, HM-A, HM-AB and HM-M

Apparently, they exhibited a strong peak centered at around 54 ppm, corresponding to tetrahedrally coordinated aluminum, and a small peak centered at around 0 ppm, corresponding to octahedrally coordinated aluminum, indicating that Al coordination in all the samples was mainly tetrahedral with a small amount octahedral. Additionally, it can be noted that for the treated samples, the peak corresponding to tetrahedrally coordinated aluminum became wide and the total peak area turned small compared with that for the parent Mordenite. This suggested that the

Al content in the treated samples decreased and some Al sites in the Mordenite framework might be slightly changed. Obviously, the resonance peak area of HM-AB is larger than that of HM-A and HM-M, indicating that the Al content in HM-AB is higher than that in HM-A and HM-M. These results are in agreement with the measurement results of the Si/Al molar ratio. Moreover, it seemed that no additional Penta aluminum was produced during desilication and further acid leaching, suggesting that the structure of Mordenite might be more stable than that of Beta zeolite.

Table 3-9 showed the number of acid sites in various samples, measured by IR-pyridine. It could be observed that the number of acid sites in zeolite Mordenite was not drastically reduced during the base treatment (in comparison, more than 60% of acid sites in Beta zeolite were lost during desilication). Moreover, subsequent acid washing successfully increased the number of acid sites in desilicated hierarchical zeolite Mordenite. The number of acid sites in HM-M is more than twice as that of HM.

Table 3-9 Number of acidic sites in various Mordenite samples

Sample	Brönsted acid sites ($\mu mol \cdot g^{-1}$)	Lewis acid sites ($\mu mol \cdot g^{-1}$)	Total acid sites ($\mu mol \cdot g^{-1}$)	Strong Brönsted acid sites ($\mu mol \cdot g^{-1}$)	Strong Lewis acid sites ($\mu mol \cdot g^{-1}$)	Total strong acid sites ($\mu mol \cdot g^{-1}$)
HM	23	104	127	28	44	72
HM-A	63	170	233	-	-	-
HM-AB	33	153	186	14	37	51
HM-M	87	201	288	65	77	142

The higher number of acid sites in HM-M than HM could be explained by the higher stability as well as the different pore structure of zeolite Mordenite. As known, Mordenite is a zeolite with one-dimensional porosity. In other dimensions, the pore is too small for allowing molecules diffusion. The additional mesopores might present acid sites in other dimensions accessible for molecules such as pyridine [72].

Due to the higher number of acid sites, HM-M could exhibit good result in acid-catalyzed reactions, even for small molecule reactions. Fig. 3-15 showed the catalytic activity of various zeolite Mordenite in the benzylation of benzene with benzyl alcohol. It could be observed that HM-M exhibited remarkably enhanced catalytic activity, which almost ended this reaction after a reaction time of 0.5 h. The apparent reaction rate constant for HM-M is 15 times that for HM and twice that for HM-A and HM-AB.

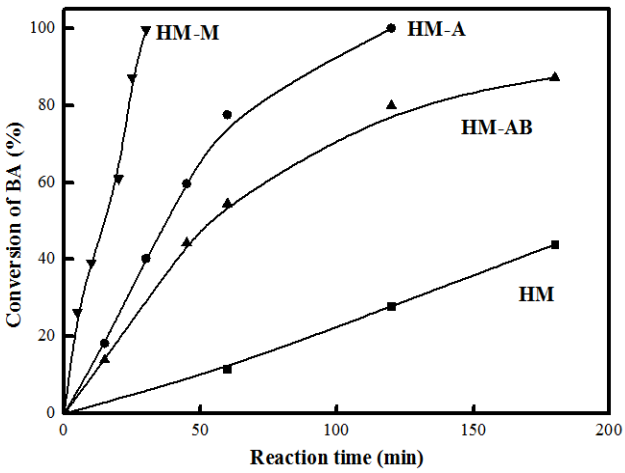

Fig. 3-15 Catalytic activities of HM, HM-A, HM-AB and HM-M in the benzylation of benzene with benzyl alcohol

In this present work, the benzylation of mesitylene with benzyl alcohol was not carried out over zeolite Mordenite. However, it was reasonable to understand that HM-M could exhibit much better activity than other samples in the acid-catalyzed reaction involving large molecules, because HM-M with more acid sites and better accessibility should possess more accessible acid sites.

3.5 Brief summary

Hierarchical Beta zeolite was firstly prepared by base treatment based on a commercial Beta with a low Si/Al molar ratio of 12.5. After desilication, the number of total acid sites in Beta zeolite was greatly decreased, which should be mainly attributed to the transformation of partial tetrahedral coordination Al into distorted tetrahedral and pentahedral coordination Al. Subsequent acid treatment may greatly increase the proportion of tetrahedral coordination Al while decreasing the proportion of the distorted tetrahedral and pentahedral coordination Al. As a result, after acid treatment the number of acid sites in Beta zeolite was greatly recovered.

Such an acid treatment is helpful for improving the catalytic performance of the desilicated hierarchical Beta in some acid-catalytic reactions. Catalytic results in the benzylation of benzene with benzyl alcohol indicated that HB-M exhibits better activity than HB-B in the acid-catalyzed reaction of small molecules, while HB-M with less active site was less active than HB. However, in the benzylation of mesitylene a larger molecule, HB-M exhibited much better catalytic performance than parent one, because the acid sites on HB-M were more accessible. These results revealed clearly that hierarchical Beta obtained by post-treatment method can find applications in acid-catalyzed reactions involving large molecules.

The same study has been extended to Mordenite zeolite. It was clearly observed that base-acid post-treatment is efficient to obtain hierarchical Mordenite. This

hierarchical Mordenite had remarkably enhanced catalytic activity in the benzylation of benzene with benzyl alcohol. The apparent reaction rate constant is 15 times that for the parent Mordenite and twice that for the acid-leaching Mordenite and base-leaching Mordenite. Such outstanding catalytic performance should be attributed to more accessible acid sites and much better mass transfer ability from rich mesoporosity in HM-M.

Chapter 4. Performance of hierarchical zeolite supported catalysts in HDS of DBT and 4,6-DMDBT

4.1 Introduction

As one important refinery process, hydrodesulfurization (HDS) of transportation fuels received much attention in recent years. Due to the stringent demand of the environmental regulations, the sulfur level in fuels must be reduced to 10 ppm in many countries. However due to the presence of refractory sulfur-containing molecules such as 4,6-dimethyldibenzothiophene (4,6-DMDBT), deep desulfurization of diesel fuels is difficult to achieve owing to the effect of steric hindrance from the alkyl groups adjacent to the sulfur atom [102-105]. Therefore, the design and development of highly efficient HDS catalysts that can eliminate the effect of steric hindrance have been pursued.

The commercial catalysts are usually composed of molybdenum disulfide promoted by Co or Ni atoms and supported on alumina. The utilization of acidic supports has been suggested to improve catalytic performance. One explanation is that they enable dealkylation and isomerization of the alkyl substituents so that the effect of steric hindrance may be relieved [106] (see Fig. 1-6). The enhancement of activity was also related to the electron-deficient character of the sulfide particles, due to electronic transfer between the acidic zeolite and the active phase particles. Additionally, it was also proposed that the interaction of active phases with acidic supports could be weakened and thus the sulfidation degree of active phases may be improved. Based on these reasons, zeolites with strong acidity have been selected as supports of HDS catalysts [1]. However, due to their relatively small pore size, several problems such as rapid deactivation and diffusion limitation [107] were generally observed.

To remedy the disadvantage of microporous zeolites, hierarchical zeolites were developed and have attracted much attention because of the introduction of additional mesopores. Several studies present their use as supports for HDS catalysts. For example, noble metal catalysts were supported on mesoporous zeolites such as ZSM-5, Beta and Y for the HDS of 4,6-DMDBT [70,108,109]. The results indicated that these catalysts exhibited higher efficiency in desulfurization than those on alumina or mesoporous silica. CoMoS sulfide phases were supported on several mesoporous materials as a zeolite L, ZSM-5, beta and Mordenite (MOR), allowing to improve their activity in the HDS of FCC gasoline, DBT and 4,6-DMDBT, compared to those obtained on catalysts supported on conventional zeolites [104,107,110-112]. However, these researches were mainly based on the hierarchical zeolite obtained by templating

method, which was much expensive and unbeneficial for large-scale production.

On the other hand, it is well known that nitrogen-containing and aromatic compounds in fuels would inhibit the HDS activity of catalysts. Therefore, catalyst with good ability of HDS, hydrodenitrogenation (HDN) and hydrodearomatation (HDA) is required. Among the studied HDS catalysts, NiW catalysts have better hydrogenation properties than CoMo catalysts and have displayed superior catalytic activity in the HDA and HDN reactions [35,113,114]. For this reason the use of NiW supported on zeolite as HDS catalysts was also reported in the literature. It was indicated that zeolite supported NiW catalyst has a relative good activity in the HDS reactions [115-117]. However, to our best knowledge, the study of NiW catalysts supported on hierarchical zeolites has not been reported.

In the present work, we prepared NiW catalysts supported either on alumina, on a Mordenite commercial zeolite or on a hierarchical Mordenite obtained by acid-base-acid post-treatment. The catalytic performance of these catalysts was measured by the HDS of two model sulfur compounds: dibenzothiophene (DBT) and 4,6-dimethyldibenzothiophene (4,6-DMDBT). The activity and selectivity of the NiW catalyst based on hierarchical zeolite was compared to those obtained using the parent zeolite and alumina.

4.2 Preparation of Mordenite supported NiW catalyst

Commercial and hierarchical zeolite Mordenite supported NiW catalysts were prepared by wetness co-impregnation technic. The detailed preparation method could be observed in Chapter 2.2.3.

4.3 Characterization of Mordenite supported NiW catalyst

The powder XRD patterns (Fig. 4-1) of all the samples exhibited well resolved diffraction peaks, characteristics of MOR framework structure (JCPDS 43-0171), indicating the preservation of the zeolitic structure after the post treatment leading to the creation of mesopores and also after the impregnation of Ni and W. Moreover, diffraction peaks assigned to WO_3 and NiO were never observed in these patterns (JCPDS 43-1035 and 022-1189, respectively). This means that tungsten and nickel oxidic species were either completely amorphous or composed of crystallites smaller than 4 nm, in agreement with a good dispersion of these species [37,114,116].

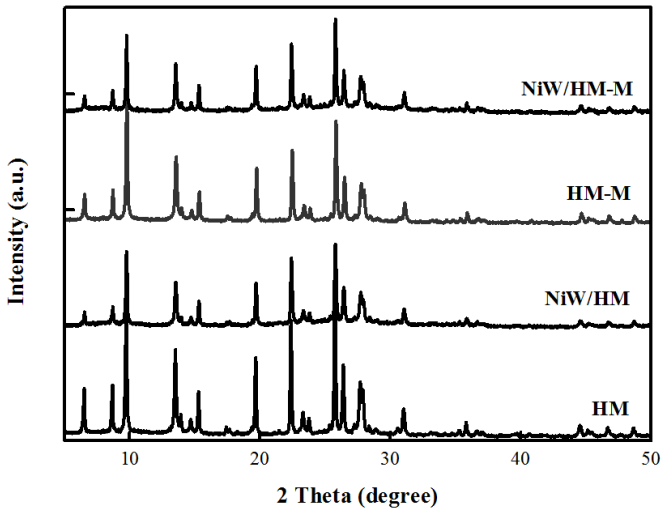

Fig. 4-1 X-ray diffraction patterns of HM and HM-M before and after impregnation

The N_2 sorption isotherms of all samples exhibited a hysteresis loop at high relative pressure characteristic of a type IV isotherm (Fig. 4-2).

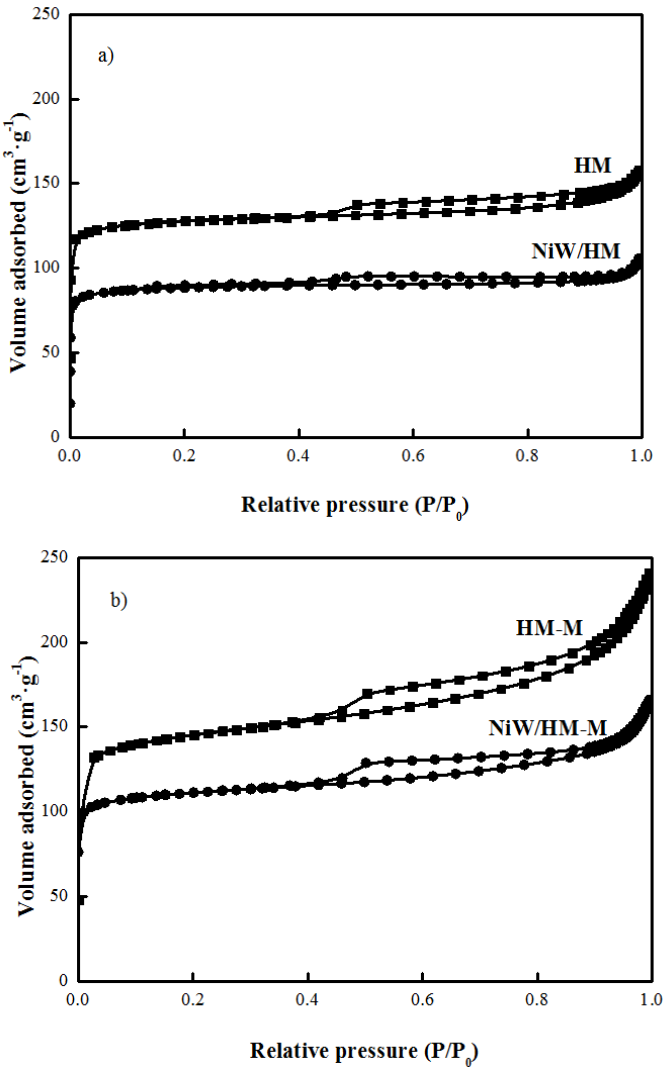

Fig. 4-2 N_2 adsorption-desorption isotherms of HM and HM-M before and after impregnation
a) HM and NiW/HM, b) HM-M and NiW/HM-M

This indicates the existence of hierarchical pores, particularly on HM-M based materials. The detailed sorption data are presented in Table 4-1. After acid-base-acid treatment, the micropore volume remained unchanged while the external surface area and the mesopore volume of the zeolite were increased by a factor of 2.5. If we assume that the area is only due to the support, we can express the surface area in m^2 of support instead of in m^2 per g of catalyst by removing the contribution of the weight gain consecutive to the introduction of the active phase, thus enabling a direct comparison with the properties of the support before impregnation. The textural properties of both HM and HM-M decreased after impregnation (except for the micropore volume), due to possible pore plugging or small collapse of the texture of the supports during impregnation. Moreover, the decrease in BET surface area and mesopore volume during impregnation appeared to be lower on HM-M than on HM support, 8% instead of 17% for the BET surface area and 17% instead of 43% for the mesopore volume, respectively. This indicates a better preservation of the textural properties in the case of hierarchical Mordenite. In addition, the micropore volume remained constant, suggesting that most of the NiW species were distributed on external surface and in the mesopores of Mordenite. Notably, the external surface area and mesopore volume for NiW/HM-M catalyst were respectively twice and four times higher than that of NiW/HM, suggesting a possible better accessibility to large molecules for this solid.

Table 4-1 Textural properties of Mordenite supports before and after impregnation

Sample	S_{BET} ($m^2 \cdot g^{-1}$)	S_{EXT} ($m^2 \cdot g^{-1}$)[a]	V_{meso} ($cm^3 \cdot g^{-1}$)[b]	V_{micro} ($cm^3 \cdot g^{-1}$)[a]
HM	411	45	0.07	0.17
NiW/HM	283 (341[c])	29 (35[c])	0.03 (0.04[c])	0.14 (0.17[c])
HM-M	471	112	0.17	0.18
NiW/HM-M	360 (434[c])	61 (73[c])	0.12 (0.14[c])	0.15 (0.18[c])

[a] *t*-plot method; [b] BJH method; [c] data calculated by deducting the effect of NiW mass.

The acidity of both HM and HM-M samples was determined by pyridine adsorption (Table 3-9). The acid-base-acid treatment of the support led to an increase of the number of Lewis and Brönsted sites, from 23 and 104 μmol g^{-1} on HM to 87 and 201 μmol g^{-1} on HM-M, respectively, despite the increase of the Si/Al ratio induced by the treatment. The higher number of acid sites in HM-M can be related to its larger specific surface area as well as to better accessibility of pyridine due to mesopore creation.

Fig. 4-3 presents the XPS spectra of W4f for the sulfided catalysts. The decomposition of the photopeaks showed three contributions attributed to W^{6+} in an oxidic environment (W4f5/2: 36.2 and W4f3/2: 38.3 eV), W^{5+} as oxysulfide species (33.2 and 35.4 eV) and W^{4+} sulfided species (32.3 and 34.4 eV) [74,75,118,119].

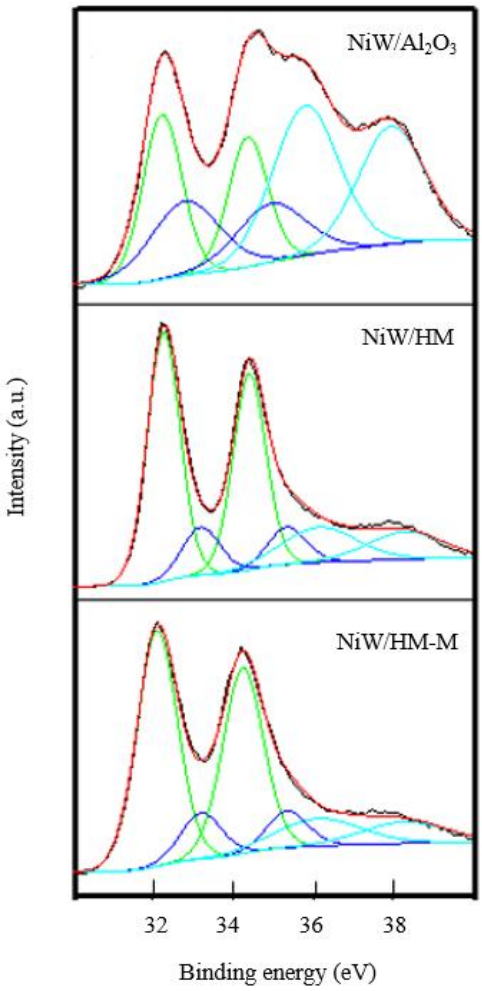

Fig. 4-3 Emission region of W4f XPS spectra of NiW/Al_2O_3, NiW/HM and NiW/HM-M sulfided at 673 K with their fit decomposition curves
experimental (black), simulation (red), WS_2 (green), WO_xS_y (blue), W^{6+} (cyan)

Table 4-2 shows the constraints between peak area, full width at half maximum (FWHM) and peak position used for the decomposition of the photopeaks in the emission region of W4f XPS spectra.

Table 4-2 Fit parameters for XPS decomposition in the energy emission region of W4f

Factor	WS 4f 7/2	WS 4f 5/2	WOS 4f 7/2	WOS 4f 5/2	WO 4f 7/2	WO 4f 5/2
Area	A_1	A_1*0.788	A_2	A_2*0.788	A_3	A_3*0.788
FWHM	B_1（1-3）	B_1*1	B_2（0.2-5）	B_2*1	B_3（1-3）	B_3*1
Pos.	C_1（31-32.5）	C_1+2.15	C_2（32-33）	C_2+2.15	C_3（34.5-37）	C_3+2.15

The results obtained from these decompositions are listed in Table 4-3. The sulfidation degree of tungsten on NiW/Al_2O_3 was found at 30%. This value can be compared to that of a NiW catalyst with a sulfidation degree of tungsten of 49% when supported on alumina (with 27% WO_3) [120], and of 42% when supported on amorphous silica alumina (with 17% WO_3) [75]. Similar sulfidation degrees were

obtained for NiW/HM and NiW/HM-M, with much higher values than on alumina, 65 and 69% respectively. This result indicates that tungsten could be well sulfided over zeolite, which might be attributed to the weak interaction between active phase and zeolite support compared to alumina as stated in the literature [37,114,116].

Table 4-3 Proportion of W species in sulfided NiW/Al_2O_3, NiW/HM and NiW/HM-M

Sample	WS_2 sulfidation degree (%)	WO_xS_y (%)	W^{6+} (%)
NiW/Al_2O_3	30	24	46
NiW/HM	65	14	21
NiW/HM-M	69	14	17

The XPS spectra for Ni2p are presented in Fig. 4-4

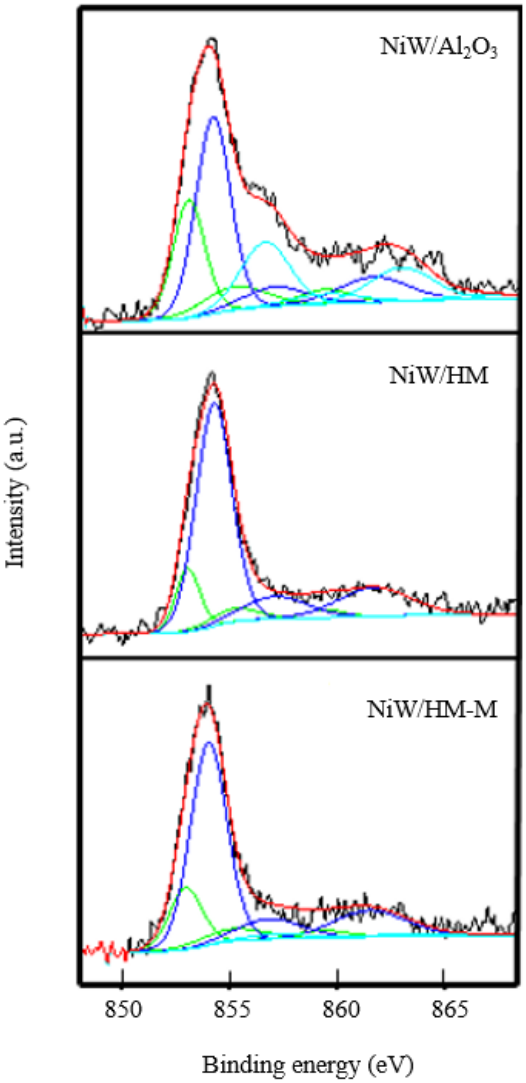

Fig. 4-4 Emission region of Ni2p XPS spectra of NiW/Al_2O_3, NiW/HM and NiW/HM-M sulfided at 673 K with their fit decomposition curves
experimental (black), simulation (red), Ni_xS_y (green), NiWS (blue), Ni^{2+} (cyan).

Their decomposition shows three contributions: sulfidic NixSy (Ni2p3/2: 852.6 eV, Ni2p1/2: 869.8 eV), NiWS (Ni2p3/2: 853.7 eV, Ni2p1/2: 870.9 eV) and an oxidic phase Ni^{2+} (Ni2p3/2: 856.4 eV, Ni2p1/2: 873.8 eV) [74,75,118,119]. The decomposition of XPS for Ni2p could be realized using the fit parameters indicated in table 4-4 [118]. Here, the satellite photopeaks (*) are the «ghost» of the main peak, such as the spin splitting, shakeup of the principal peak.

Table 4-4 Fit parameters for XPS decomposition in the energy emission region of Ni2p

	Area	FWHM	Pos.
NiS	A1	B1（1-2）	C1（852.8-853）
NiS*	A1*0.4	B1*2	C1+2.1
NiS*	A1*0.2	B1*1.6	C1+6.2
NiWS	A2	B2（1-2.5）	C2（853.9-854.2）
NiWS*	A2*0.18	B2*1.8	C2+2.8
NiWS*	A2*0.26	B3*2	C3+7.3
NiO	A3	B3（1-3.5）	C3（855.5-857）
NiO*	A3*0.22	B3*1.4	C3+2.8
NiO*	A3*0.67	B3*1.3	C3+6.2
NO*	A3*0.11	B3*1.3	C3+10.1

The proportion of NiO, NixSy and NiWS (promotion degree) in the catalysts were calculated and are listed in Table 4-5. A proportion of 44% NiWS was obtained in NiW/Al_2O_3, which was similar to the value of 37% reported on a sulfided NiW/ASA catalyst [75]. Interestingly, the use of HM and HM-M as supports led to better promotion of the sulfide phase, the proportion of NiWS being 82% in NiW/HM and 73% in NiW/HM-M. If the sulfidation degree of molybdenum or tungsten has been evaluated in the literature, no studies reported the promotion degree of the sulfide phase supported on zeolites determined by decomposition of the XPS Ni2p photopeak.

Table 4-5 Proportion of Ni species in sulfided NiW/Al_2O_3, NiW/HM and NiW/HM-M

Sample	NiWS promotion degree (%)	Ni_xS_y (%)	Ni^{2+} (%)
NiW/Al_2O_3	44	27	29
NiW/HM	82	18	<5
NiW/HM-M	73	23	<5

Representative TEM images of all the sulfided catalysts are shown in Fig. 4-5. All samples exhibited the typical structure of the layered WS_2 phase, with an interplanar spacing of 0.65 nm, corresponding to the (002) planes of the WS_2 crystal [121]. The

WS_2 slabs appeared to be well dispersed over Al_2O_3 and HM-M (Fig. 4-5a and 4-5c), the sulfided NiW/Al_2O_3 sample showing mainly mono slabs, while more stacked slabs were present on the sulfided NiW/HM-M. On the contrary large agglomerations of slabs were observed on NiW/HM (Fig. 4-5b), probably in relation with the low external surface of the support. As observed on the images, the size of active phase is larger than the micropore size in Mordenite, indicating that the WS_2 slabs are mainly located outside the micropores, in accordance with results obtained from N_2 sorption. These observations clearly show that the presence of mesopores on HM-M allowed a better dispersion of the active phase, by offering larger surface for WS_2 deposition.

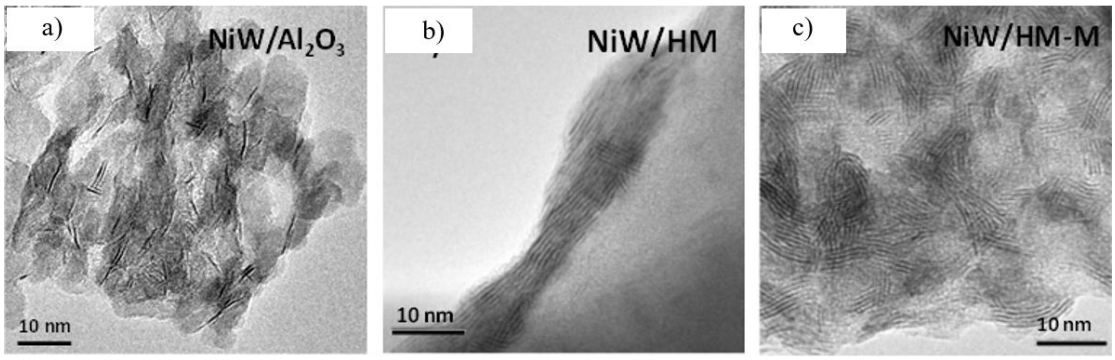

Fig. 4-5 HRTEM images of NiW catalysts supported on HM, HM-M and Al_2O_3 after sulfidation at 673 K
a) NiW/Al_2O_3, b) NiW/HM, c) NiW/HM-M

By statistical analysis of the images, the distribution in slab length and stacking of the WS_2 slabs were obtained, as shown in Fig. 4-6. Due to the heavy agglomeration observed on sulfided NiW/HM, the statistical data is not available for this sample. On the sulfided NiW/Al_2O_3, the WS_2 slab length was between 1 and 10 nm with an average length L of 4.8 nm and an average stacking N of 1.2, values similar to those reported in the literature (L = 3.3 nm and N = 1.3 for 19% WO_3, L = 4.1 nm and N = 1.8 for 27% WO_3 [120,122]). Comparatively, the length of WS_2 slabs in NiW/HM-M was distributed in a relatively wide range, the majority of the slabs showing a length between 1 and 13 nm. The calculated average length of 5.6 nm and the calculated average stacking degree of 4.8 on sulfided NiW/HM-M appeared to be much larger than those obtained on alumina, in agreement with literature data obtained on NiW supported on Y zeolites. Average length between 9 and 16 nm and average stacking between 2.4 and 3.7 were reported by Ding et al., for NiW catalysts supported on zeolites beta [37,114,116]. This can be explained by a weaker interaction developed on the zeolite support by the sulfide phase compared to alumina, well known for its dispersion ability.

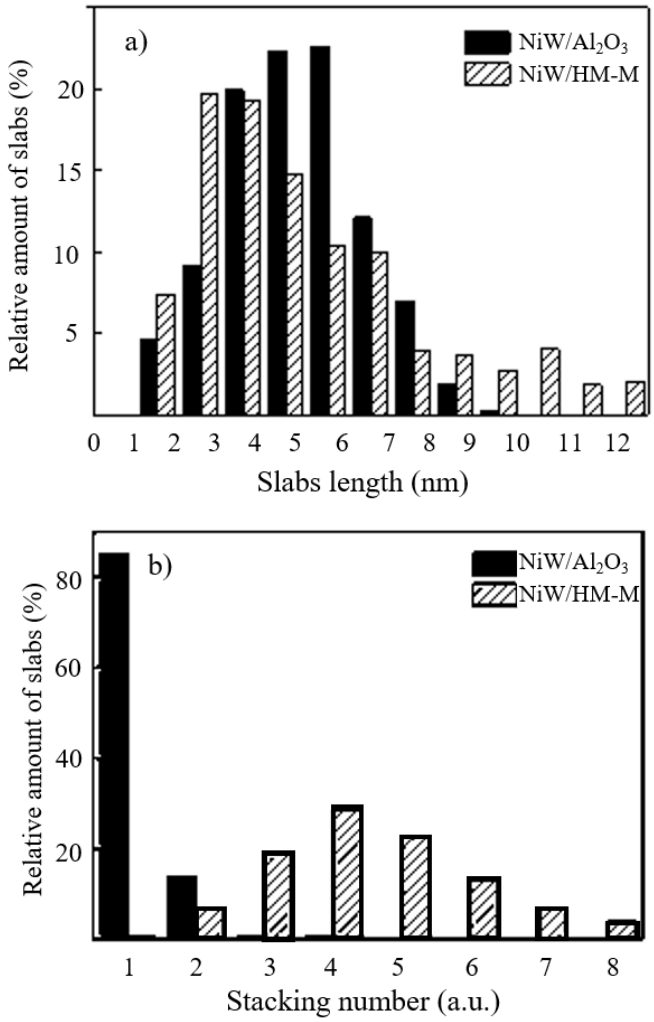

Fig. 4-6 Statistic results of the WS_2 slabs over NiW/Al_2O_3 and NiW/HM-M
a) Length distribution, b) Stacking number

4.4 Performance of Mordenite supported NiW catalyst

To test the deep desulfurization ability of the synthesized catalysts (NiW/Al_2O_3, NiW/HM and NiW/HM-M), their catalytic performances were evaluated in desulfurization of dibenzothiophene (DBT) and 4,6-dimethyldibenzothiophene (4,6-DMDBT) at 613K under 4 MPa as total pressure.

4.4.1 Activity in the HDS of DBT

Over sulfide catalysts supported on alumina, it is generally accepted that DBT and 4,6-DMDBT convert by two routes: the direct desulfurization pathway (DDS) yielding biphenyls and the hydrogenation pathway (HYD) yielding cyclohexylbenzenes. However, the use of sulfide catalysts containing acidic supports (HM and HM-M) in DBT HDS led to the presence of other products compared to those obtained over NiW/Al_2O_3. In addition to products already observed from DBT

on the conventional catalyst (tetrahydrodibenzothiophene and biphenyl), three methyldibenzothiophene isomers (MDBT), four dimethyldibenzothiophene isomers (DMDBT), two methylbiphenyl isomers (MBPh), three dimethylbiphenyl isomers (DMBPh) and benzene (Bz) were observed in the reactional mixture. Under these experimental conditions, we verified that cyclohexylbenzene (the main HYD product obtained over NiW/Al_2O_3) was totally converted into cyclohexane and benzene likely by hydrocracking due to the presence of strong acid sites on zeolites. This observation is in good agreement with results reported by several authors [105,123]. Moreover, it was verified that biphenyl was unreactive in presence of NiW/HM. In addition, MDBT and DMDBT isomers and their desulfurized products were also observed in very low amounts over NiW/HM and NiW/HM-M. The formation of these compounds can be explained by alkylation reaction (methylation) due to the presence of DMDS in the model feed. Such reaction was already observed for the transformation of DBT by Bataille et al. using a CoMo/HY catalys [21]. According to the detected products, the main reaction routes of DBT over Mordenite supported catalysts could be drawn, as indicated in Fig. 4-7.

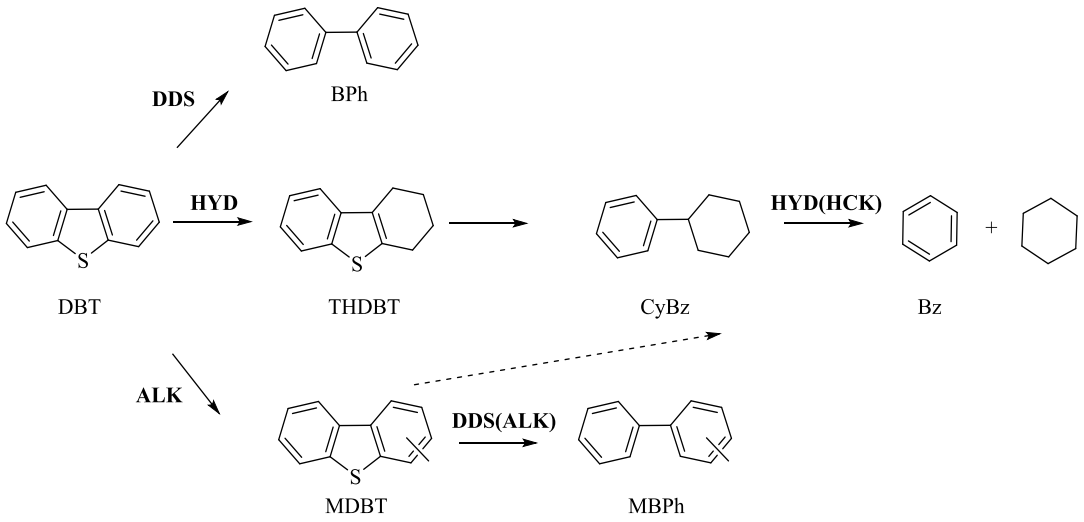

Fig. 4-7 Proposed main reaction pathways of DBT over Mordenite supported catalysts

Both NiW sulfide phase supported on Mordenite zeolites (NiW/HM and HM-M) appeared to be less efficient than NiW/Al_2O_3 for the HDS of DBT, the HDS activity being higher on alumina (2.19 $mmol \cdot h^{-1} \cdot g^{-1}$) than on zeolite based catalysts (0.37 $mmol \cdot h^{-1} \cdot g^{-1}$ for NiW/HM and 0.98 mmol h^{-1} g^{-1} for NiW/HM-M) as illustrated in Fig. 4-8. Nevertheless XPS analysis evidenced a higher NiWS percentage on catalysts supported on HM (82%) and HM-M (73%) than on alumina (44%), indicating that the promotion degree is not linked to catalytic activity. This suggests that a great amount of sites are inaccessible for reactants or deactivated, when the Mordenite zeolite is used as support. The occurrence of deactivation will be further discussed in chapter 5. The agglomerated active phase or active phase located in micropores would exhibit

low accessibility to reactants. Another possibility is that the use of zeolite support could lead to less active site than alumina as a result of support effect on the active phase.

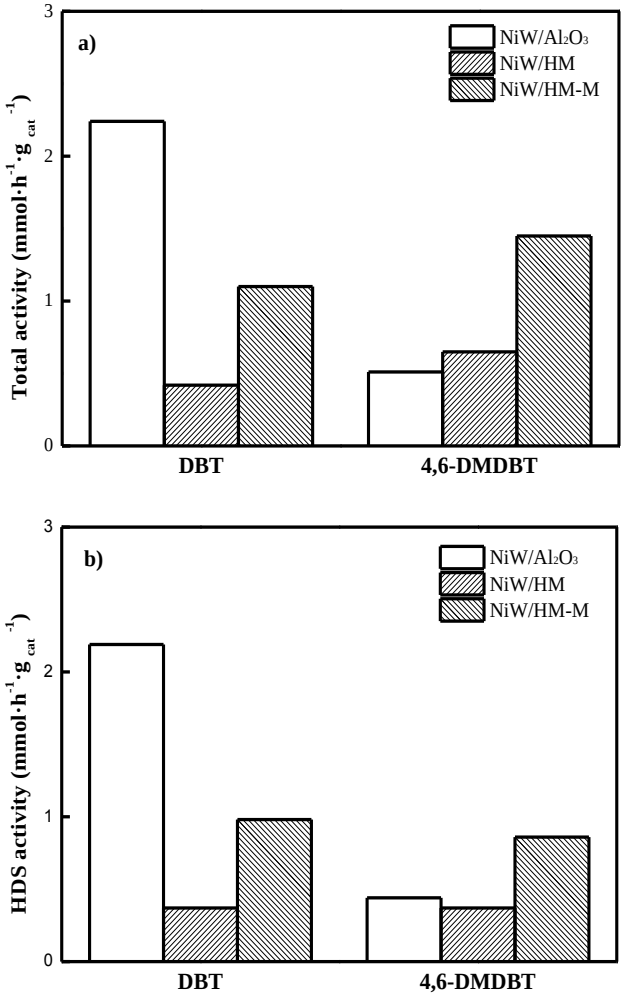

Fig. 4-8 Transformation of DBT and 4,6-DMDBT at 613K under 4 MPa of total pressure over NiW/Al_2O_3, NiW/HM and NiW/HM-M
a) total activity, b) desulfurization activity

The differences in activity between NiW/HM and NiW/HM-M supported the hypothesis about accessibility. The use of the modified Mordenite zeolite as catalytic support of the sulfide phase (NiW/HM-M) instead of the parent zeolite (NiW/HM) allows an increase of the HDS activity by a factor of 2.6 (Fig. 4-8b). This result can be attributed to the presence of the mesopores allowing a better dispersion of the active phase as evidenced by TEM (Fig. 4-5) as well as a better diffusion of reagents, and hence a higher accessibility of sulfur molecules to active sites.

4.4.2 Activity in the HDS of 4,6-DMDBT

In the presence of both NiW/HM and Ni/HM-M catalysts, other sulfur and desulfurized products were detected. Two isomers of 4,6-dimethyldibenzothiophene (iDMDBT) were observed in large quantities, 3,6-dimethyldibenzothiophene being the main isomer formed. By the DDS route, 3,6-dimethyldibenzothiophene yielded 3,4'-dimethylbiphenyl, the main product of the DDS(ISOM) pathway. As in the case of DBT, the main hydrogenation product of 4,6-DMDBT (MCHT) was totally converted into toluene and methylcyclohexane. Similarly to results observed with DBT, alkylation products were also observed in trace amounts. According to the detected products, the main reaction routes of 4,6-DMDBT over Mordenite supported catalysts could be drawn, as indicated in Fig. 4-9.

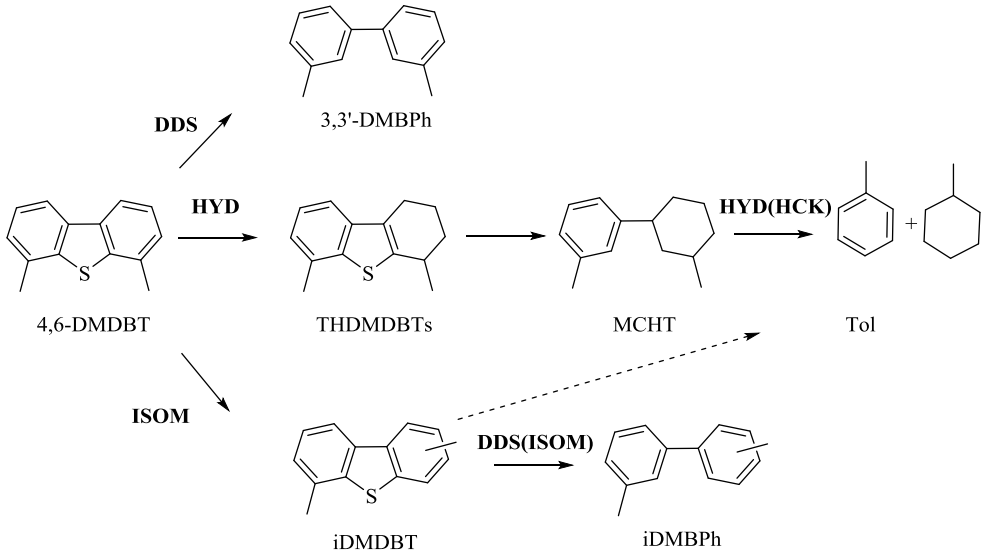

Fig. 4-9 Proposed main reaction pathways of 4,6-DMDBT over Mordenite supported catalysts

On NiW/Al_2O_3, the total activity using DBT and 4,6-DMDBT was largely dominated by HDS activity. As expected, 4,6-DMDBT was found 4.4 times less reactive than DBT over NiW/Al_2O_3 (Fig. 4-8a) and 5 times less reactive in desulfurization (Fig. 4-8b). This difference in reactivity between both model molecules is of the same order of magnitude than the values measured over a $NiMo/Al_2O_3$ commercial catalyst using the same experimental conditions [21]. It is well known that the presence of methyl groups in position of 4 and 6 leads to a significant inhibition of the desulfurization rate of dibenzothiophenic compounds due to steric hindrance [21,124-127].

Interestingly, the 4,6-DMDBT HDS activity of NiW/Al_2O_3 is relatively close to the value measured over NiW/HM (0.44 $mmol \cdot h^{-1} \cdot g^{-1}$ for the former and 0.37 $mmol \cdot h^{-1} \cdot g^{-1}$ for the latter), indicating that the activity of the sulfide phase in the HDS of 4,6-DMDBT does not follow the trend observed for the HDS of DBT. This could

correspond to the presence of two types of sites, active either only in DBT HDS or in both DBT and 4,6-DMDBT HDS, hypothesis already suggested in the literature [11,128], depending probably on their localization on the slabs and/or on the intrinsic nature induced by the nature of the support. Zeolites based catalysts could thus contain mainly sites active in both DBT and 4,6-DMDBT. 4,6-DMDBT was 2.3 times more reactive over NiW/HM-M than over the NiW/HM catalyst, this ratio being of the same order of magnitude as that mentioned above in the HDS of DBT. As previously proposed, this improvement can be related at least in part to the presence of mesopores in HM-M support.

4.4.3 Selectivity in the HDS of DBT

Table 4-6 indicated the distribution of obtained products over various catalysts in the HDS of DBT.

Table 4-6 Distribution of products obtained from the transformation of dibenzothiophene (DBT) over NiW/Al_2O3, NiW/HM and NiW/HM-M at 613K under 4 MPa as total pressure

Routes	Products	NiW/Al_2O_3	NiW/HM	NiW/HM-M
	Bz	0	34	32
HYD	CyBz	31	0	0
	THDBT	2	5	6
DDS	BPh	67	48	47
DDS（ALK）	iMBPh+iDMBPh	0	8	10
ALK	iMDBT+iDMDBT	0	5	5
DDS/HYD		1.98	1.25	1.27

Figure 4-10 shows the activity of the different routes of DBT transformation described above over the three catalysts. Over NiW/Al_2O_3, DBT is mainly desulfurized by the DDS route (DDS/HYD selectivity close to 2). In the presence of NiW/HM catalyst, both main desulfurization routes (HYD and DDS) were affected compared to the NiW/Al_2O_3 catalyst. Moreover, the comparison of the DDS/HYD ratios on NiW/Al_2O_3 (1.98) and on NiW/HM (1.25) indicates that the DDS route was more affected than the HYD route when zeolite was used as support. As evidenced by TEM analysis, the stacking of the WS_2 phase appears to be much higher on zeolite support than on alumina. In accordance with the rim-edge model [129], the DDS activity should be less reduced than the HYD activity. As the opposite was observed, the selectivity difference cannot be explained by the modification of the morphology of the sulfide phase. The differences in DDS/HYD selectivity could thus be related to the nature of the active sites depending on the support used. Moreover XPS analysis indicated that the promotion degree was much higher on zeolite supported catalyst

(82%) compared to alumina catalyst (44%), which could support the fact that zeolite used as support induces modifications in the active sites.

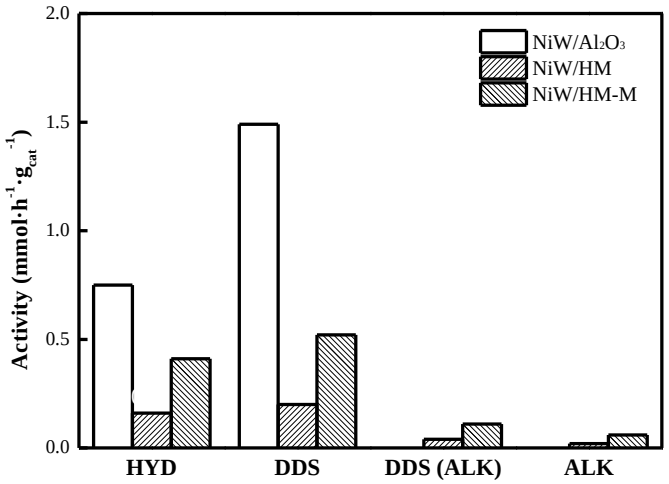

Fig. 4-10 Activity of the different desulfurization pathways for the transformation of DBT at 613K under 4 MPa of total pressure over NiW/Al_2O_3, NiW/HM and NiW/HM-M.

The use of the hierarchical zeolite as support led to the same DDS/HYD ratio than on NiW/HM, indicating that the creation of mesoporosity has no influence on the selectivity and in the nature of the active sites. As a matter of fact similar sulfidation and promotion degrees were obtained by XPS over both NiW/HM and NiW/HM-M.

4.4.4 Selectivity in the HDS of 4,6-DMDBT

Concerning the reactivity of 4,6-DMDBT over NiW/Al_2O_3, the conversion was mainly through the HYD route leading to 3-(3'-methylcyclohexyl)toluene (MCHT) and three dimethyltetrahydrodibenzothiophene isomers (iDMTHDBT) (Table 4-7), whereas 3,3'-dimethylbiphenyl was the only product formed by the DDS route. Contrary to the reactivity of DBT, the main reaction route of 4,6-DMDBT was the HYD way (DDS/HYD selectivity near 0.3). These results are in agreement with those reported in the literature over Mo based catalysts [21], confirming that the presence of methyl groups in position 4 and 6 strongly inhibits the DDS way whereas the HYD route is less affected. On the zeolite supported catalysts, the DDS/HYD ratios obtained from 4,6-DMDBT transformation were lower than the ratio measured over NiW/Al_2O_3 (Table 4-7), in accordance with the results observed from DBT reaction already discussed.

Table 4-7 Distribution of products obtained from the transformation of 4,6-DMDBT over NiW/Al_2O_3, NiW/HM and NiW/HM-M at 613K under 4 MPa as total pressure

Routs	Products	NiW/Al_2O_3	NiW/HM	NiW/HM-M
	Tol	0	36	32
HYD	MCHT	63	0	0
	THDMDBT	9	7	6
DDS	3,3-DMBPh	23	8	9
DDS（ISOM）	3,4-DMBPh+4,4-DMBPh	0	10	12
HCK	iMBPh	0	3	7
ISOM	iDMDBT	5	33	33
ALK	iMBPh	0	3	1
	DDS/HYD	0.32	0.18	0.24

Due to the acidic properties of the zeolitic supports, 4,6-DMDBT was mainly isomerized into 3,6-DMDBT (ISOM way), which is known to be more reactive than 4,6-DMDBT [20,105]. The use of a mesoporous support (NiW/HM-M) allowed to favor isomerization of 4,6- DMDBT, the ISOM activity being doubled, and hence the production of dimethylbiphenyl isomers (Fig. 4-11). This result explains why the desulfurization is the most favored over NiW/HM-M.

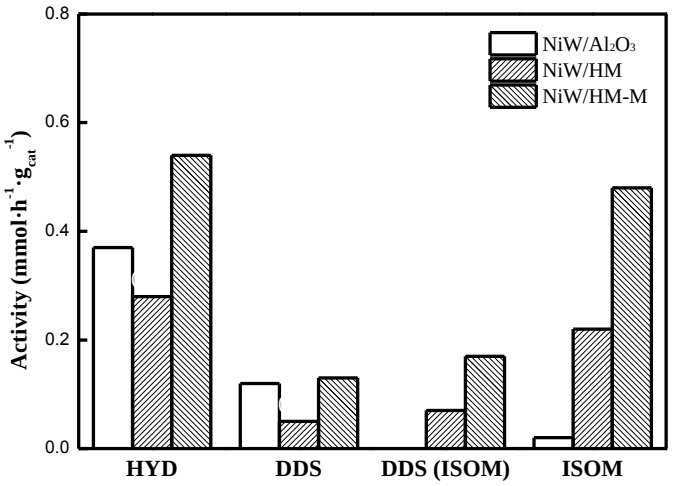

Fig. 4-11 Activity of the different desulfurization pathways for the transformation of 4,6-DMDBT at 613K under 4 MPa of total pressure over NiW/Al_2O_3, NiW/HM and NiW/HM-M

The higher reactivity of 4,6- DMDBT over the hierarchical zeolite supports catalyst due to this new transformation route (ISOM) can be related to the acidity properties of the supports: indeed HM-M possessed a larger number of Lewis and Brönsted acid sites (87 and 201 $\mu mol \cdot g^{-1}$ respectively) than HM (23 and 104

μmol·g^{-1}). In addition, the rate of 4,6-DMDBT isomerization is most likely higher than its direct desulfurization since isomerized products were observed in large quantities compared to the 3,3-dimethylbiphenyl formed by the DDS way. Moreover, 3,6-DMDBT, the main isomer of 4,6-DMDBT, can be converted into 3,4'-dimethylbiphenyl by the DDS(ISOM) route and into toluene and methylcyclohexane by HYD(HCK). The highest value of the HYD activity measured over NiW/HM-M (0.54 mmol·h^{-1}·g^{-1}) compared to the one determined over NiW/Al_2O_3 (0.37 mmol·h^{-1}·g^{-1}) could be explained through the participation of the HYD route of the isomerized products (3,6-DMDBT mainly), which led to the same products (toluene and methylcyclohexane) as those formed from the HYD route of 4,6-DMDBT.

4.5 Extended study on Beta supported NiW catalsyts

Catalytic evaluation of hierarchical Beta supported catalysts (NiW/HB-M) was carried out. Hierarchical zeolite Beta HB-M was prepared by the base-acid post treatment. The preparation method of commercial and hierarchical Beta supported catalysts was similar to that of hierarchical Mordenite supported catalysts. The detailed preparation method was described in Chapter 2.2.3.

The detailed characterizations of zeolite Beta supported catalysts could be observed in Chapter 5. The particle size of HB was much smaller (about 150 nm) than that of HM (0.5-1 μm), and the external surface area of HB was larger than that of HM and HM-M. Thus, HB could offer more available surface for WS_2 deposition. Indeed, no agglomeration of sulfided NiW active phase could be observed over both NiW/HB and NiW/HB-M. Moreover, NiW/HB exhibited higher sulfidation degree and promotion degree than NiW/HB-M.

4.5.1 Activity of Beta supported catalysts

Fig. 4-12 illustrates the activity of NiWcatalysts supported on Al_2O_3, HB, HB-M and HM-M. As in the case of Mordenite supported solids, Beta zeolite supported catalysts also exhibited less efficient activity than NiW/Al_2O_3 in the HDS of DBT. The total activity of NiW/HB (1.26 mmol·h^{-1}·g^{-1}) and NiW/HB-M (1.10 mmol·h^{-1}·g^{-1}) was only about half of that of NiW/Al_2O_3 (2.24 mmol·h^{-1}·g^{-1}) (Fig. 4-12a). Similar trend was observed in the comparison of desulfurization activities (Fig. 4-12b). XPS analysis revealed higher promotion degree on NiW/HB (52%) than on NiW/Al_2O_3 (44%) suggesting that parti of active phase over Beta zeolite supported catalyst is inaccessible or less active compared to NiW/Al_2O_3, as in the case of Mordenite supported solids.

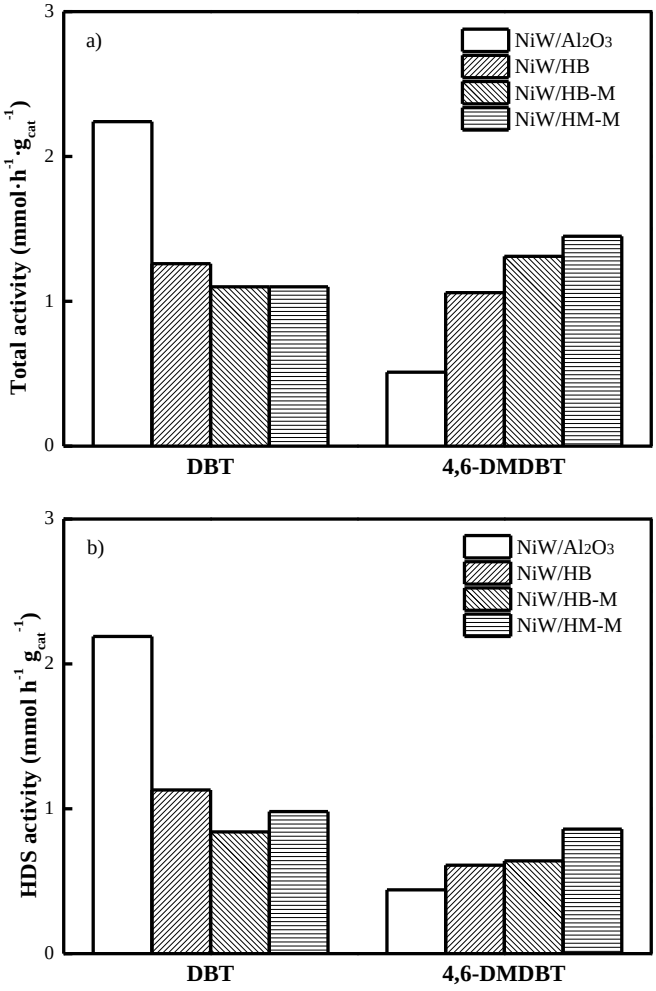

Fig. 4-12 Transformation of DBT and 4,6-DMDBT at 613K under 4 MPa of total pressure over NiW/Al_2O_3, NiW/HB and NiW/HB-M
a) total activity, b) desulfurization activity

Contrary to Mordenite support, the use of hierarchical zeolite Beta instead of microporous zeolite Beta as the catalyst support did not improve the performance of the catalysts. Total and HDS activities in transformation of DBT are even slightly decreased: from 1.26 $mmol \cdot h^{-1} \cdot g^{-1}$ to 1.1 $mmol \cdot h^{-1} \cdot g^{-1}$. This might be explained by the fact that no agglomeration was observed over NiW/HB, contrary to HM supported catalyst. Thus, the use of hierarchical zeolite could not greatly improve the dispersion of active phases. Moreover active phase on NiW/HB-M was less sulfided and promoted than that over NiW/HB (sulfidation degree: NiW/HB 73%; NiW/HB-M 58%; Promotion degree: NiW/HB 52%, NiW/HB-M 33%). However, the activity of NiW/HB and NiW/HB-M were similar to that of NiW/HM-M.

In the transformation of 4,6-DMDBT, NiW/HB-M exhibited 30% higher total activity than NiW/HB (1.31 $mmol \cdot h^{-1} \cdot g^{-1}$ and 1.06 $mmol \cdot h^{-1} \cdot g^{-1}$ respectively), while HDS activities were found similar (0.64 $mmol \cdot h^{-1} \cdot g^{-1}$ and 0.61 $mmol \cdot h^{-1} \cdot g^{-1}$

respectively). This might be attributed to the higher number of accessible acid sites in HB-M (more than 3 times as that of HB), beneficial to the isomerization of 4,6-DMDBT. This result confirmed that hierarchical zeolite supported catalyst had potential application in HDS of 4,6-DMDBT due to their enhanced accessible acidity. Moreover, the similar HDS activity of NiW/HB and NiW/HB-M could be explained by the low activity of low steric hindrance molecules over NiW/HB-M (as illustrated by their activity in the HDS of DBT), which would influence the further desulfurization of 4,6-DMDBT isomers. This result suggested that the improvement of NiW/HB-M might be focused on its low activity with low steric hindrance molecules.

4.3.2 Selectivity of Beta supported catalysts

The detected products over NiW/HB and NiW/HB-M in the HDS of DBT are listed in Table 4-8. They were similar to those obtained over NiW/HM and NiW/HM-M, indicating that the reaction routes obtained by Mordenite supported catalysts could be applied in Beta supported catalysts. Moreover, it could be observed that the product distribution over NiW/HB and NiW-HB-M are slightly different, which might be related to their slightly different sulfidation and promotion degree.

Table 4-8 Distribution of products obtained from the transformation of dibenzothiophene (DBT) over NiW/Al_2O_3, NiW/HB and NiW/HB-M at 613K under 4 MPa as total pressure

Routes	Products	NiW/Al_2O_3	NiW/HB	NiW/HB-M
	Bz	0	34	32
HYD	CyBz	31	0	0
	THDBT	2	3	4
DDS	BPh	67	48	33
DDS（ALK）	iMBPh+iDMBPh	0	9	12
ALK	iMDBT+iDMDBT	0	6	19
DDS/HYD		1.98	1.20	0.92

Fig. 4-13 compares the activities of the different routes of DBT transformation over the four catalysts. It could be observed that NiW/HB-M exhibited higher ALK and DDS(ALK) activity than NiW/HB, which might be attributed to the higher number of accessible acid sites in HB-M. However, NiW/HB-M showed lower DDS and HYD activity than NiW/HB, which might be due to its lower sulfidation and promotion degree.

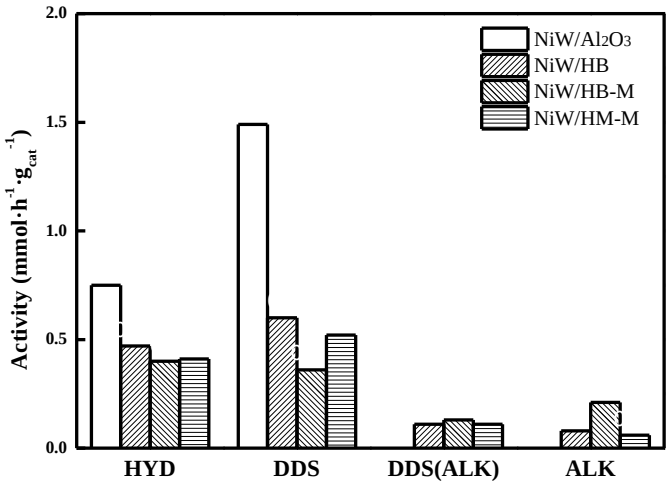

Fig. 4-13 Activity of the different desulfurization pathways for the transformation of DBT at 613K under 4 MPa of total pressure over NiW/Al_2O_3, NiW/HB and NiW/HB-M

The detected products over NiW/HB and NiW/HB-M in the HDS of 46-DMDBT were listed in Table 4-9. They are similar to those detected over NiW/HM and NiW/HM-M, suggesting again that the reaction routes obtained by Mordenite supported catalysts was suitable for Beta supported catalysts.

Table 4-9 Distribution of products obtained from the transformation of 4,6-DMDBT over NiW/Al_2O_3, NiW/HB and NiW/HB-M at 613K under 4 MPa as total pressure

Routes	Products	NiW/Al_2O_3	NiW/HB	NiW/HB-M
	Tol	0	30	21
HYD	MCHT	63	0	0
	THDMDBT	9	8	5
DDS	3,3-DMBPh	23	9	9
DDS（ISOM）	3,4-DMBPh+4,4-DMBPh	0	14	12
HCK	iMBPh	0	-	-
ISOM	iDMDBT	5	30	37
ALK	iMBPh	0	-	-
DDS/HYD		0.32	0.24	0.35

Fig. 4-14 compares the activities of the different routes of 4,6-DMDBT transformation over the four catalysts. As discussed before, more acid sites on support could help to decrease the difficulty of 4,6-DMDBT HDS by increasing the activity of ISOM routes. However, The size of 4,6-DMDBT should be taken in count here. 4,6-DMDBT is much larger than micropores in zeolite. Thus, only accessible acid

sites are available for the isomerization of 4,6-DMDBT. Although HB-M possessed less acid sites than HB, acid sites on HB-M exhibited much better accessibility for large molecules. Based on this understanding, the higher ISOM activity of NiW/HB-M than that of NiW/HB could be attributed to their different number of accessible acid sites. Additionally, it could be clearly observed in Fig. 4-14 that the higher activity of NiW/HB-M than that of NiW/HB in the HDS of 4,6-DMDBT was fully due to the improved ISOM activity (because the activity of NiW/HB-M in other reaction routes were lower or similar than that of NiW/HB), which was in accordance with the result obtained over hierarchical zeolite Mordenite supported catalyst.

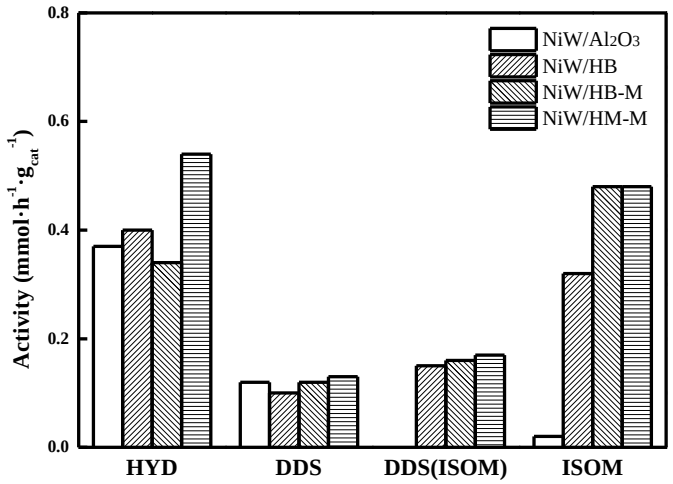

Fig. 4-14 Activity of the different desulfurization pathways for the transformation of 4,6-DMDBT at 613K under 4 MPa of total pressure over NiW/Al_2O_3, NiW/HB and NiW/HB-M

4.6 Brief summary

NiW catalysts supported on Al_2O_3, commercial Mordenite and hierarchical Mordenite obtained by acid-base-acid treatment were prepared by co-impregnation technique. NiW/Al_2O_3 catalyst exhibited better HDS activity than NiW/HM and NiW/HM-M in the transformation of DBT even if higher promotion degree was determined by XPS on the zeolite supported catalysts. This suggests that sites active on the alumina supported catalyst are inaccessible or less active when Mordenite, modified or not, is used as support.

Comparatively, NiW/HM and NiW/HM-M displayed superior catalytic performance than NiW/Al_2O_3 in the transformation of 4,6-DMDBT due to the introduction of additional reaction route (isomerization) resulting from the acidity of the zeolitic supports. Furthermore, NiW/HM-M exhibited higher catalytic activity than NiW/HM in the transformation of both DBT and 4,6-DMDBT. This can be explained by (i) better dispersion of the sulfide NiW phase observed by TEM when

deposited on the hierarchical zeolite; (ii) enhanced accessibility of the sulfur model compounds to the active sites due to the creation of mesoporosity by base-acid treatment; (iii) in the case of 4,6-DMDBT, the higher acidity and better accessibility of acid sites in NiW/HM-M compared to that of NiW/HM leading to an improvement of its reactivity in isomerization.

This study clearly demonstrates that the use of hierarchical Mordenite as support of NiW based HDS catalyst is beneficial in the desulfurization of refractory sulfur molecules, combining the acidic properties of the zeolite and the mesoporosity allowing better accessibility to the active sites. Additionally, such an improvement could also be observed with hierarchical zeolite Beta supported catalyst in the HDS of 4,6-DMDBT.

Chapter 5. Restraining deactivation of hierarchical zeolite supported catalysts

5.1 Introduction

Transition metal Ni(Co)Mo(W) sulfide (TMS) catalysts are important industrial catalysts for hydrodesulfurization (HDS) of transportation fuels in oil refinery. Generally, TMS catalysts need to be supported on a carrier like alumina and the support plays a vital role in determining the catalytic activity and stability [130,131]. It is generally accepted that a support with strong Brönsted acid sites is beneficial for promoting the HDS performance of catalysts [26,132,133] because it could enhance the adsorption property of sulfur-containing molecules and optimizes the electron property of active phases [48,134,135]. Thus, zeolites with such acid sites have been widely investigated as support of HDS catalysts [1]. However, some studies indicated that zeolites supported TMS catalysts exhibited lower catalytic activity than alumina supported TMS catalysts in some HDS reactions [19,20,105,107,117]. One explanation is that active phases located in micropores of zeolites might be difficult to access for the reactants. Additionally, it has been reported that microporous zeolite based TMS catalysts underwent a significant deactivation, which could be stabilized during the first few hours [20,136]. Such an initial deactivation would remarkably decrease the activity of zeolite supported catalysts.

To overcome the drawbacks associated to microporous zeolites, the utilization of hierarchical zeolites as support of TMS catalyst has been considered as the active phases located in mesopores/macropores could be more easily accessible to the reactants and the diffusion ability can also be improved due to the introduction of these additional pores. Indeed, there are some reports about this subject. For examples, Ni(Co)Mo catalyst was supported on hierarchical zeolite L, ZSM-5, and Mordenite for HDS reactions [110,107-112]. The results indicated that hierarchical zeolites supported Ni(Co)Mo catalyst exhibited superior catalytic performance than microporous zeolites supported one. This demonstrated that the introduction of additional mesopores/macropores in zeolite supports is helpful for enhancing the HDS catalytic performance in agreement with better accessibility of active phases.

On the other hand, it is well known that conventional zeolites deactivated easily in some acid-catalytic reactions and the introduction of hierarchical pores into zeolites can improve the resistance ability to deactivation [137-139]. One explanation is that external active sites outside micropores were able to perform the catalytic function even after active sites inside micropores were deactivated [138]. Thus, from the viewpoint of deactivation the use of hierarchical zeolites as the support of TMS

catalysts might inhibit deactivation of catalysts to some extent. Nevertheless, the study about deactivation situation of hierarchical zeolites supported TMS catalysts in the HDS reactions has not been presented.

In this present work, hierarchical zeolite Beta was used as a probe to study the deactivation of hierarchical zeolites supported TMS catalysts. Moreover, HDS of thiophene was used to evaluate the performance of catalysts. In this case, the influence of accessibility and agglomeration of active phase could be avoided as much as possible, due to the small size of thiophene and the large external surface of zeolite Beta.

5.2 Preparation of modified Beta supported catalysts

The preparation method of two modified catalysts, mixed catalysts and sodium exchanged catalysts could be observed in Chapter 2.2.3.

5.3 Characterization of Beta supported catalyst before and after modification

The powder XRD patterns of all the samples are presented in Fig. 5-1. HB and HB-M exhibited well resolved diffraction peaks, which are characteristic for beta zeolite framework structure. After supporting NiW catalyst, the zeolite structure was still maintained and no detectable diffraction peaks assigned to WO_3 and NiO were observed. This suggested that tungsten and nickel oxidic species were either completely amorphous or composed of crystallites smaller than 4 nm [37,114,116], indicating a good dispersion of the metals.

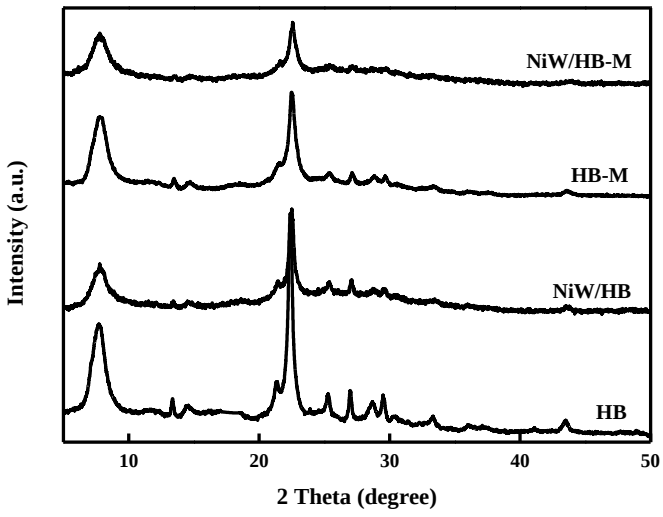

Fig. 5-1 X-ray diffraction patterns of HM and HM-M before and after impregnation

The N_2 sorption isotherms of HB, HB-M and their corresponding catalysts are shown in Fig. 5-2. They exhibited a type I isotherm at low relative pressure and a type IV isotherm with a hysteresis loop at high relative pressure, indicating the existence of hierarchical pores.

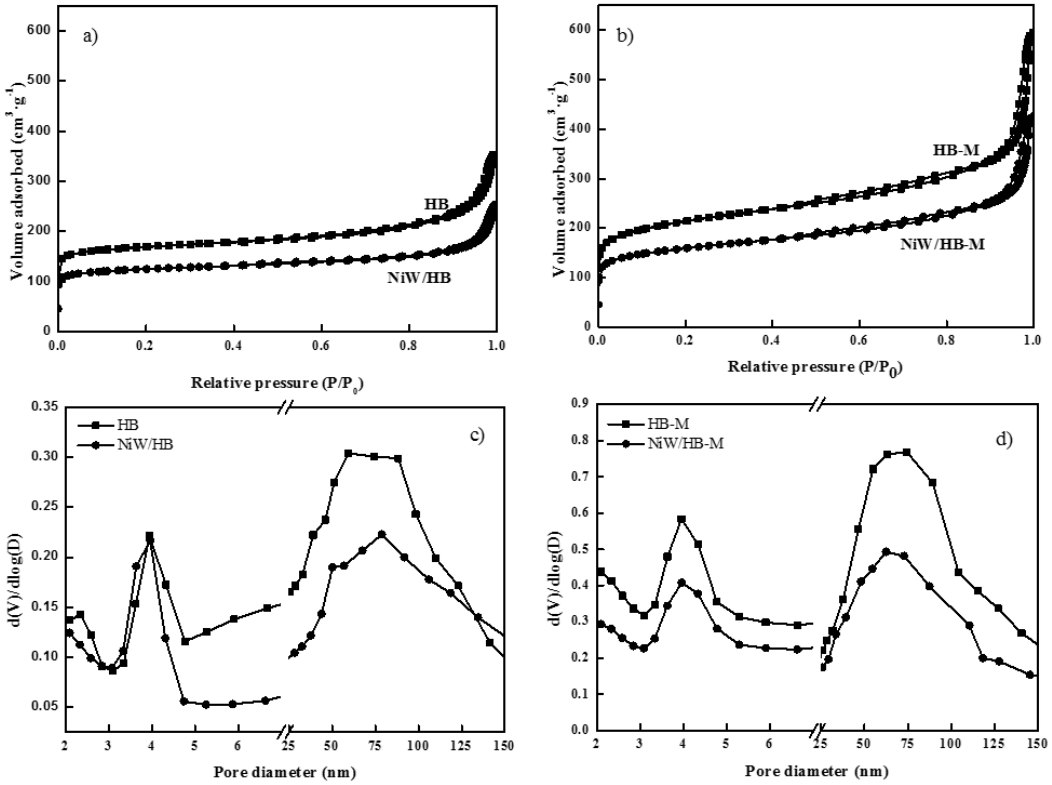

Fig. 5-2 N_2 sorption isotherms and pore distribution of HM and HM-M before and after impregnation
a) isotherm of HB and NiW/HB, b) isotherm of HB-M and NiW/HB-M, c) pore distribution of HB and NiW/HB, d) pore distribution of HB-M and NiW/HB-M

The detailed sorption data are listed in Table 5-1. For the catalysts, surface areas and pore volumes were also expressed per gram of support, by deducing the weight gain due to the active phase, in order to estimate the variations of the textural properties of the support itself.

Table 5-1 Textural properties of Beta supports before and after impregnation

Sample	S_{BET} ($m^2 \cdot g^{-1}$)	S_{Ext}($m^2 \cdot g^{-1}$)[a]	V_{micro}($cm^3 \cdot g^{-1}$)[a]	V_{meso} ($cm^3 \cdot g^{-1}$)[b]
HB	550	134	0.20	0.34
NiW/HB	407(507[c])	98(121[c])	0.15(0.18[c])	0.24(0.30[c])
HB-M	717	348	0.18	0.74
NiWHB-M	531(623[c])	242(284[c])	0.14(0.16[c])	0.52(0.61[c])

[a] t-plot； [b] BJH（adsorption branch）； [c] Data calculated by deducting the effect of NiW mass.

It can be observed that the micropore volume, external surface area and mesopore volume of HB and HB-M decreased after impregnation, suggesting that NiW active

phase could be dispersed in both micropores and mesopores (which is different to that of zeolite Mordenite). The pore distribution of the samples (Fig. 5-2) appeared not affected after impregnation step.

The acidity of various supports was measured by NH_3-TPD and IR study of pyridine adsorption, to reflect the acidity of catalysts. It can be seen from NH_3-TPD results that both HB and HB-M exhibited two desorption peaks, at about 260°C and 450°C (Fig. 5-3). However, the strong acid sites in zeolite Beta was disappeared after sodium ion-exchange.

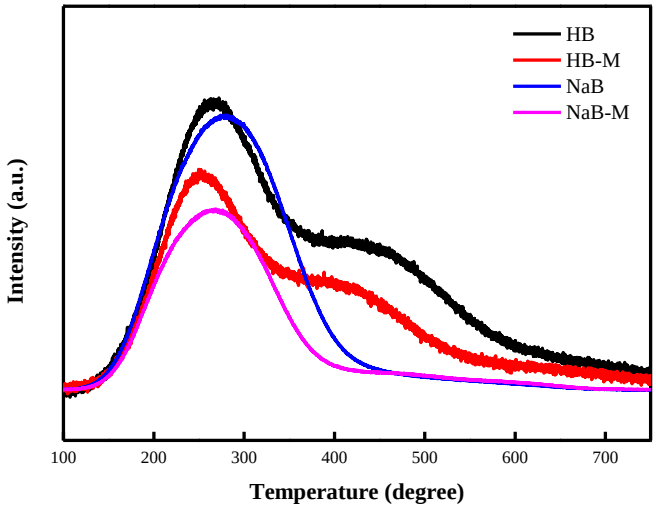

Fig. 5-3 NH_3-TPD profiles for HB, HB-M, NaB and NaB-M

Table 5-2 showed the detailed acidity of various supports obtained by NH_3-TPD. The number of acid sites in HB and HB-M was 1170 μmol·g^{-1} and 920 μmol·g^{-1} respectively. However, The number of acid sites in NaB and NaB-M was only 910 μmol·g^{-1} and 600 μmol·g^{-1} respectively. Moreover, it could be observed that alumina don't have strong acid sites, and the number of acid sites in alumina was much lower than that of other supports.

Table 5-2 Acidity of different supports measured by NH_3-TPD

Support	Desorption temperature 1 (°C)	Desorption temperature 2 (°C)	Number of acid sites (μmol·g^{-1})
Al_2O_3	249	-	204
HB	280	450	1170
HB-M	260	440	920
NaB	290	-	910
NaB-M	280	-	600

By IR studies of pyridine adsorption (Table 5-3), it is also shown that HB-M

possessed less number of Brönsted acid sites (209 μmol·g^{-1}) than HB (269 μmol·g^{-1}) as observed on the global acidity. In order to try to discriminate between Brönsted acid sites present in micropores and mesopores, a larger basic molecule, pivalonitrile, was used to probe the accessible acid sites. The number of these external Brönsted acid sites is is five times larger in HB-M than that in HB in agreement with the larger pore volume of the treated zeolite.

Table 5-3 Chemical composition and acidity of NiW/HB and NiW/HB-M

Sample	Si/Al	WO_3 (%)[a]	W/Ni	Number of Brönsted acid sites (μmol·g^{-1})[b]	Number of Brönsted acid sites (f μmol·g^{-1})[c]
NiW/HB	17	16.6	2.4	269	2.0
NiW/HB-M	15	13.1	2.6	209	9.5

[a] ICP-OES； [b] Pyridine-IR； [c] Pivalonitrile-IR

Fig. 5-4 showed the XPS spectra of W4f for the sulfided catalysts. The decomposition of the photopeaks revealed three contributions attributed to W^{6+} in an oxidic environment (W4f5/2: 36.2eV and W4f3/2: 38.3eV), W^{5+} as oxysulfide species (33.2eV and 35.4eV) and W^{4+} sulfided species (32.3eV and 34.4 eV) [74,75,118,119].

By the interaction between photopeaks (Table 4-2), the XPS spectra could be decomposed. The data obtained from these decompositions are listed in Table 5-4. The sulfidation degree of tungsten in NiW/Al_2O_3 was about 30%, which was in agreement with previous works [120]. In comparison, higher sulfidation degree was obtained for NiW/HB (73%) and NiW/HB-M (58%), which is in accordance with other reported works about that the use of zeolite support improving the sulfidation degree of Ni(Co)Mo(W) catalyst [75]. This result might be related to the relatively weak interaction between active phase and zeolitic support because Si species had weaker interaction than Al species with Mo(W) active phase [140].

Table 5-4 Proportion of W species in sulfided NiW/Al_2O_3, NiW/HB and NiW/HB-M

Sample	WS_2 sulfidation degree (%)	WO_xS_y (%)	W^{6+} (%)
NiW/Al_2O_3	30	24	46
NiW/HB	73	0	27
NiW/HB-M	58	3	39

Therefore, the higher sulfidation degree of NiW/HB than NiW/HB-M might be due to the higher Si/Al ratio in HB. Generally, the higher sulfidation degree of NiW/HB and NiW/HB-M suggested that they could exhibit better activity in the HDS reactions.

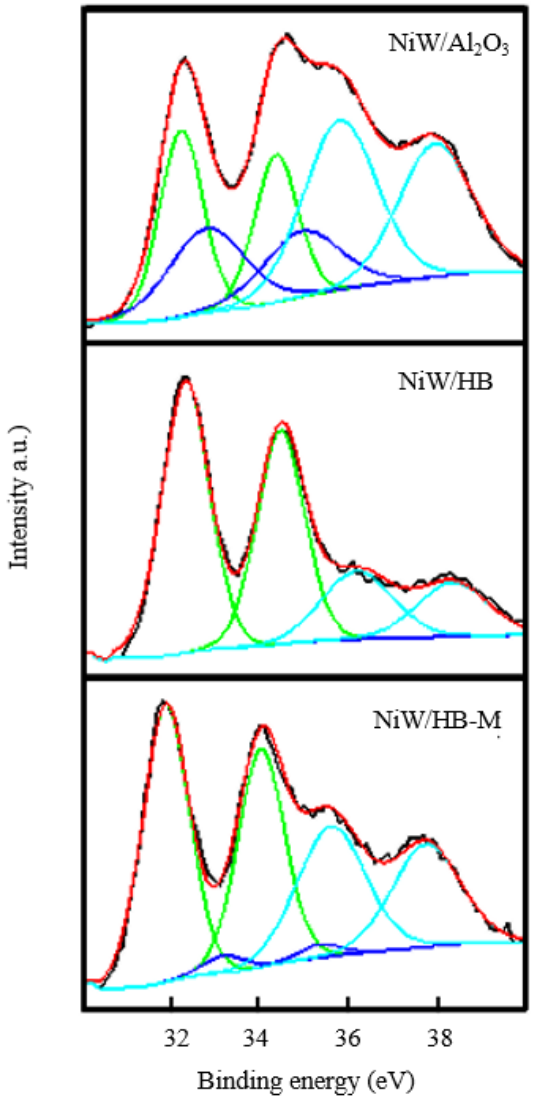

Fig. 5-4 Emission region of W4f XPS spectra of NiW/Al_2O_3, MiW/HB and NiW/HB-M sulfided at 673 K with their fit decomposition curves
experimental (black), simulation (red), WS_2 (green), WO_xS_y (blue), W^{6+} (cyan)

The XPS spectra for Ni2p are presented in Fig. 5-5 and their decomposition evidenced three contributions: sulfidic NixSy (Ni2p3/2: 852.6 eV, Ni2p1/2: 869.8 eV), NiWS (Ni2p3/2: 853.7 eV, Ni2p1/2: 870.9 eV) and an oxidic phase Ni^{2+} (Ni2p3/2: 856.4 eV, Ni2p1/2: 873.8 eV) [74,75,118,119]. The proportions of NiO, NixSy and NiWS in the catalysts were calculated and listed in Table 5-5, based on the interaction between photopeaks (Table 4-4). The proportion of NiWS species represented the promoting degree of Ni. A proportion of 44% NiWS was obtained in NiW/Al_2O_3, which was similar to that in the previous work [75,159]. Comparatively, the promotion degree of Ni was 52% and 33% in NiW/HB and NiW/HB-M, respectively.

Although the sulfidation degree of molybdenum or tungsten has been evaluated in the literature, no studies reported the promotion degree of the sulfide phase supported on zeolites determined by decomposition of the XPS Ni2p photopeak. Thus, the comparison between our result and reported values were difficult. However, it could

be observed in our previous work that Mordenite supported catalyst NiW/HM and NiW/HM-M and alumina supported catalyst NiW/Al_2O_3 revealed higher promotion degree than Beta supported catalysts NiW/HB and NiW/HB-M. This might be attributed to the distribution of active phases in micropores and mesopores, which would be further discussed 5.4.2.

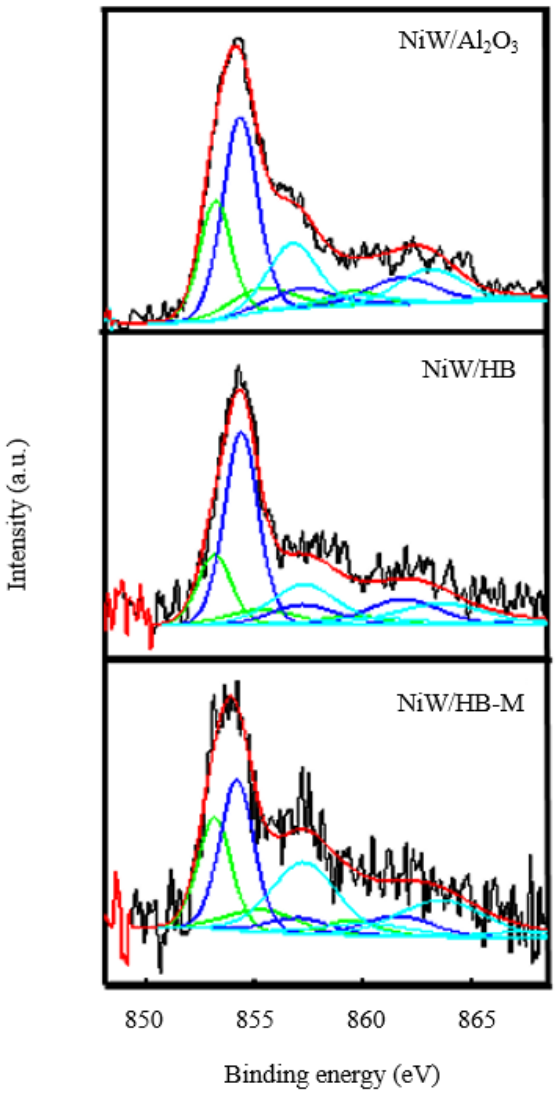

Fig. 5-5 Emission region of Ni2p XPS spectra of NiW/Al_2O_3, MiW/HB and NiW/HB-M sulfided at 673 K with their fit decomposition curves
experimental (black), simulation (red), Ni_xS_y (green), NiWS (blue), Ni^{2+} (cyan)

Table 5-5 Proportion of Ni species in sulfided NiW/Al_2O_3, NiW/HB and NiW/HB-M

Sample	WS_2 sulfidation degree (%)	WO_xS_y (%)	W^{6+} (%)
NiW/Al_2O_3	44	27	29
NiW/HB	52	20	28
NiW/HB-M	33	26	41

Representative HRTEM images of the sulfided catalysts are shown in Fig. 5-6. All the samples exhibited the typical structure of the layered WS_2 phase, with an interplanar spacing of 0.65 nm, corresponding to the (002) planes of the WS_2 crystal [121]. No agglomeration could be observed over NiW/HB, which was different to that of NiW/HM. This could be explained by the following reason: the particle size of HB was much small than that of HM, and the external surface area of HB was larger than that of HM and HM-M (Chapter 3). Therefore, HB could offer enough external surfaces area for WS_2 deposition, and avoid the appearance of WS_2 active phases agglomeration.

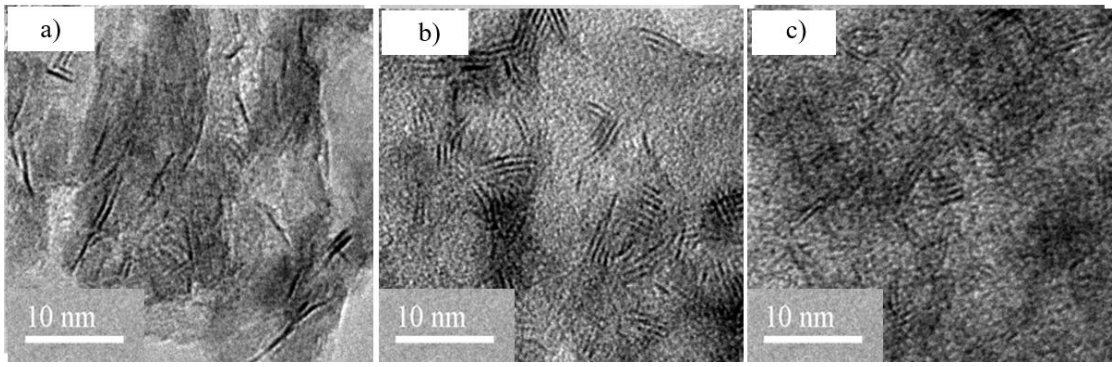

Fig. 5-6 HRTEM images of sulfided NiW/Al_2O_3, NiW/HB and NiW/HB-M.
a) NiW/Al_2O_3, b) NiW/HB, c) NiW/HB-M

By the statistical analysis of the images, the distributions in slab length and stacking of the WS_2 slabs were obtained. On sulfided NiW/Al_2O_3, the WS_2 slab length was between 1 and 10 nm with an average length (L) of 4.8 nm and an average stacking number (N) of 1.2 (Fig. 5-7). The length of WS_2 slabs in NiW/HB was distributed between 1 to 13 nm. The calculated average length was about 4.8 nm and the average stacking number was 3.3. Additionally, the length of WS_2 slabs in NiW/HB-M was distributed in a narrower range of 1~7 nm. The average length was about 2.6 nm and the average stacking number was 2.6.

From this results, it could be observed that active phases supported on HB and HB-M was larger than that over alumina support and more stacked, similar to previous results. This might be caused by the interaction between support and active phase. The interaction between alumina and WS_2 active phases was relative high. The active phases could be fastened on the surface of alumina. Therefore, less stacked active phases could observed.

In comparison, active phases over zeolite Beta supports seemed to be smaller than that over Mordenite supported catalysts. According to the Rim-Adge model, the active phases over zeolite Beta supports should be better promoted (higher promotion degree could be obtained). However, this was different to the results obtained by XPS analysis.

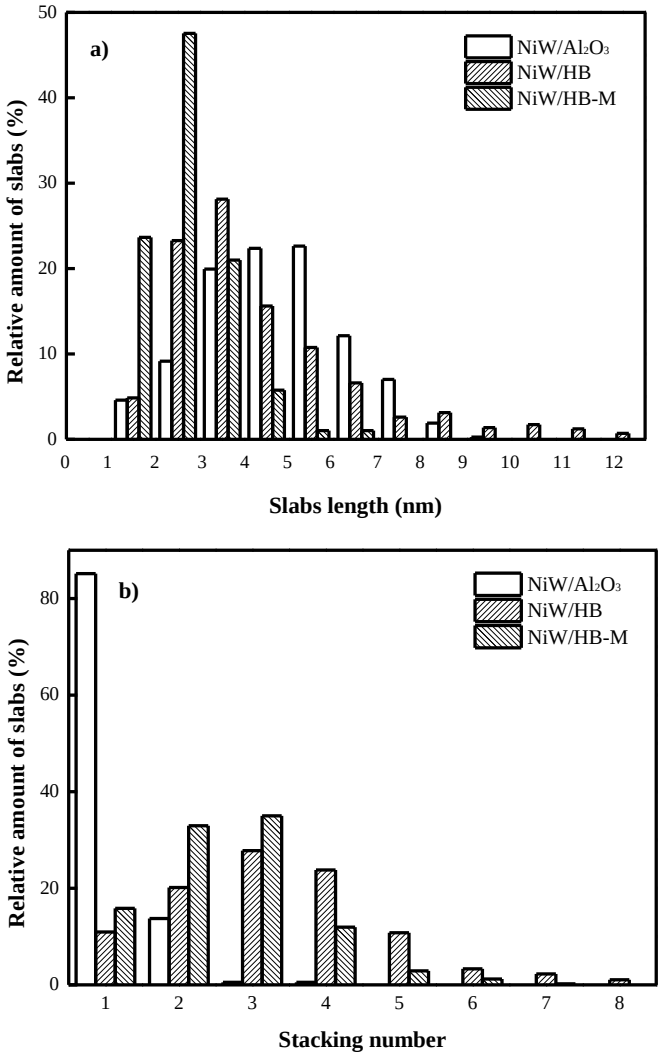

Fig. 5-7 Statistic results of the WS2 slabs over NiW/Al_2O_3, MiW/HB and NiW/HB-M
a) Length distribution, b) Stacking number

5.4 Performance of Beta supported catalysts in the HDS of thiophene

5.4.1 Deactivation of Beta supported catalysts

The catalytic performance of these catalysts was evaluated in the HDS of thiophene. Only four products (1-butene, cis- and trans-2-butene, n-butane) can be detected over NiW/Al_2O_3. In comparison, some additional products (such as ethane, ethylene, propane and propene) were detected over NiW/HB and NiW/HB-M due to the strong acidity of the support. No dihydrothiophene, tetrahydrothiophene and 1,3-butadiene were detected because they can be quickly converted into butane and

butenes. Moreover, a small amount of unidentified large molecules were detected over NiW/HB and NiW/HB-M, which might be attributed to the polymerization of olefins. The main HDS reaction pathway in this reaction was shown in Fig. 5-8.

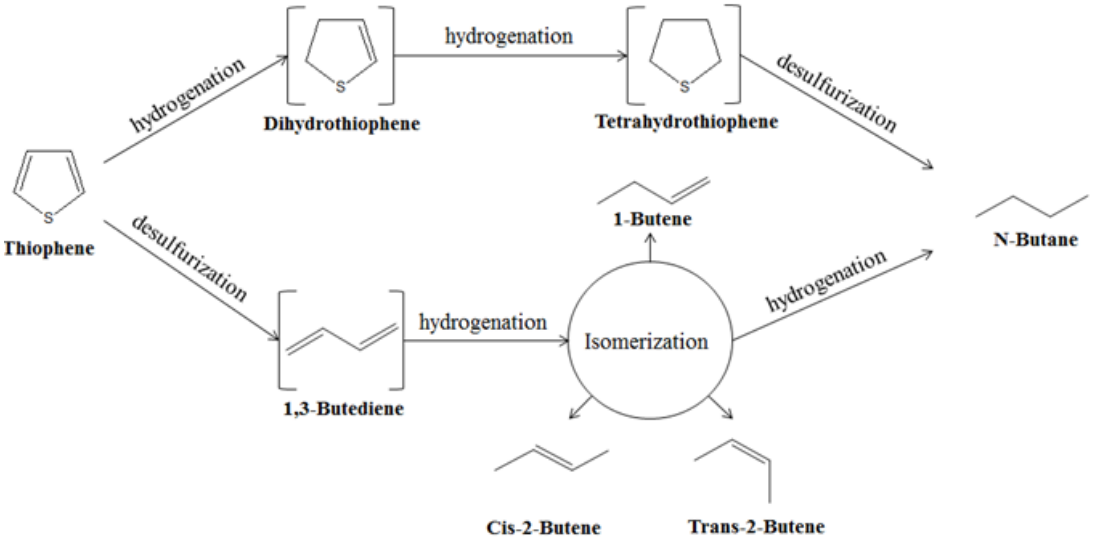

Fig. 5-8 Main reaction pathway for thiophene hydrodesulfurization

The reaction rate of thiophene over various catalysts with time on stream was shown in Fig. 5-9. The activities after 15 minutes and 3 hours of reaction over these catalysts are listed in Table 5-6. Here, we can consider the activity at a reaction time of 3 h as the steady-state because activity tended to be stable after this time. Obviously, no deactivation was observed over NiW/Al_2O_3 within a reaction time of 8 h with an activity around 177 $L \cdot h^{-1} \cdot mol^{-1}$ W. In comparison, NiW/HB displayed higher initial activity (385 $L \cdot h^{-1} \cdot mol^{-1}$ W) than NiW/Al_2O_3. However, rapid deactivation occurred and the catalytic activity was stabilized after a reaction time of 3 h. The steady-state activity of NiW/HB was 71 $L \cdot h^{-1} \cdot mol^{-1}$ W, which was much lower than that of NiW/Al_2O_3. Further, NiW/HB-M exhibited highest initial activity (473 $L \cdot h^{-1} \cdot mol^{-1}$ W) among these catalysts. Nevertheless, rapid deactivation was also observed over NiW/HB-M. After a reaction time of 3 h, the activity reached 195 $L \cdot h^{-1} \cdot mol^{-1}$ W.

Table 5-6 Initial and steady-state activity of NiW/Al_2O_3, NiW/HB and NiW/HB-M

Sample	Initial activity ($L \cdot h^{-1} \cdot mol^{-1}$ W)	Steady-state activity ($L \cdot h^{-1} \cdot mol^{-1}$ W)
NiW/Al_2O_3	177	177
NiW/HB	385	71
NiW/HB-M	473	195

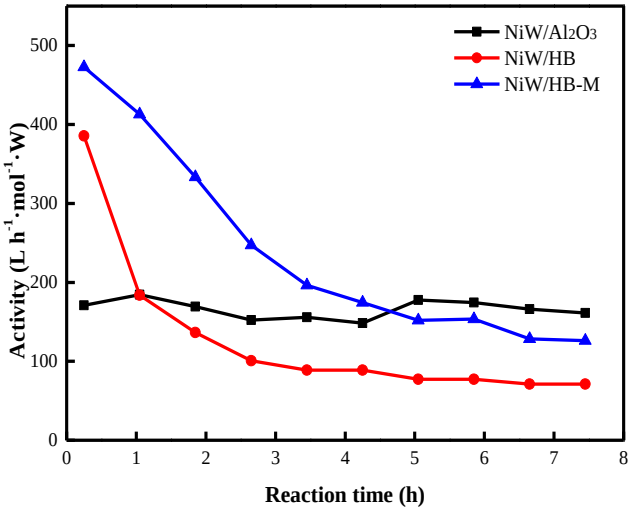

Fig. 5-9 Catalytic activity of NiW/Al_2O_3, MiW/HB and NiW/HB-M with time-on-stream in HDS of thiophene

The steady-state selectivity of products over various catalysts was shown in Fig. 5-10. Only n-butane, 1- and 2-butenes (C4 products) were observed over NiW/Al_2O_3. For NiW/HB, some cracking products (C2 2%, C3 12%) as well as polymerized products (others 14%) could be detected besides major C4 products (72%). Comparatively, NiW/HB-M exhibited higher cracking activity (C2 3%, C3 19%) than NiW/HB, which might be related to the larger number of accessible acid sites in HB-M as the number of acid sites located in mesopores/macropores could be less reduced than that in micropores during deactivation [138,142].

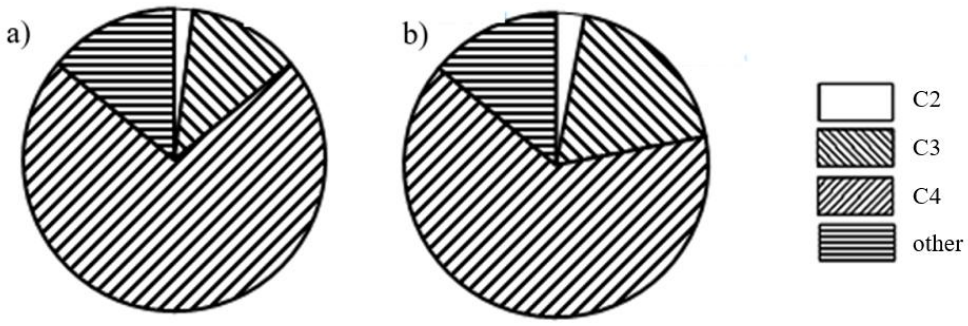

Fig. 5-10 Steady-state product selectivity of NiW/HB and NiW/HB-M in HDS of thiophene
a) NiW/HB, b) NiW/HB-M

As shown in Fig. 5-9, NiW/HB-M and NiW/HB exhibited largely higher initial activity than NiW/Al_2O_3. The higher initial activity of NiW/HB than NiW/Al_2O_3 might be partly attributed to its higher sulfidation/promotion degree. However, NiW/HB-M showed higher initial activity than NiW/HB, which was different to the order of their sulfidation/promotion degrees. It could be assumed that due to very fast deactivation at the beginning of the reaction observed in Fig. 5-9 for zeolite based

catalysts, the initial activity value is difficult to measure with a good accuracy. On the other hand, the additional mesopores in zeolite support could improve the performance of zeolite based catalysts as already reported [143]. This phenomenon was confirmed by our results that hierarchical zeolite supported catalysts could always reveal higher steady-state activity than the parent ones in the HDS of thiophene (Fig. 5-11).

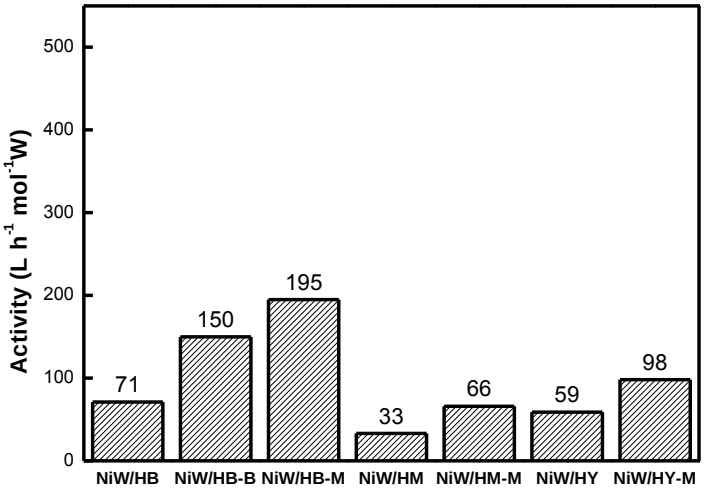

Fig. 5-11 Steady-state activities of various catalysts in HDS of thiophene

Activity after 3 hours of NiW/HB and NiW/HB-M is much lower than their corresponding initial activity and after 6 hours it becomes below that of NiW/Al_2O_3. It is well known that zeolite deactivated easily in many acid-catalytic reactions due to coke formation [137-139,142,144]. Such initial deactivation caused by rapid coke formation has also been reported when zeolite was used as support of Ni hydrotreating catalyst [145]. It was indicated that the amount of coke in zeolite supported catalyst quickly increased during the beginning of reaction, and then tended to be stable. In this work, the initial deactivation over NiW/HB and NiW/HB-M in HDS reaction of thiophene could be possibly attributed to coke formation due to the strong acidity from zeolite Beta.

5.4.1 Distribution of active phases & its influence on the deactivation

In general, the promotion degree in TMS catalysts should have a good relationship with the sulfidation degree because the existence of more species like $W(Mo)S_2$ can result in higher possibility of formation for the species like NiW(Mo)S. In this work, although NiW/HB-M exhibited higher sulfidation degree (58%) than NiW/Al_2O_3 (30%), the promotion degree in NiW/HB-M (33%) was lower than that in NiW/Al_2O_3 (44%). Similarly, the sulfidation degree in NiW/HB (73%) was twice

more than that in NiW/Al_2O_3 (30%) while the promotion degree (52%) in NiW/HB was only slightly higher than that (44%) in NiW/Al_2O_3. This means that Ni species might not efficiently promote the sulfided W species in HB and HB-M.

To explain the above results, an imaginative diagram about the distribution of active phase in micropores and mesopores/macropores of zeolite Beta was proposed (Fig. 5-12). As shown, Ni species might be located in both micropores and mesopores/macropores of zeolite Beta, whereas W species could be only located in mesopores/macropores. Such supposition was mainly based on the consideration of preparation process for the introduction of the active phase. In this work, the precursors of active phase were nickel nitrate hexahydrate and ammonium metatungstate. During the impregnation, Ni^{2+} from the precursor of Ni species can enter the pores of zeolite Beta, including micropores, due to its small cation size. However, it will be more difficult for $H_2W_{12}O_{40}^{6-}$ from the precursor of W species to enter the micropores because the size of the anion is relatively large. Ni species might thus be located in both micropores and mesopores/macropores of zeolite Beta and W species only in mesopores/macropores. This means that only Ni species located in mesopores can play a promotion role on WS_2. This hypothesis can explain why NiW/HM and NiW/HM-M with high sulfidation degree did not accordingly display high promotion degree.

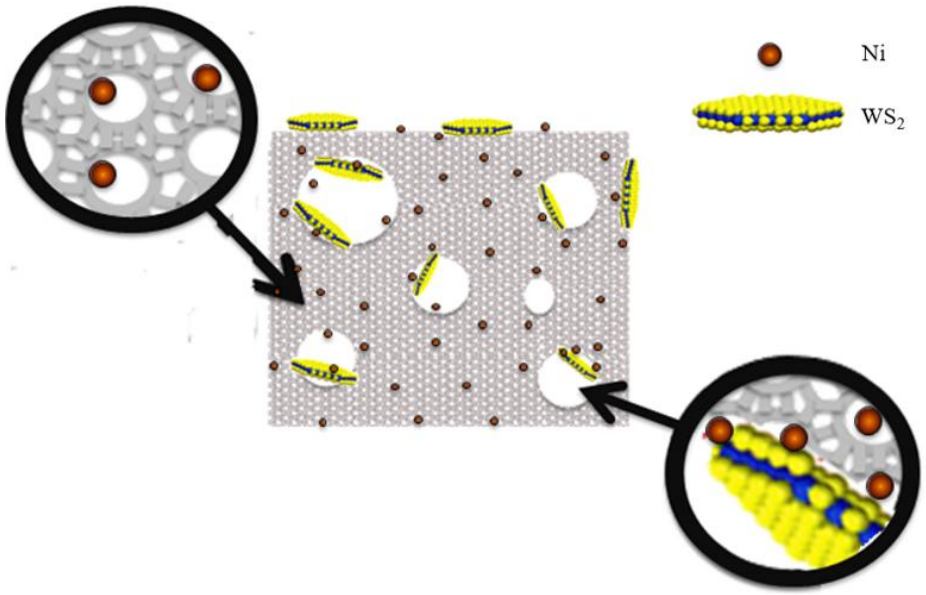

Fig. 5-12 Proposed imaginative diagram about location of active phase in hierarchical Beta

Obviously, it could be observed from N_2-sorption that the active phases could go into the micropores and mesopores of zeolite Beta. Based on our hypothesis, the decreased micropore volume after impregnation was mainly caused by the location of Ni species. However, the situation was different when using zeolite Mordenite as support. It could be observed from the N_2-sorption of NiW/HM and NiW/HM-M that

the micropore volume was not decreased after impregnation, suggesting that both Ni species and W species could be only located on the external surface of zeolite Mordenite. Therefore, both the high sulfidation degree and promotion degree could be obtained over zeolite Mordenite supported catalysts. This might be due to the immigration of Ni species during calcination and pre-sulfidation. It has been proposed that Ni species over zeolite supports would redistribute during calcination and presulfidation [48]. Therefore, it was possible that all Ni species over Mordenite immigrated on the external surface due to the relative low interaction between Mordenite and Ni species.

In this work the introduction of additional mesopores/macropores in zeolite Beta did not inhibit the deactivation tendency even if in literature data, introduction of hierarchical pores in zeolite is reported to remarkably retard the deactivation caused by coke formation [137-139,142]. Indeed, coke formation is known to preferably occur inside the micropores that can block or cover active sites [146]. In this case external active sites outside micropores are available to perform the catalytic function even when active sites inside micropores are deactivated [138]. The distribution of active sites in both micropores and mesopores/macropores in hierarchical zeolite could then explain the anti-deactivation ability. In our case, NiW/HB-M did not exhibit better anti-deactivation ability than NiW/HB that can be due to the single distribution of active species in mesopores/macropores as shown in Fig. 5-12.

5.5 Performance of Modified Beta supported catalysts in the HDS of thiophene

5.5.1 Performance of mixed catalysts

Considering that this deactivation might be caused by the coke formation, it was attempted to mix NiW/HB-M with NiW/Al_2O_3 in different proportions to inhibit deactivation as the additional alumina could trap coke precursors on the alumina surface and decrease the acidity of the catalyst [147].

The catalytic activities of mixed catalysts in the HDS of thiophene are presented in Fig. 5-13. Obviously, the addition of NiW/Al_2O_3 into NiW/HB-M greatly inhibited the deactivation of the catalysts. The deactivation of NiW/HB-M was remarkably inhibited when the content of NiW/Al_2O_3 was increased to 80 wt% (NiW/20HB-M). The steady-state activity of NiW/20HB-M (276 $L \cdot h^{-1} \cdot mol^{-1}$ W) was about 1.5 times as that of NiW/HB-M (195 $L \cdot h^{-1} \cdot mol^{-1}$ W) and NiW/Al_2O_3 (177 $L \cdot h^{-1} \cdot mol^{-1}$ W). The same method was also used to prepare the mixed catalyts of NiW/HB and NiW/Al_2O_3. The result indicated that deactivation can be also inhibited by this strategy. However, the steady-state activity (212 $L \cdot h^{-1} \cdot mol^{-1}$ W) of NiW/20HB with the same content of

NiW/Al_2O_3 was still lower than that of NiW/20HB-M.

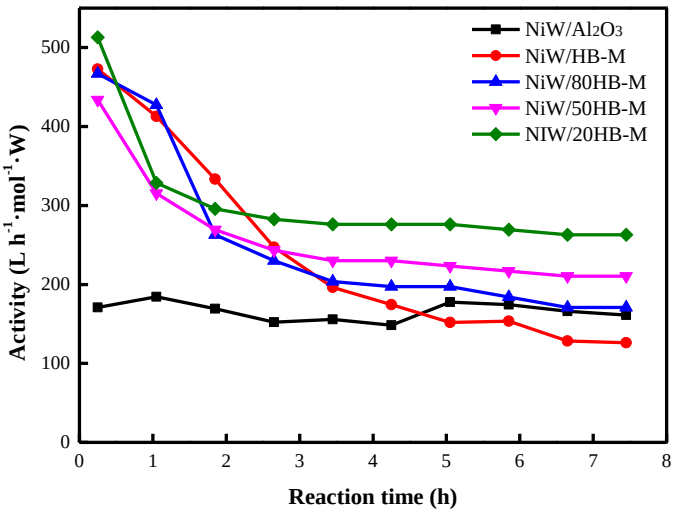

Fig. 5-13 Catalytic activity of mixed catalysts with time-on-stream in HDS of thiophene

The steady-state selectivity of mixed catalysts was shown in Fig. 5-14. It could be observed that the cracking ability could be maintained in mixed catalysts, suggesting that mixed catalysts still had relative high acidity. However, the cracking ability of these catalysts was lower than that of NiW/HB and NiW/HB-M, which was due to the lower acidity of mixed catalysts than NiW/HB and NiW/HB-M.

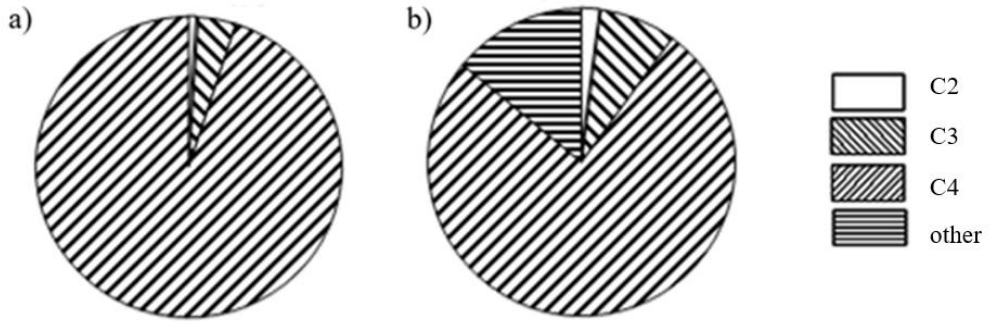

Fig. 5-14 Steady-state product selectivity of NiW/20HB and NiW/20HB-M in thiophene HDS
a) NiW/20HB, b) NiW/20HB-M

5.5.2 Performance of sodium exchanged catalysts

Another strategy to inhibit the deactivation was to use Na^+-exchanged Betas as support of NiW catalysts, by reducing the acidity of the support. Their catalytic activities were shown in Fig. 5-15 and show that deactivation can be restrain by using Na^+ exchanged zeolites. NiW/NaB-M exhibited a steady-state activity 330 $L \cdot h^{-1} \cdot mol^{-1}$ W that can be compared to that of NiW/HB-M equal to 195 $L \cdot h^{-1} \cdot mol^{-1}$ W. Also, a

similar effect was observed over NiW/NaB presenting an improved steady-state activity reaching 190 $L \cdot h^{-1} \cdot mol^{-1}$ W.

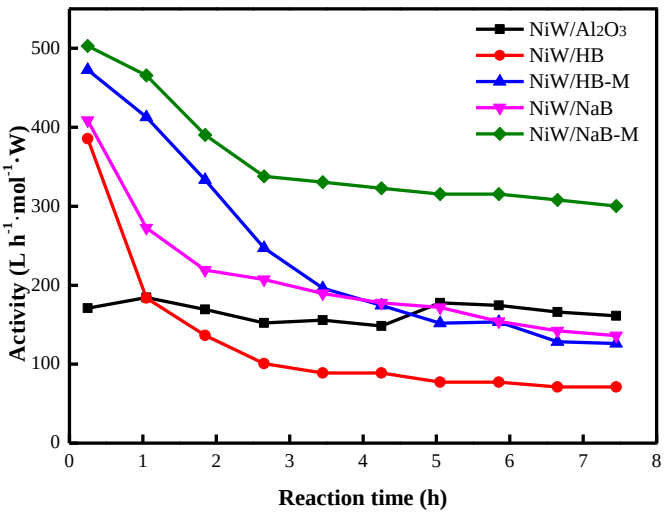

Fig. 5-15 Catalytic activity of various Na^+-exchanged Beta zeolite supported catalysts with time-on-stream in HDS of thiophene

The steady-state selectivity of Na^+-exchanged Beta zeolite supported catalysts was shown in Fig. 5-16. Similar to that of mixed catalysts, Na^+-exchanged Beta zeolite supported catalysts exhibited lower cracking ability than NiW/HB and NiW/HB-M, which might be attributed to their lower acidity. Moreover, more polymerization products were observed over NiW/NaB and NiW/NaB-M, which might be due to the presence of alkaline earth metal in catalysts.

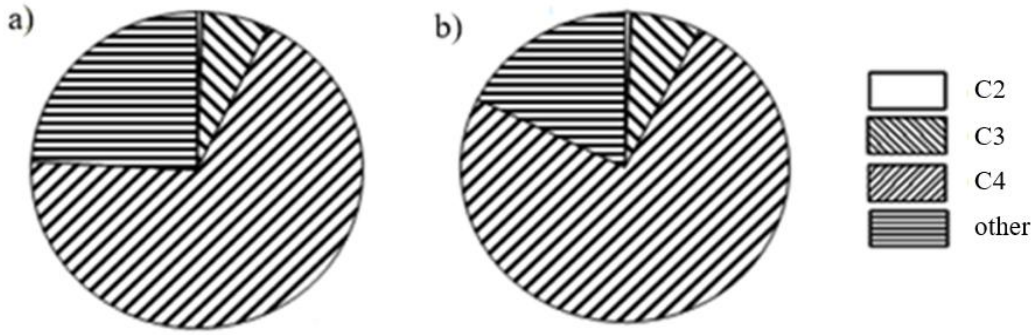

Fig. 5-16 Steady-state product selectivity of NiW/NaB and NiW/NaB-M in HDS of thiophene a) NiW/NaB, b) NiW/NaB-M

5.5.3 Expended studies

Such an enhancement could also be observed with hierarchical Mordenite zeolite supported TMS catalysts. The steady-state activity of various Mordenite zeolite-based catalysts in HDS of thiophene was illustrated in Fig. 5-17. Obviously, Na^+-exchanged

hierarchical Mordenite zeolite supported catalyst and hierarchical zeolite Mordenite mixed catalyst could exhibit much higher steady-state activity than that of NiW/HM-M, which might be mainly due to their improved anti-deactivation ability.

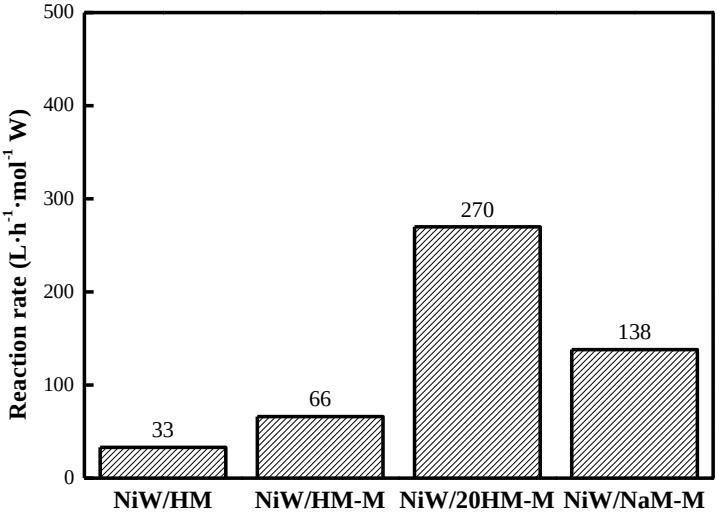

Fig. 5-17 Steady-state catalytic activity of modified Mordenite zeolite supported catalysts in HDS of thiophene

These results clearly indicate that deactivation could be greatly inhibited by adding NiW/Al_2O_3 or Na^+ into the zeolite supported catalysts, and the steady-state activity of catalyst could be further improved by this optimization. Actually, using zeolite with higher Si/Al should be another way to improve the anti-deactivation ability of hierarchical zeolite supported catalyst because zeolite with higher Si/Al possessed lower acidity. Previous works already indicated that the TMS catalyst using microporous zeolite support with higher Si/Al exhibited higher steady-state activity than that with low Si/Al ratio (Chapter 1.4.3), which could be well explained by our results. However, these experiments cannot be carried out in our system because hierarchical zeolite with high Si/Al is hard to be prepared by post-treatment.

5.6 Brief summary

NiW catalysts supported on γ-Al_2O_3 (NiW/Al_2O_3), commercial Beta (NiW/HB) and hierarchical Beta (NiW/HB-M) were prepared and their catalytic performance was evaluated by HDS of thiophene. NiW/HB and NiW/HB-M exhibited higher initial catalytic activity than NiW/Al_2O_3. However, important deactivation occurred over NiW/HB and NiW/HB-M showing that the introduction of additional mesopores/macropores in HB-M support could not prevent the deactivation tendency. This could be explained by the location of active phase (WS_2 and NiWS species) supposed to be located outside micropores.

Additionally, two methods have been attempted to improve the catalytic performance of NiW/HB-M in HDS of thiophene by inhibiting the deactivation of catalyst. One method is the mechanical mixing of NiW/HB-M with NiW/Al_2O_3. The other one is the use of Na^+-exchanged zeolite as support of NiW catalyst. Both methods are very efficient and lead to steady-state activities 1.5 times and twice higher respectively than that of NiW/Al_2O_3, reference catalyst. Moreover, these two methods may be utilized to enhance the anti-deactivation ability of zeolites with different framework types supported NiW catalysts in the HDS of thiophene, such as Mordenite supported catalyst.

Chapter 6. Conclusion

6.1 General conclusion

In order to overcome the limitations of conventional HDS catalyst, NiW catalyst based on hierarchical zeolite Beta and Mordenite supports were prepared. The current work was focused on the following three points: preparation of hierarchical zeolite, The catalytic performance of the prepared catalysts in the hydrodesulfurization (HDS) of dibenzothiophene (DBT) and 4,6-dimethyldibenzothiophene (4,6-DMDBT), and the anti-deactivation ability of hierarchical zeolite supported catalysts. According to the present research, following conclusions were obtained:

(1) Hierarchical Beta could be obtained by desilication, based on a commercial Beta with a low Si/Al molar ratio of 12.5. However, the number of total acid sites in zeolite Beta would be greatly decreased, which was attributed to the transformation of tetrahedral aluminum during desilication. Subsequent acid treatment after desilication could recover the content of tetrahedral aluminum in zeolite Beta, and further compensate the loss of acid sites during desilication. Moreover, our results demonstrated that acid treatment after desilication could be applied in other zeolite frameworks, such as Mordenite.

(2) Hierarchical zeolite Beta prepared by base-acid treatment possessed less active sites than parent Beta zeolite. Thus, it could not exhibit better activity than HB in the benzylation of benzene with benzyl alcohol. However, in the benzylation of mesitylene with relatively large molecular size, hierarchical zeolite Beta exhibited much better catalytic performance than parent one, because the acid sites on hierarchical zeolite Beta were more accessible. These results revealed clearly that hierarchical Beta obtained by post-treatment method can find applications in acid-catalyzed reactions involving large molecules.

(3) Zeolite Beta and Mordenite supported catalysts cannot reveal better activity than alumina supported catalyst in the HDS of DBT because sites active on the alumina supported catalyst were inaccessible or deactivated when zeolite is used as support. However, these catalysts could reveal better activity in the HDS of 4,6-DMDBT than alumina supported one because the use of zeolite as support could create an additional isomerization reaction route, which could decrease the difficulty of 4,6-DMDBT HDS.

(4) Hierarchical zeolite Mordenite supported NiW catalyst (NiW/HM-M) exhibited higher catalytic activity than microporous zeolite Mordenite supported catalyst (NiW/HM) in the transformation of both DBT and 4,6-DMDBT. This can be explained by (i) better dispersion of the sulfide NiW phase observed by TEM when deposited on the hierarchical zeolite; (ii) enhanced accessibility of the sulfur model

compounds to the active sites due to the creation of mesoporosity by base-acid treatment; (iii) in the case of 4,6-DMDBT, the higher acidity and better accessibility of acid sites in NiW/HM-M compared to that of NiW/HM leading to an improvement of its reactivity in isomerization. This study clearly demonstrates that the use of hierarchical Mordenite as support of NiW based HDS catalyst is beneficial in the desulfurization of refractory sulfur molecules.

(5) The use of hierarchical zeolite Beta (NiW/HB-M) instead of microporous zeolite Beta (NiW/HB) as the catalyst support didn't improve the performance of catalyst in the HDS of DBT. This might be explained by (i) no agglomeration was observed over NiW/HB. Thus, the use of hierarchical zeolite could not greatly improve the dispersion of active phases. (ii) active phase on NiW/HB-M was less sulfided and promoted than that over NiW/HB. However, NiW/HB-M could exhibit higher activity in the HDS of 4,6-DMDBT, because HB-M possessed more accessible acid sites, which could enhance the isomerization of 4,6-DMDBT.

(6) Catalytic evaluation of NiW/HB in the HDS of thiophene indicated that NiW/HB possessed high initial activity. Then, important and rapid deactivation would occur. After 3h, the reaction rate of NiW/HB would tend stable. However, more than 60% activity of NiW/HB was lost during such a deactivation. Moreover, the introduction of additional mesopores/macropores in support could not prevent the deactivation tendency. This made the steady-state activity of NiW/HB and NiW/HB-M lower than that of NiW/Al_2O_3, because no deactivation was observed over NiW/Al_2O_3.

(7) The anti-deactivation ability of the catalysts could be remarkably improved by mixing NiW/HB or NiW/HB-M with NiW/Al_2O_3 and using Na^+-exchanged Beta as support. As a result, the catalysts NiW/NaB-M (NiW catalyst supported on Na^+-exchanged hierarchical Beta) and NiW/20HB-M (20% NiW/HB-M mixed with 80% NiW/Al_2O_3) gave superior catalytic activity than NiW/HB-M and NiW/Al_2O_3. Moreover, these two methods may be utilized to enhance the anti-deactivation ability of zeolites with different framework types supported NiW catalysts in the HDS of thiophene.

6.2 Innovation points

(1) Hierarchical Beta was prepared by base-acid post-treatment. This hierarchical zeolite Beta has a better catalytic activity than parent zeolite Beta in benzylation of mesitylene with benzyl alcohol. Moreover, the change of local structure during treatment and its effect on the acidity was deeply discussed.

(2) Hierarchical zeolite supported NiW catalyst was prepared. These catalysts could exhibit more than doubled activity as that of NiW/Al_2O_3 in the HDS of 4,6-DMDBT, suggesting that these catalysts has potential application in deep HDS process.

(3) Two methods were proposed to effectively inhibit the deactivation of hierarchical zeolite supported catalyst. By these methods, the steady-state activity of hierarchical zeolite supported catalyst in the HDS of thiophene could be greatly improved.

6.3 Perspectives

(1) Realumination could be used to produce hierarchical zeolite with high acidity or hetero-atom. In this present work, it could be observed that realumination might occur in the subsequent acid washing. In the further research, we should confirm the existence of realumination.

(2) Acidity of zeolite support should have two influences in the HDS of 4,6-DMDBT: (i) improve the isomerization of 4,6-DMDBT, (ii) cause the initial rapid deactivation of catalyst. Thus, the performance of hierarchical zeolite supported catalyst in deep HDS could be optimized by tuning the acidity of support. This could be realized by changing the mixing ratio, ion-exchange degree or using other ion such as K^+.

Reference

[1] Wang Y., Wang B, Rives A. et al. Energy and Environment Focus, 2014, 3: 1-8.
[2] Shi Y. Desulfurization in Petroleum. Beijing: China Petrochemical Press, 2008.
[3] Xu J., Ding G., Yan P., et al. J. Appl. Meteo. Sci., 2007, 5: 645-653.
[4] Srivastava V.C. RSC Adv., 2012, 2: 759-783.
[5] GB19147-2013, China, 2013.
[6] Yin C. Xia D., J. Fuel Chem. Technol., 2001, 29: 256-258.
[7] Fadeev A.G., Meagher M.M. Chem. Comm., 2001: 295-296.
[8] Bakar W.A.W.A.，Ali R.，Kadir A.A.A. et al. Fuel Process. Technol., 2012, 101: 78-84.
[9] Dinamarca M.A., Rojas A. Baeza P. et al. Fuel, 2014, 116: 237-241.
[10] Tang M., Zhou L., Du M., et al. Catal. Comm., 2015, 61: 37-40.
[11] Tuxen A.K., Füchtbauer H.G., Temem B., et al. J. Catal., 2012, 295: 146-154.
[12] Whitehurst D.D., Isoda I., Mochida I. Adv. Catal., 1998, 42: 345-357.
[13] Shafi R., Hutchings G.J. Catalysis Today, 2000, 3-4: 428-442.
[14] Nag N.K., Sapre A.V., Broderick D.H., et al. J. Catal., 1979, 57: 509-512.
[15] Kilanowski, D.R., Teeuwen H., Beer V.H.J., et al. J. Catal., 1978, 55: 129-137.
[16] Isoda T., Takase Y., Kusakabe K., et al. Energy & Fuels, 2000, 14, 585-590.
[17] Houalla M., Broderick D.H., Sapre A.V., et al. J. Catal., 1980, 61: 523-527.
[18] Meille V., Schulz E., Lemaire M., et al. J. Catal. 1997, 170: 29-36.
[19] Solis D., Agudo A.L., Ramirez J., et al. Catal. Today, 2006, 116: 469-477.
[20] Bataille F., Lemberton J.L., Perot G., et al. Appl. Catal. A, 2001, 220: 191-205.
[21] Bataille F., Lemberton J.L., Michaud P., et al. J. Catal., 2000, 191: 409-422.
[22] Bej S.K., Maity S.K., Turaga U.T. Energy & Fuels, 2004, 18: 1227-1237.
[23] Lecrenay E., Sakanishi K., Mochida I., Catal. Today, 1997, 39: 13-20.
[24] Isoda T., Nagao S. Ma X.L., et al. Energy & Fuels, 1996, 10: 482-486.
[25] Hedoire C.E., Louis C., Davidson A., et al. J. Catal., 2003, 220: 433-441.
[26] Chen W., Mauge F., van Gestel J., et al. J. Catal., 2013, 304: 47-62.
[27] Nava R., Infantes-Molina A., Castano P., et al. Fuel, 2011, 90: 2726-2737.
[28] Peng P., Zhang Z., Wang Y., et al. Progress in Chemistry, 2013, 25:2028-2037.
[29] Serrano D.P., Escola J.M., Pizarro P. Chem. Soc. Rev., 2013, 42: 4004-4035.
[30] Na K., Choi M., Ryoo R. Micropor. Mesopor. Mater., 2013, 166: 3-19.
[31] Rahimi N., Karimzadeh R. Appl. Catal. A, 2011, 398: 1-17.
[32] Navarro R., Pawelec B., Fierro J.L.G., et al. Fuel Process. Technol., 1999, 61, 73-88.
[33] Azizi N., Ali S.A., Alhooshani K., et al. Fuel Process. Technol., 2013, 109: 172-178.
[34] Kumaran G.M., Gary S., Soni K., et al. Energy & Fuels, 2006, 20: 1784-1790.
[35] Kumaran G.M., Gary S., Kumar M., et al. Energy & Fuels, 2006, 20: 2308-2313.

[36] Ali M.A., Tatsumi T., Masuda T. Appl. Catal. A, 2002, 233: 77-90.
[37] Ding L., Zheng Y., Zhang Z., et al. J. Catal., 2006, 241: 435-445.
[38] Ding L., Zheng Y., Zhang Z., et al. Appl. Catal. A, 2007, 319: 25-37.
[39] Tatsumi T., Taniguchi M., Ishige H., et al. Appl. Surf. Sci., 1997, 121-122: 500-504.
[40] Corma A., Fornes V., Bonton J.B., et al. J. Catal., 1987, 107: 288-295.
[41] Camblor M.A., Corma A., Martinez A., J. Catal., 1998, 179: 537-547.
[42] Sarbak Z, Applied Catal. A, 2001, 207: 309-314.
[43] Ismagilov Z.R., Yashnik S.A., Startsev A.N., et al. Catal. Today, 2009, 114: 235-250.
[44] Lara G., Escobar J., De los Reyes J., et al. The Canadian Journal of Chemical Engineering, 2005, 83: 685-694.
[45] Marin C., Escobar J., Galvan E., et al. Fuel Process. Technol., 2004, 86: 391-405.
[46] Kadono T., Chatani H., Kubota T., et al. Micropor. Mesopor. Mater., 2007, 101: 191-199.
[47] Chen X., Liu X., Wang L., et al. RSC Adv., 2013, 3: 1728-1731.
[48] Marques J., Guilaume D., Merdrignac I., et al. Appl. Catal. B, 2011, 101: 727-737.
[49] Perez-Ramirez J., Christensen C.H., Egeblad K., et al. Chem. Soc. Rev., 2008, 37: 2530-2542.
[50] Davis M.E., Saldarriage C., Montes C., A Nature, 1988, 331: 698-699.
[51] Moller K., Bein T. Chem. Soc. Rev., 2013, 42: 3689-3707.
[52] de Jong K.P., Zecevic J., Friedrich H., et al. Angew. Chem., 2010, 49: 10074-10078.
[53] Ogura M., Shinomiya S.-Y., Tateno J., et al. ChemInform Abstract: Formation of Uniform Mesopores in ZSM-5 Zeolite through Treatment in Alkaline Solution., Weinheim: WILEY-VCH Verlag GmbH & Co. KGaA, 2000.
[54] Holm M.S., Svelle S., Joensen F., et al. Appl. Catal. A, 2009, 356: 23-30.
[55] Verboekend D., Vile G., Perez-Ramirez J. Adv. Funct. Mater., 2012, 22: 916-928.
[56] Verboekend D., Perez-Ramirez J. Catal. Sci. Technol., 2011, 1: 879-890.
[57] Verboekend D., Mitchell S., Milina M., et al. J. Phys. Chem. C, 2011, 115: 14193-14203.
[58] Verboekend D., Vile G., Perez-Ramirez J. J. Cryst. Growth Des., 2012, 12: 3123-3132.
[59] Bonilla A., Baudouin D., Perez-Ramirez J. J. Catal., 2009, 265: 170-180.
[60] Perez-Ramirez J., Abello S., Bonilla A., et al. Adv. Funct. Mater., 2009, 19: 164-172.
[61] Greon J.C., Peffer L.A.A., Moulijn J.A., et al. Micropor. Mesopor. Mater., 2004, 69: 29-34.

[62] Greon J.C., Perez-Ramirez J., Peffer L.A.A. Catal. Lett., 2002, 31: 94-95.
[63] Greon J.C., Jansen J.C., Moulijn J.A., et al. J. Phys. Chem. B, 2004, 108: 13062-13065.
[64] Greon J.C., Bach T., Ziese U., et al. J. Am. Chem. Soc., 2005, 127: 10792-10793.
[65] Greon J.C., Moulijn J.A., Perez-Ramirez J. Micropor. Mesopor. Mater., 2005, 87: 153-161.
[66] Greon J.C., Peffer L.A.A., Moulijn J.A., et al. Colloids Surf. B, 2004, 241: 53-58.
[67] Greon J.C., Peffer L.A., Perez-Ramirez J. Chemistry, 2005, 11: 4983-4994.
[68] Greon J.C., Abello S., Vilaescusa L.A., et al. Micropor. Mesopor. Mater., 2008, 114: 93-102.
[69] Sun Y., Prins R. Angew. Chem., 2008, 47: 8478-8481.
[70] Tang T., Yin C., Wang L., et al. J. Catal., 2008, 257: 125-133.
[71] Hojholt K.T., Vennestrom P.N.R., Tiruvalam R., et al. Chem. Comm., 2011, 47: 12864-12866.
[72] van Laak A.N.C., Sagala S.L., Zecevic J., et al. J. Catal., 2010, 276: 170-180.
[73] Leng K., Wang Y., Hou C., et al. J. Catal., 2013, 306: 100-108.
[74] Tayeb K.B., Lamonier C., Lancelot C., et al. Catal. Today, 2010, 150: 207-212.
[75] Tayeb K.B., Lamonier C., Lanceot C., et al. Appl. Catal. B, 2012, 126 : 55-63.
[76] Frydman L., Harwood J.S. J. Am. Chem. Soc., 1995, 117: 5367-5368.
[77] Tamura M., Shimizu K.-I., Satasuma A. Appl. Catal. A, 2012, 433-434: 135-145.
[78] Sadowska K., Gora-Marek K., Datka J. J. Phys. Chem. C, 2013, 117: 9237-9244.
[79] Giraldo S.A., Centeno A. Catal. Today, 2008, 133-135: 255-260.
[80] Srivastava R. Chem. Comm., 2006, 43: 4489-4491.
[81] Kim J.-C., Cho K., Ryoo R. Appl. Catal. A, 2014, 470: 420-426.
[82] Holm M.S., Hansen M.K., Christensen C.H. Eur. J. Inorg. Chem., 2009, 9: 1194-1198.
[83] Sexena S.K., Viswanadham N., Sharma T. J. Mater. Chem. A, 2013, 2: 2487-2490.
[84] Wu Y., Tian F., Liu J., et al. Micropor. Mesopor. Mater., 2012, 162: 168-174.
[85] Tian F., Wu Y., Shen Q., et al. Micropor. Mesopor. Mater., 2013, 173: 129-138.
[86] Narender N., Mohan K.V.V.K., KulKarni S.J., et al. Catal. Comm., 2006, 7: 583-588.
[87] Nakashima S., Takahashi Y., Kiguchi M. Beilstein J. Nanotechnol., 2011, 2: 755-759.
[88] McMillan M., Brinen J.S., Carruthers J.D., et al. Colloids Surf., 1989, 38: 133-148.
[89] Thomas J.M., Klinowski J. Adv. Catal., 1985, 33: 199-374.
[90] Sazama P., Sobalik Z., Jakubec I., et al. Angew. Chem., 2013, 52: 2038-2041.
[91] Fyfe C.A., Strobl H., KoKotailo G.T., et al. Zeolite, 1988, 8: 132-136.

[92] Stelzer J., Paulus M., Hunger M., et al. Micropor. Mesopor. Mater., 1998, 22: 1-8.
[93] Fujita H., Kanougi T., Atoguchi T. Appl. Catal. A, 2006, 313: 160-166.
[94] van Bokhoven J.A., Lee T.-L., Drakopoulos M., et al. Nature Mater. 2008, 7: 551-555.
[95] Newsam J.M., Treacy M.M.J., Koetsier W.T., et al. Proc. R. Soc. Lond. A, 1988, 420: 375-405.
[96] van Bokhoven J.A., Koningsberger D.C., Kentgens A.P.M. J. Am. Chem. Soc., 2000, 122: 12842-12847.
[97] Omegna A., Vasic M., van Bokhoven J.A., et al. Phys. Chem. Chem. Phys., 2004, 6: 447-452.
[98] Chen T.-H., Houthoofd K., Grobet P.J. Micropor. Mesopor. Mater., 2005, 86: 31-37.
[99] de Ménorval L.C., Buckermann W., Figueras F., et al. J. Phys. Chem., 1996, 100 : 465-467.
[100]Oumi Y., Mizuno R., Azuma K., et al. Micropor. Mesopor. Mater., 2001, 49: 103-109.
[101]Oumi Y., Nemoto S., Nawata S., Mater. Chem. Phys., 2003, 78: 551-557.
[102]Song C., Ma X. Appl. Catal. B, 2003, 41: 207-238.
[103]Duan A., Wan G., Zhao A., et al. Catal. Today, 2007, 119: 13-18.
[104]Zhang D., Duan A., Zhao Z., et al. Catal. Today, 2011, 175: 477-484.
[105]Michaud P., Lemberton J.L., Perot G. Appl. Catal. A, 1998, 169: 343-353.
[106]Richard F., Boita T., Perot G. Appl. Catal. A, 2007, 320: 69-79.
[107]Huo Q., Dou T., Zhao Z., et al. Appl. Catal. A, 2010, 381 : 101-108.
[108]Fu W., Zhang L., Tang T., et al. J. Am. Chem. Soc., 2011, 133: 15346-15349.
[109]Sun Y., Wang H., Prins R. Catal. Today, 2010, 150: 213-217.
[110]Huo Q., Gong Y., Dou T., et al. Energy & Fuels, 2010, 24: 3764-3771.
[111]Duan A., Li T., Zhao Z., et al. Appl. Catal. B, 2015, 165: 763-773.
[112]Tang T., Zhang L., Fu W., et al. J. Am. Chem. Soc., 2013, 135: 11437-11440.
[113]Ren J., Wang A.J., Li X., et al. Appl. Catal. A, 2008, 344: 175-182
[114]Ding L., Zheng Y., Yang H., et al. Appl. Catal. A, 2009, 353: 17-23.
[115]Bendezu S., Cid R., Fierro J.L.G., et al. Appl. Catal. A, 2000, 197: 47-60.
[116]Tian R., Shen B., Wang F., et al. Energy & Fuels, 2009, 23: 55-59.
[117]Fan Y., Xiao H., Shi G., et al. J. Catal., 2011, 279: 27-35.
[118]Diaz de Leon J.N., Michel P., Massin L., et al. J. Mol. Catal. A, 2012, 363-364: 311-321.
[119]Reinhoudt H.R., Crezee E., van Langeveld A.D., et al. J. Catal., 2000, 196: 315-329.
[120]Wan G., Duan A., Zhang Y., et al. Energy & Fuels, 2009, 23: 3846-3852.
[121]Zhang B, Yi Y.J., Zhang W., et al. Mater. Chara., 2011, 62: 684-690.

[122]Hensen E.J.M., van der Meer Y., van Veen J.A.R. Appl. Catal. A, 2007, 322: 16-32.
[123]Landau M.V., Berger D., Herskowitz M. J. Catal., 1996, 159: 536-245.
[124]Michel V., Dorothée L., Christophe G. Appl. Catal. B, 2012, 128: 3-9.
[125]Egorova M., Prins R. J. Catal., 2004, 225: 417-427.
[126]Da Costa P., Potvin C., Manoli J., et al. J. Mol. Catal. A, 2002, 184: 323-333.
[127]Saih Y., Segawa K. Catal. Surv. Asia, 2003, 7: 235-249.
[128]Philippe M., Richard F., Hudebine D., et al. Appl. Catal. B, 2013, 132-133: 493-498.
[129]Daager M., Chinanelli R.R. J. Catal., 1994, 149: 414-427.
[130]Stanislaus A., Marafi A., Rana M.S. Catal. Today, 2010, 153: 1-68.
[131]Nikulshin P.A., Salnikov V.A., Mozhaev A., et al. J. Catal., 2014, 309: 386-396.
[132]Pawelec B., Fierro J.L.G., Montesinos A., et al. Appl. Catal. B, 2008, 80: 1-14.
[133] Venezia A.M., Murania R., La Parola V., et al. Appl. Catal. A, 2010, 383: 211-216.
[134]La Parola V., Testa M.L., Venezia A. Appl. Catal. B, 2012, 119-120: 248-255.
[135]Giraldo S.A., Centeno A. Catal. Today, 2008, 133-135: 255-260.
[136]Solis D., Klimova T., Cuevas R., et al. Catal. Today, 2004, 98: 201-206.
[137]Srivastava R. Chem. Comm., 2006, 43: 4489-4491.
[138]Kim J.-C., Cho K., Ryoo R. Appl. Catal. A, 2014, 470: 420-426.
[139]Liu Y., Zhao N., Xian H., et al. Appl. Mater. Interfaces, 8398-8403.
[140] Joshi Y.V., Ghosh P., Daagge M., et al. J. Catal., 2008, 257: 71-80.
[141]Kogan V.M., Nikulshin P.A., Rozhdestvenskaya R.N., et al. Fuel, 2012, 100: 2-16.
[142]Yang H., Liu Z., Gao H., et al. Appl. Catal. A, 2010, 379: 166-171.
[143]Wang Y., Wu J., Wang S., RSC Adv., 2013, 3: 12635-12638.
[144]Guidotti M., Canaff C., Coustard J.-M., et al. J. Catal., 2005, 230: 375-383.
[145]Aguado J., Serrrano D.P., Escola J.M., et al. Fuel, 2013, 109: 679-686.
[146]Occelli M.L., Olivier J.P., Auroux A. J. Catal., 2002, 209: 385-393.
[147]Hargreaves J.S.J., Munnoch A.L., Catal. Sci. Technol., 2013, 3: 1165-1171

Publications in the period of Ph.D. education

(1) Publications

[1] Y. Wang, C. Lancelot, C. Lamonier, et al. Hierarchisation of Mordenite as NiW Sulfide Catalysts Support: Towards Efficient Hydrodesulfurization. ChemCatChem, 2015, 7: 3936-3944

[2] Y. Wang, C. Lancelot, C. Lamonier, et al. Restraining Deactivation of Hierarchical Zeolite supported NiW Catalyst in the HDS of Thiophene, RSC Adv., 2015, 5: 74150-74158

[3] Y. Wang, Y. Sun, C. Lancelot, et al. Effect of Post Treatment on the Local Structure of Hierarchical Beta Prepared by Desilication and the Catalytic Performance in Friedel-Crafts Alkylation. Micropor. Mesopor. Mater., 2015, 206: 42-51.

[4] Y. Wang, B. Wang, A. Rives, et al. Hydrodesulfurization of Transportation Fuels over Zeolite-Based Supported Catalysts. Energy and Environment Focus, 2014, 3: 1-8.

[5] K. Leng, Y. Wang, C. Hou, et al. Enhancement of Catalytic Performance in the Benzylation of Benzene with Benzyl Alcohol over Hierarchical Mordenite. J. Catal., 2013, 306: 100-108.

(2) Communications

[1] Y. Wang, Y. Sun, K. Leng, et al. Hydrodesulfurization of dibenzothiophene and 4,6-dimethyldibenzothiophene over NiW catalyst supported on hierarchical Mordenite. XII European Congress on Catalysis, Kasan, Russia, 2015

[2] Y. Wang，K. Leng, C. Lancelot, et al. Preparation of hierarchical Beta and its catalytic performance in Friedel-Crafts alkylations. 11th International Symposium on the Scientific Bases for the Preparation of Heterogeneous Catalysts, Louvain, Belgium, 2014.

[3] Y. Wang，K. Leng, C. Lancelot, et al. Desilicated hierarchical zeolite supported NiW catalysts for thiophene HDS. Gecat, France, 2014.

[4] K. Leng, Y. Wang, C. Hou, et al. Enhancement of catalytic performance in the benzylation of benzene with benzyl alcohol over hierarchical Mordenite. GFZ, France, 2014